

# THESIS

## HYPERPYCNAL FLOW DEPOSITION AND SEQUENCE STRATIGRAPHY OF A CRETACEOUS NEAR-SHORE MUDSTONE UNIT — THE SKULL CREEK SHALE FORMATION, COLORADO, USA

Submitted by

Kathleen J. Masterson

Department of Geosciences

In partial fulfillment of the requirements

For the Degree of Master of Science

Colorado State University

Fort Collins, Colorado

Fall 2015

Master's Committee:

Advisor: Sven Egenhoff

Ellen Wohl

Michelle Stanley

Copyright by Kathleen J. Masterson 2015

All Rights Reserved

## ABSTRACT

### HYPERPYCNAL FLOW DEPOSITION AND SEQUENCE STRATIGRAPHY OF A CRETACEOUS NEAR-SHORE MUDSTONE UNIT — THE SKULL CREEK SHALE FORMATION, COLORADO, USA

The middle shale member of the Cretaceous Dakota Group, the Skull Creek Formation (Fm.), is a proximal mudstone unit deposited in a delta-fed system within the Cretaceous Interior Seaway. Based on lithology, sedimentary structures, bioturbation intensity, and TOC values, the Skull Creek Fm. was divided into twelve facies which were grouped into five facies associations (FAs). All facies and FAs record deposition along proximal to distal regions within an ancient mud-dominated continental shelf. Sediment transport and deposition were strongly influenced by both river flooding and storm events that generated hyperpycnal flows. Sediments in the Skull Creek Fm. were transported as bed load by a combination of wave and current energy above storm wave-base (FA 5, FA 4, and parts of FA 5) or exclusively by currents as the flow traveled below storm wave-base (parts of FA 3, FA 2, and FA 1). Mud-rich siltstones and sandstones (FA 4) and bioturbated siltstones and sandstones (FA 5) are the most proximal FAs and were deposited above storm wave-base while ripple- to planar-laminated siltstones and mudstones (FA 3) were interpreted to be “medial” expressions of hyperpycnal flows due to the low occurrence of wave generated structures. The most distal FA's include massive, bioturbated mudstones (FA 1) that were deposited in a sediment starved area, most likely located laterally or in a more distal location to the

laminated mudstones (FA 2). Laminated mudstones (FA 2) were transported as bed load within turbulent flows below storm wave-base.

Fining-upward parasequences containing fine-grained FAs (FA 1 and FA 2) represent decreasing energy conditions and a rise in sea level, while stacked successions of more proximal units (FA 3, FA 4, and FA 5) are indicative of high energy levels and lower sea levels. Based on the stacking patterns of the five FAs, the Skull Creek Fm. was divided into five laterally traceable stratigraphic intervals. Transgressive system tracts are observed in interval 1 and interval 2, which are fining-upward successions composed of FA 5, FA 4 at the base and FA 1, FA 2, and FA 3 at the top. Interval 3 contains mainly HCS sandstones and siltstones which thicken vertically and it represents the only highstand system tract (HST) within the Skull Creek Fm. A regressive sequence is preserved in interval 4 which is composed of the most proximal FAs (mainly FA 5) and is abruptly overlain by interval 5, which is a fining-upward succession, and represents a final transgressive system tract within the Skull Creek Fm.

TOC (total organic carbon) content is highest, and contains the most oil-prone organic matter, within interval 2 which is composed of mainly laminated mudstones (FA 2). The high TOC values within FA 2 are due to low levels of bioturbation and low levels of sediment accumulation, whereas in other FAs moderate to high bioturbation intensities and high sedimentation rates decrease the likelihood of preserving organic matter. "Sweet spots" within other similar, proximal mudstone units that were deposited as hyperpycnal flows are therefore predicted to be found in distal deposits, where there was limited sediment reworking by organisms.

## ACKNOWLEDGMENTS

I would like to acknowledge my advisor, Dr. Sven Egenhoff for the countless comments and feedback that helped to improve my writing and made this thesis possible. I would like to thank ConocoPhillips for giving us access to their core of the Skull Creek Fm. which contributed greatly to this project. I would also like to thank the United States Geological Survey (USGS) for allowing us to sample and view the cores at the Core Research Facility (CRC).

Thank you to my committee members, Dr. Sven Egenhoff, Dr. Ellen Wohl, and Dr. Michelle Stanley for their comments and feedback that improved the quality of this thesis. I would also like to thank Heather Lowers at the USGS for her help navigating the SEM and Dr. Frank Ethridge for his help locating and visiting outcrops.

A very special thank you to my fellow graduate students in the CSU Sedimentology Group and in office 319. I would like to thank my undergraduate field assistants as well, Olivia Verma and Sean Horne. I would like to especially thank Katharine Compton, Kate Shervais, and Travis Wadkins for their friendship, love, and support which got me through the trials of graduate school.

## TABLE OF CONTENTS

ABSTRACT .....	II
ACKNOWLEDGMENTS .....	IV
TABLE OF CONTENTS .....	V
1.0 INTRODUCTION .....	1
2.0 GEOLOGICAL SETTING .....	4
4.0 SEDIMENTOLOGY .....	11
4.1 INTRODUCTION .....	11
4.2 SEDIMENTARY FACIES .....	12
4.3 FACIES ASSOCIATIONS .....	22
4.3.1 Facies Association 1 – Massive mudstone and siltstone .....	23
4.3.2 Facies Association 2- Laminated siltstone and mudstone .....	23
4.3.3 Facies Association 3 – Ripple to planar laminated siltstone .....	24
4.3.4 Facies Association 4 – Mud-rich sandstone and siltstone .....	24
4.3.5 Facies Association 5 – Bioturbated siltstone and sandstone .....	25
5.0 FACIES ARCHITECTURE .....	26
6.0 INTERPRETATION .....	31
6.1 DEPOSITIONAL MODEL .....	31
6.2 SEQUENCE STRATIGRAPHY .....	35
7.0 DISCUSSION .....	41

7.1 TRANSPORT MECHANISM OF FINE-GRAINED SEDIMENTS.....	41
7.2 ICHNOFACIES .....	44
7.3 TOC CONTENT .....	46
7.4 GUTTER CASTS.....	47
8.0 CONCLUSIONS .....	50
9.0 BIBLIOGRAPHY.....	53
10.0 APPENDICES .....	59
APPENDIX 1: TOC DATA .....	60
APPENDIX 2: STRATIGRAPHIC SECTIONS .....	70
APPENDIX 3: SCANNING ELECTRON MICROSCOPE (SEM) REPORT .....	86

## 1.0 INTRODUCTION

The high productivity of oil and gas exploration from unconventional reservoirs has led to a plethora of research focusing on fine-grained sedimentary mudstones (Baas and Best 2002; Bohacs et al. 2014; Ghadeer and Macquaker 2011; Macquaker et al. 2007; Schieber et al. 2007; Taylor and Macquaker 2000). Originally thought to have been deposited exclusively by suspension settling (Potter et al. 1980), it has recently become clear that mudstones can also be deposited from bed load processes and produce structures similar to their coarse-grained counterparts (Schieber et al. 2007; Schieber and Southard 2009). Many recent papers focus on deep shelf shale depositional systems and the siliciclastic mudstones that link shallow shelf sand- to siltstones and deep shelf mudstones have been largely left aside. For this reason, the sedimentary processes that shape the proximal part of continental shelves are still largely enigmatic. This study therefore aims at describing one example of such mudstone units, the Cretaceous Skull Creek Formation, which is well-exposed within hogbacks along the Front Range of Colorado, USA. The structures observed in this unit are characteristic not only for the Cretaceous of the Interior Seaway but will probably also characterize other proximal mudstone successions of all geological ages worldwide.

Serving as an example of relatively shallow-water mudstone deposition, the Skull Creek Fm. is interpreted to represent the distal portion of a delta system that shed siliciclastic material from the advancing orogenic front during the Sevier orogeny (Graham and Ethridge 1994; Weimer 1996). Within the Cretaceous Interior Seaway, the



humid environment and tectonically active margins are very favorable for producing hyperpycnal flows during river-flooding events (Bhattacharya and MacEachern 2009). Sediments within the Skull Creek Fm. are interpreted to have been deposited as a result of these flooding events, which have recently been found to play a large role in transporting mud from the delta front to the continental shelf (Friedrichs and Scully, 2007; Pattison et al. 2007; Traykovski et al. 2000). Because of changing sea level during the development of the Skull Creek Fm., this unit reflects deposition at varying distances from the sediment source and allows for a reconstruction of a proximal to distal transect through this delta-fed mudstone system.

The Skull Creek Fm. study is based on detailed descriptions of four outcrops and two cores (Fig. 1). The outcrops are arranged along two transects: one is positioned north-south along the western edge of the Denver basin and the other extends from the southernmost outcrop location (Turkey Creek) basinward, along an east-west transect. Based on detailed lithology descriptions, sedimentary structures, stacking patterns, TOC data, and bioturbation intensities, the Skull Creek Fm. was divided into 12 facies, 5 facies associations, and five distinct stratigraphic intervals.

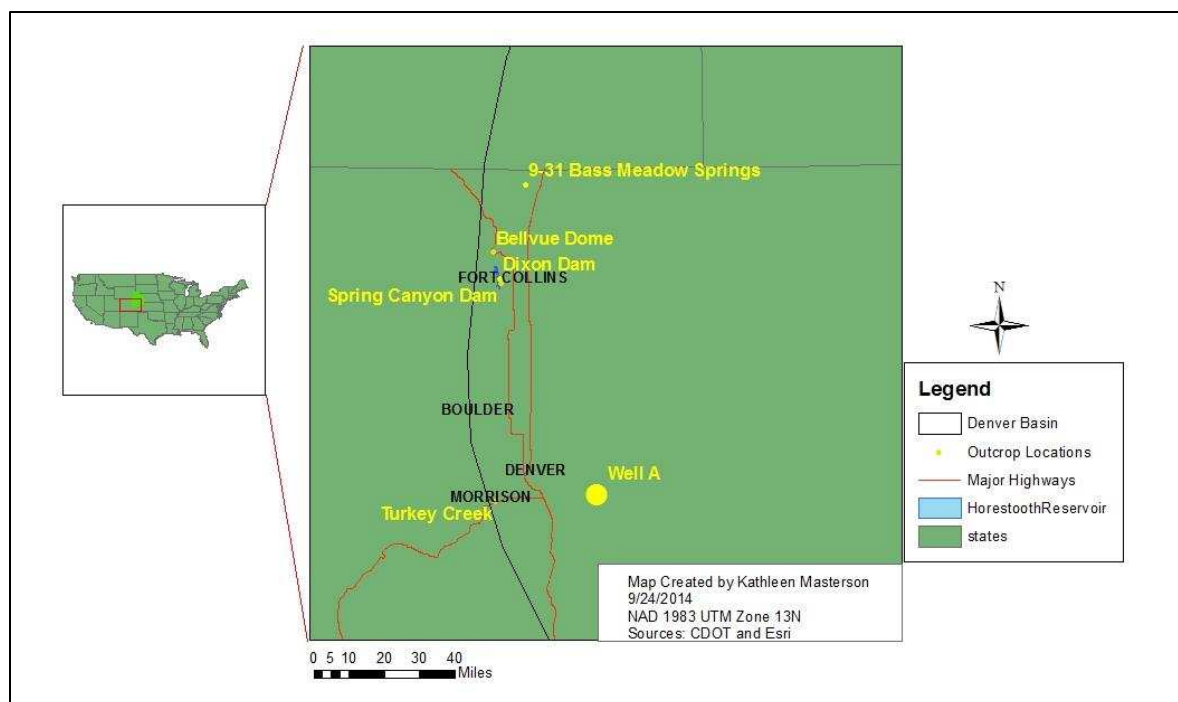


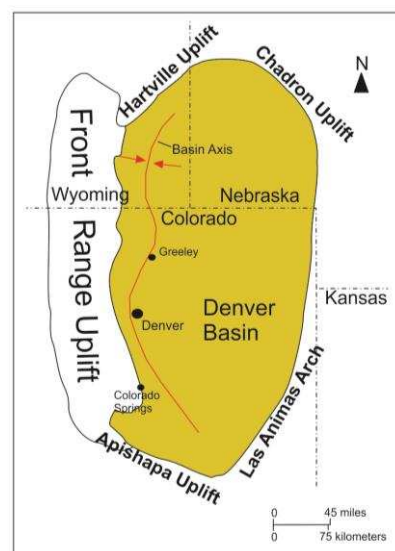
**Figure 1:** Overview map of outcrop and core locations of the study area.

## 2.0 GEOLOGICAL SETTING

The Denver basin covers an area of 60,000 mi.<sup>2</sup> (155,399 km<sup>2</sup>) and spans from northeast Colorado, and parts of southeast Wyoming to southwestern Nebraska (Fig. 2) (Dechesne et al. 2011). It is bounded by the Hartville and Chadron uplifts to the north and by the Apishapa Arch to the south. Sediments in the Denver Basin range from Paleozoic to Early Cenozoic in age. This basin is economically important due to its estimated reserves of 104.23 MMBO (million barrels of oil) and 2,519 BCFG (billion cubic feet of gas) where most of the












oil-producing units are within Upper Cretaceous formations (Fig. 3) (Dechesne et al. 2011; U.S. Geological Survey 2003). The Lower Cretaceous Dakota Group is both an oil- and gas-producing unit and is composed of two basal sandstones (Lytle and Plainview Fm.), a middle mudstone unit (Skull Creek Fm.) and the overlying Muddy (J) sandstones. The Skull Creek Fm. is speculated to be the source rock for the Muddy (J) sandstones and it is Albian in age (Weimer, 1996). The Skull Creek Fm., and other fine-grained units of the Denver basin, were deposited within the Cretaceous Interior Seaway, which is an inland sea that covered the interior of North America and would periodically stretch from Canada to the Gulf of Mexico (Decelles 2004).

It is speculated that transgressions and regressions in the Cretaceous Interior Seaway were heavily influenced by lithospheric loading along the developing foreland



**Figure 2:** Overview map of the Denver Basin. Modified from Knepper 2002.

thrust belt in the North America Cordillera (Jordan, 1981). This orogenic system can be divided into two major events; the Sevier and Laramide orogenies. The Sevier orogeny occurred from the mid-Jurassic to the Late Cretaceous, and began as the Farallon plate subducted under the North American Plate (Ethridge and Holbrook, 1996). During this orogenic event, the central US was affected by crustal shortening and uplift as the Sevier foreland basin system developed (DeCelles 2004; Dickinson and Lawton 2001; Ethridge and Holbrook 1996). Regional uplift increased subsidence in areas located to the east of the thrust belt (e.g. Colorado and Wyoming) and during the Albian (~112-98.5 Mya) the first major transgression of the Cretaceous Interior Seaway occurred (DeCelles 2004). The seaway was connected to the Gulf of Mexico by mid-Albian time (Fig. 4) (Burtner and Warner 1984). During this initial transgression, sediments of the early Skull Creek Fm. were eroded from uplifted areas in central Utah and deposited within an estuarine to prodeltaic environment (Burtner and Warner 1984; Graham and Ethridge 1994). The late Skull Creek and Muddy (J) sandstones were deposited mainly from a western source (e.g. the Bear River Delta, Bow Island Delta Complex) and a southern shoreline facies originating from the Mogollan high (Burtner and Warner 1984; Dolson et al. 1991). The Laramide orogeny (Late Cretaceous to Eocene) began after the Skull Creek Fm. was deposited. During the Laramide orogeny, the Sevier foreland basin broke-up into different uplifts and basins (e.g. Raton Basin, Powder River Basin, Crazy Mountains Basin) as a result of the flat subduction of the Farallon plate below the North America plate (DeCelles 2004; Weimer 1996).

	DENVER BASIN	
	Source Rocks	Production
		<ul style="list-style-type: none"> <li> Mainly oil</li> <li> Mainly gas</li> <li> Oil and Gas</li> </ul>
Upper Cretaceous	Laramie Formation	
	Fox Hills Sandstone	
	Pierre Shale	Terry "Sussex" Ss. Mbr. 
		Hygiene "Shannon" Ss. Mbr. 
		Sharon Springs Mbr. 
	Niobrara Formation	Smoky Hill Shale Mbr. 
		Fort Hays Limestone Mbr.
		Codell Sandstone Mbr. 
	Carlile Shale	
	Greenhorn Limestone	
	Graneros Shale  "D" sandstone	
Lower Cretaceous	Huntsman and Mowry Shales	
	Dakota Group	Muddy (J) Sandstones 
		Skull Creek Shale
		Plainview Sandstone member
		Lytle Formation
Jurassic	Morrison Formation	
	Ralstone Creek Formation	
	Entrada Sandstones	

**Figure 3:** Stratigraphic column of oil and gas producing units in the Denver basin. The Pierre shale is mainly oil producing, the Niobrara and Benton group are gas producing, and the Dakota Group (specifically the Muddy (J) sandstones) are oil and gas producing (from Knepper 2002)

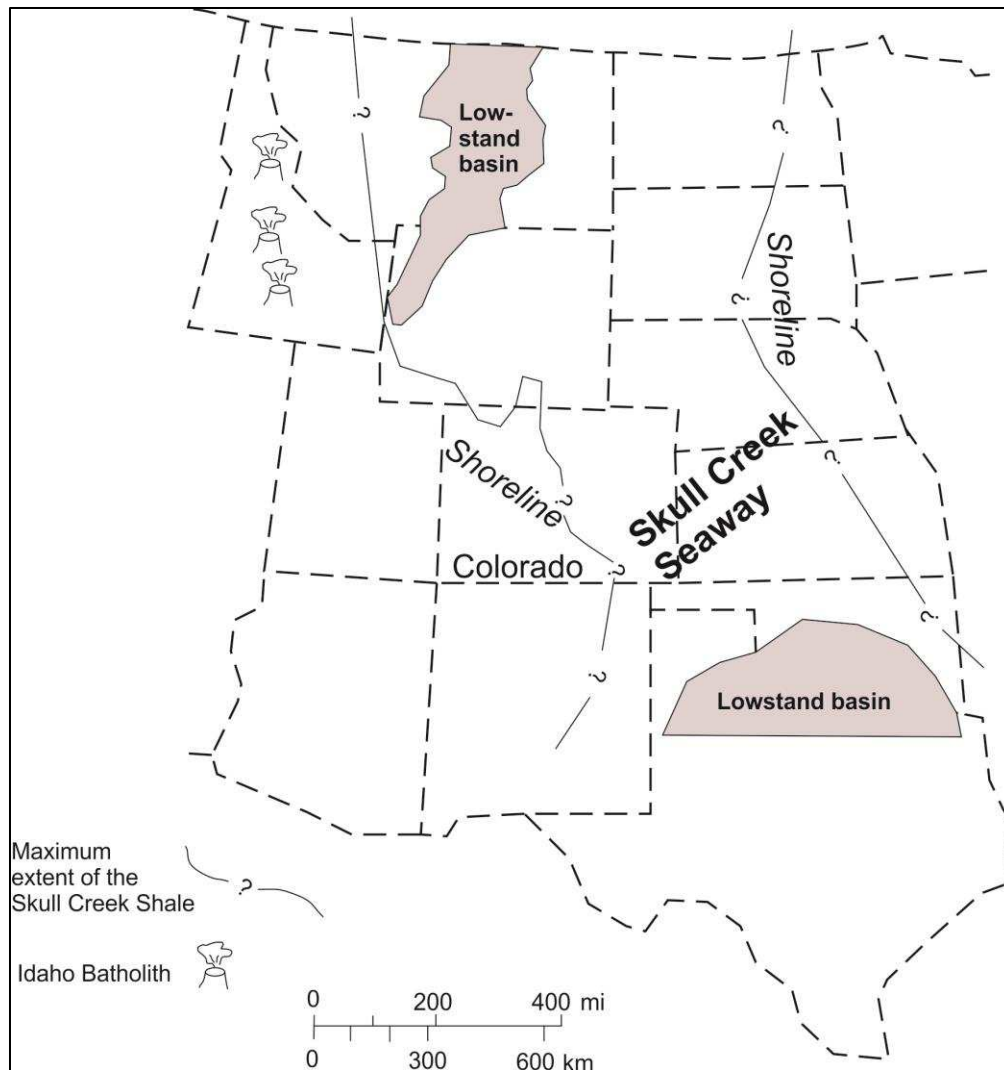


**Figure 4:** Map showing the maximum transgression during Skull Creek deposition and maximum regression during the deposition of the Muddy (J) sandstones (from Cobban et al. 1994; Dolson and Muller 1994; Weimer 1996)

### 3.0 METHODOLOGY

The data for this study included four outcrop locations and two cores, spanning about 90.35 mi. (145.41 km) along a north-south and an undisclosed distance along an east-west transect. Four outcrops and one core were chosen along the western boundary of the Denver basin, near the western edge of the Skull Creek Seaway (Burtner and Warner 1984). These locations are named (from north to south) 9-31 Bass Meadow Springs (USGS core library number D313), Bellvue Dome, Dixon Dam, Spring Canyon Dam, and Turkey Creek. The second core, located farther to the east within the basin, was provided by ConocoPhillips and will be referred to as Well A. Detailed stratigraphic sections were hand-drawn in the field, at the USGS core research center in Denver, CO, and at the Weatherford core viewing rooms in Houston, TX, and include fine-scale (mm-cm) observations recording grain size, sedimentary structures, bioturbation index, nature of contacts, and stacking patterns. The bioturbation index (BI) was used after Taylor and Goldring (1993), who described the level of bioturbation on a grade of 0-6, where 0 is no bioturbation and 6 is complete bioturbation or sediment reworking (Table 1). Representative samples were taken throughout the succession to document composition and sedimentary structures in detail (which will give an indication of the processes that formed the sample) and for measuring TOC values within different sedimentary facies.

A total of fifty ultra-thin (20  $\mu\text{m}$  thickness) polished thin sections were prepared with both clear and blue epoxy impregnation by Wagner Petrographic and TPS Enterprises. Two petrographic microscopes were used (Nikon Eclipse Ci-E and Nikon

SMZ 1500) to identify mineral composition and the degree of bioturbation from characteristic thin sections of cores and outcrops. The blue epoxy was used to estimate porosity of the samples. Organic matter type and composition of concretions was recognized using a scanning electron microscope (SEM) at the United States Geological Survey in Denver, CO. Thin sections were carbon-coated and investigated using a Quatra 450 FEG scanning electron microscope equipped with an energy-dispersive X-ray spectroscopy (EDS) that includes a backscattered electron (BSE) detector.

Thirty-one hand samples were collected for measuring total organic carbon content (TOC) from proximal, intermediate, and distal facies of mudstone units. For the TOC analysis, all of the samples were treated with hydrochloric acid to remove any carbonate; the analyses were carried out using standard induction furnace techniques by Weatherford Laboratories with a Leco-CS230 instrument. Five of the TOC samples were analyzed using programmed pyrolysis to identify the maturity and kerogen type of the mudstones on a RockEval-II instrument. This was achieved by heating of organic matter under an inert helium atmosphere.

**Table 1:** Bioturbation Index, from Taylor and Goldring, 1993.

Grade	Percent Bioturbated	Classification
0	0	No bioturbation
1	1-4	Sparse bioturbation, bedding distinct, few discrete traces and/or escape structures
2	5-30	Low bioturbation, bedding distinct, low trace density, escape structures often common
3	31-60	Moderate bioturbation, bedding boundaries sharp, traces discrete, overlap rare



4	61-90	High bioturbation, bedding boundaries indistinct, high trace density with overlap common
5	91-99	Intense bioturbation, bedding completely disturbed (just visible), limited reworking, later burrows discreet
6	100	Complete bioturbation, sediment reworking due to repeated overprinting

## 4.0 SEDIMENTOLOGY

### 4.1 Introduction

Detailed descriptions of macroscopic and microscopic observations from four outcrop locations, two cores and forty-nine thin sections (Appendix 2) were used to subdivide the Skull Creek Fm. into eleven facies and five facies associations. The facies are distinguished based on grain size, sedimentary structures, and composition. All eleven facies are mostly composed of siliclastic and carbonate grains, with only some phosphatic remains of organisms. High TOC values are exclusively found within fine-grained facies that either lack or show only rare bioturbation. Heavily bioturbated facies have the lowest recorded TOC values in the succession. Organic matter types are both terrestrial and marine in origin and include vitrinite (terrestrial), telalginite, bituminite, and amorphous organic matter (identification of organic matter types based on Fishman et al. 2012). Telalginite is orange to yellow in color, orientated parallel to bedding, and is ~1.5mm in length. Bituminite is non-fluorescent and is preserved as thin, wispy laminae. Vitrinite is orange to red in color under plane polarized light, has well defined boundaries, and preserved as small round clasts (~.05mm) or thin laminae. Amorphous organic matter types are black, irregular clasts and are composed of a mixture of clay and carbon.

## 4.2 Sedimentary Facies

Facies Name	Laminae/Bed Thickness	Feature Description	Composition	Interpretation
<b>Massive Mudstone (Facies 1)</b>	Beds: 10mm-3500mm	<ul style="list-style-type: none"> <li>Poorly sorted mudstones of mainly clay-sized grains with some floating silt grains.</li> <li>Rare to frequent <i>Planolites</i> and <i>Phycosiphon isp</i>; BI (bioturbation index)= 1-4, <i>Planolites</i> are oval in shape and filled with silt</li> <li>Wt. % TOC: 0.31- 1.39</li> <li>Contains large concretions (up to 15cm diameter)</li> </ul>	<ul style="list-style-type: none"> <li>Clay: 55-65%</li> <li>Siliciclastic and carbonate silt: 10-30%</li> <li>Pyrite: 0-5%</li> <li>Organic matter: 0-10%</li> </ul>	<ul style="list-style-type: none"> <li>Large “floating” quartz grains could have originated by two processes: (1) either they originally formed siltstone laminae, likely deposited by bed load processes, that were disturbed by bioturbation, and silt grains pushed into adjacent mudstones, or (2) the clasts were originally deposited in the muddy matrix from fluid mud of the upper cohesive layer within hyperpycnal flows and are preserved as massive mudstone deposits (Wilson and Schieber 2014).</li> <li>High levels of bioturbation intensity indicate slow sediment deposition or deposition in a sediment starved area where there was ample time for organisms to colonize the beds (Taylor and Gawthorpe 1993).</li> <li>The overall low TOC values are due to feeding organisms (<i>Planolites</i>) who likely consumed some of the organic matter.</li> </ul>
<b>Regularly laminated mudstone (Facies 2a)</b>	Laminae: <1.5 mm, Beds: 100mm-300mm	<ul style="list-style-type: none"> <li>Mudstones of mainly clay-size grains interbedded with thin silt laminae (&lt;0.5mm)</li> <li>Planar laminae are normally or inversely graded laminae</li> <li>Basal scours at the base of normally graded beds, in places low angle crossbeds at the base of graded beds.</li> <li>Siltstone laminae are</li> </ul>	<ul style="list-style-type: none"> <li>Clay: 40-80%</li> <li>Siliclastic and carbonate silt: 30-8%</li> <li>Pyrite: 1-5%</li> <li>Organic matter: 1-20%</li> </ul>	<ul style="list-style-type: none"> <li>Siltstone laminae containing low-angle crossbeds and a basal scour were formed by a turbulent flow that 1) eroded into underlying sediment 2) silt-size grains were deposited as the flow decelerated, formed siltstone laminae, and were partly reworked by currents to form low angle crossbeds 3) mud was deposited on top of silt laminae as the flow waned to form normally graded laminae. Alternatively, if the flow gained energy (accelerated) it formed inversely graded laminae (Mulder and Alexander 2001; Wilson and Schieber</li> </ul>

		<ul style="list-style-type: none"> <li>even in thickness</li> <li>Rare to intermediate <i>Phycosiphon isp.</i> are lined with silt grains and filled with mud, can be up to 1mm in length, BI=0-2</li> <li>Wt. % TOC: 1.63-3.86</li> </ul>		<ul style="list-style-type: none"> <li>2014).</li> <li>Siltstone laminae are even in thickness since they were not disturbed by bioturbation.</li> <li>This facies was deposited in a stressed environment due to low diversity of ichnofossils, and rapid deposition interpreted from low bioturbation intensities.</li> </ul>
<b>Irregularly laminated mudstone (Facies 2b)</b>	Laminae: 0.1mm-1mm Beds: 0.09cm-0.4cm	<ul style="list-style-type: none"> <li>Mudstones of mainly clay-size grains with thin siltstone laminae that are irregular in thickness (&lt;0.1mm); some floating silt-size quartz grains</li> <li>Sharp contact between siltstone and mudstone laminae</li> <li>Lamellar AOM (amorphous organic matter)</li> <li>Rare to intermediate <i>Planolites</i> and <i>Phycosiphon</i>, BI=0-3</li> <li>Wt. % TOC: 0.7–3.86</li> </ul>	<ul style="list-style-type: none"> <li>Clay: 40-80%</li> <li>Siliclastic and carbonate silt: 10-40%</li> <li>Pyrite: 1-5%</li> <li>Organic matter: 3-15%</li> </ul>	<ul style="list-style-type: none"> <li>Siltstone laminae are interpreted to have been regular originally; they are envisioned to have been formed by mixing of silt-size sediment in the lower turbulent layer with the fine-grained material of the upper cohesive layer of hyperpycnal flows (Macquaker et al. 2010).</li> <li>Irregularity of laminae thickness is due to bioturbation. The floating grains may be the remnants of siltstone laminae that were disrupted by bioturbation or formed from the upper cohesive layer (fluid mud layer) of the hyperpycnal flow and were deposited within the mudstones.</li> <li>Low diversity of ichnofossils suggests a stressed environment.</li> <li>There are in places bioturbated, &lt;0.6 mm thick laminae (BI=3) that represent a break in deposition.</li> </ul>
<b>Mudstones with downlapping laminae (Facies 3)</b>	Laminae: 0.1mm-0.7mm Beds: 0.2mm-0.4mm	<ul style="list-style-type: none"> <li>Mudstones of mainly clay-size grains with thin (&lt;0.5mm) siltstone laminae</li> <li>Low-angle, uni-directional crossbeds that downlap onto underlying mudstone beds. Bounded by a basal scour.</li> <li>Lamellar to rounded AOM</li> </ul>	<ul style="list-style-type: none"> <li>Clay: 50-70%</li> <li>Siliclastic and carbonate silt: 10-42%</li> <li>Pyrite: 1-5%</li> <li>Organic matter: ~15%</li> </ul>	<ul style="list-style-type: none"> <li>Downlapping laminae are formed from lower flow regime by currents indicated by low-angle crossbeds.</li> <li>Uni-directional cross beds and a basal scour suggest sediment was transported as a traction current; the current eroded underlying sediment, silt and mud was deposited and reworked by currents to form low-angle crossbeds.</li> <li>Low diversity of ichnofauna suggests a</li> </ul>

		<ul style="list-style-type: none"> <li>(0.1mm-0.01mm)</li> <li>Contains rare <i>Phycosiphon</i> isp. BI=0-1</li> <li>Wt. % TOC: 0.91-2.97</li> </ul>		stressed environment; alternatively, sediment was deposited rapidly and organisms did not have time to colonize the sediment.
<b>Siltstones with downlapping laminae (Facies 4)</b>	Laminae: less than 0.5 mm, Beds: 2mm-40mm	<ul style="list-style-type: none"> <li>Siltstones with mainly silt-size quartz grains and minimal mud size grains</li> <li>Well-preserved, uni-directional cross beds with alternating siltstone and mudstone laminae</li> <li>Lamellar to rounded AOM (0.1mm-0.01mm)</li> <li>Water-escape structures and slumps common</li> <li>Usually there is a sharp contact at the base</li> <li>Rare to absent <i>Phycosiphon</i> isp. BI= 0-1</li> <li>Wt. % TOC: ~2.49</li> </ul>	<ul style="list-style-type: none"> <li>Clay: 20-50%</li> <li>Siliclastic and carbonate silt: 50-70%</li> <li>Pyrite: 0-5%</li> <li>Organic matter: 1-20%</li> </ul>	<ul style="list-style-type: none"> <li>Deposited in lower flow regime by unidirectional currents indicated by crossbeds.</li> <li>The downlapping siltstone laminae, or uni-directional crossbeds, bounded by a basal scour suggest sediment was deposited from turbulent flows where the incoming flow eroded into underlying sediment; as energy waned, siltstone was deposited and reworked by currents preserving low angle crossbeds.</li> </ul>
<b>Laminated Siltstones (Facies 5)</b>	Laminae: less than 1.5mm Beds: 10mm-90mm	<ul style="list-style-type: none"> <li>Siltstones with mainly silt-size quartz grains and some thin (&lt;1mm) clay laminae</li> <li>Planar siltstone laminae are continuous in thickness and normally and inversely graded</li> <li>Top and basal contacts are sharp between mudstone and siltstone laminae.</li> <li>Water-escape structures and slumps common</li> <li>Bioturbation is absent and OM is rare</li> <li>Rare to absent <i>Phycosiphon</i> isp. BI=0-1</li> </ul>	<ul style="list-style-type: none"> <li>Clay: 30-50%</li> <li>Siliclastic and carbonate silt: 50-70%</li> <li>Pyrite: 0-5%</li> <li>Organic matter: 1-15%</li> </ul>	<ul style="list-style-type: none"> <li>Planar laminae that are normally and inversely graded are found in "transitional flows" which are formed from the interaction of a lower, turbulent layer that has a high shear component and an upper cohesive layer that has a low shear component. Turbulent flows erode underlying beds and deposit silt-size particles at the base of the flow, the overlying mudstone laminae are deposited as the flow decelerates (Baas and Best 2002).</li> <li>Normal grading is formed from a decelerating (waning) flow. Inverse grading is formed from flows that are accelerating (waxing).</li> </ul>

		<ul style="list-style-type: none"> <li>Wt. % TOC: 0- 0.44</li> </ul>		
<b>Massive siltstone (Facies 6)</b>	Beds: 20mm-6000mm	<ul style="list-style-type: none"> <li>Siltstones with mainly silt-size quartz grains, rare siltstone to mudstone rip-up clasts, and rare, thin (&lt;1mm) siltstone and clay laminae</li> <li>Alternating, regular siltstone and mudstone laminae are orientated parallel to bedding and have a basal scour</li> <li>Siltstone and mudstone rip-up clasts are in places deformed and are 0.2mm-5mm in size</li> <li>Pyrite concretions are concentrated in burrows</li> <li>Massive siltstone with some wavy mudstone layers, contains <i>Planolites</i>, <i>Chondrites</i>, <i>Phycosiphon</i>, <i>Teichichnus</i>, <i>Schaubcylindrichnus</i>, <i>Skolithos</i>, <i>Arenocolites</i>, <i>Zoophycos</i>, <i>Asterosoma</i>, <i>Ophiomorpha</i>, <i>Thalassinoids</i> and <i>Cylindrichnus</i>. BI= 3-6</li> <li>Wt. % TOC: 0-0.40</li> </ul>	<ul style="list-style-type: none"> <li>Clay: 10-40%</li> <li>Siliclastic and carbonate silt: 58-80%</li> <li>Pyrite: 1-5%</li> <li>Organic matter: 1-5%</li> <li>Porosity: 0-5%</li> </ul>	<ul style="list-style-type: none"> <li>There are two pieces of evidence for sediment transport in turbulent flow: 1) siltstone and mud clasts are intraclasts that were eroded from unconsolidated sediment and transported as bed load within a turbulent flow and 2) siltstone and mudstone laminae were formed as siltstone and mudstone grains were transported as bed load in a turbulent flow that eroded underlying sediment, deposited silt-size particles at the base of the flow and overlying mud-size particles as the flow waned.</li> <li>Sedimentary beds where structures are preserved (BI=3) were formed in areas of the basin where sediment was deposited rapidly, with frequent input from turbulent flows, and organisms did not have enough time to colonize the sediment. Heavily bioturbated (BI=4-6) beds were deposited in areas that had low rates of sediment input and organisms had plenty of time to rework the beds.</li> <li>Heavy bioturbation suggests an overall oxic environment.</li> <li>Pyrite concretions filling in burrows are formed from early diagenetic reactions within mucus trails which serve as a site for "microbial sulfate reduction" and subsequent iron sulfide precipitation (Schieber 2002).</li> </ul>
<b>Fossil-bearing siltstones (Facies 7)</b>	Laminae: 0.3mm-1mm, Beds: 200mm-4000mm	<ul style="list-style-type: none"> <li>Composed of poorly sorted silt-size carbonate grains, broken shell debris, and minimal quartz grains</li> <li>Shell debris is mainly bivalves (<i>Inoceramus</i>)</li> </ul>	<ul style="list-style-type: none"> <li>Clay: 30-15%</li> <li>Siliclastic and carbonate silt: 70-80%</li> <li>Phosphate: 2-5%</li> <li>Pyrite: 0-5%</li> </ul>	<ul style="list-style-type: none"> <li>Shell debris is allochthonous. Because shell debris is preserved as broken pieces, it can be interpreted that they were transported as bed load from proximal areas in the basin during high-energy events and deposited as the flow decelerated.</li> </ul>

		<ul style="list-style-type: none"> <li>• Rare phosphatic concretions are 1.1mm-0.5mm in diameter (Appendix 3)</li> <li>• Shell layers are in places found at the base of hummocks.</li> <li>• BI=0</li> </ul>		<ul style="list-style-type: none"> <li>• Phosphate concretions are diagenetic and nucleated by organic remains (Taylor and Macquaker 2000; Trappe 2001).</li> </ul>
<b>Fine-grained sandstone to siltstone with draping laminae (facies 8)</b>	Beds: 1 mm-38 mm	<ul style="list-style-type: none"> <li>• Composed of silt to vfg (very fine grained) sand-size quartz grains</li> <li>• Shows two different symmetrical ripple types; one with undiscernible internal laminations to low angle bi-directional and one with uni-directional cross beds.</li> <li>• Sharp basal contact</li> <li>• Beds are connected by draping forsets or are separated to form isolated "swollen" lenses.</li> <li>• BI=0-1</li> </ul>	<ul style="list-style-type: none"> <li>• Clay: 10-40%</li> <li>• Siliclastic silt to vfg sand: 55-85%</li> <li>• Pyrite: 0-5%</li> </ul>	<ul style="list-style-type: none"> <li>• Symmetric lenses, draping forsets, internal laminations, and irregular lower boundaries suggest sediment reworking by a combination of wave and current action and are indicative of transport in combined flow to predominately oscillatory flows (de Raaf et al. 1977).</li> <li>• Symmetric ripples with weak, bi-directional internal laminations are formed when sand or silt settles out of a flow, and is subsequently reworked by wave action. Internal uni-directional cross beds are formed when sediment is transported in a current-dominated flow; the upper symmetric boundaries of the ripples represent an oscillatory component that affects the upper boundaries of the flow (de Raaf et al. 1977).</li> </ul>
<b>Fine-grained sandstone to siltstone with HCS (Facies 9)</b>	Beds: 2mm-400mm	<ul style="list-style-type: none"> <li>• Composed of silt to vfg sand-size quartz grains</li> <li>• Hummocky-bedded sandstones are lenticular (1cm - 38cm thick)</li> <li>• Sharp basal contact</li> <li>• Often overlain by thin mudstone beds (facies 1) (0.5cm-4cm)</li> <li>• Wt. % TOC: ~0.44</li> </ul>	<ul style="list-style-type: none"> <li>• Clay: 10-0%</li> <li>• Detrital siliclastic and carbonate silt to vfg sand: 90-100%</li> <li>• Phosphate: 0-2%</li> <li>• Pyrite: 0-5%</li> <li>• Organic matter: 1-10%</li> </ul>	<ul style="list-style-type: none"> <li>• Bottom currents scour the sea floor; silt to sand to silt particles are transported in combined flows to waning oscillatory flows indicated by 1) flat laminations at the base; produced by a combination of current and oscillatory motion 2) hummocks and overlying high angle cross beds with symmetrical upper boundaries were produced by waning flows or very strong oscillatory combined flows. Low-angle crossbeds with symmetrical upper boundaries were formed in low velocity combined flows (Duke et al. 1991).</li> </ul>

<b>Massive mud-rich sandstone to siltstone (Facies 10)</b>	Beds: 10mm-20mm	<ul style="list-style-type: none"> <li>• Composed of silt to vfg sand-size quartz grains with mud matrix</li> <li>• Sandstones and siltstones are very well sorted</li> <li>• Massive siltstones and sandstones fill gutter casts and sand lenses</li> <li>• Contains <i>Arenicolites</i> and <i>Diplocraterion</i></li> <li>• Wt. % TOC: 0-0.11</li> </ul>	<ul style="list-style-type: none"> <li>• Clay: 10-0%</li> <li>• Siliclastic silt to vfg sand: 90-100%</li> <li>• Pyrite: 0-5%</li> <li>• Organic matter: 0-1%</li> </ul>	<ul style="list-style-type: none"> <li>• Scours were formed by incoming currents and after the current passed the depression was filled with sand.</li> <li>• Massive beds indicate sediment was deposited very quickly.</li> <li>• Presence of <i>Arenicolites</i> and <i>Diplocraterion</i> represent pauses in sedimentation between high energy events (e.g. storm events) and subsequent normal marine conditions after the storm as passed (MacEachern et al. 1991)</li> </ul>
--	-----------------	---	--	--



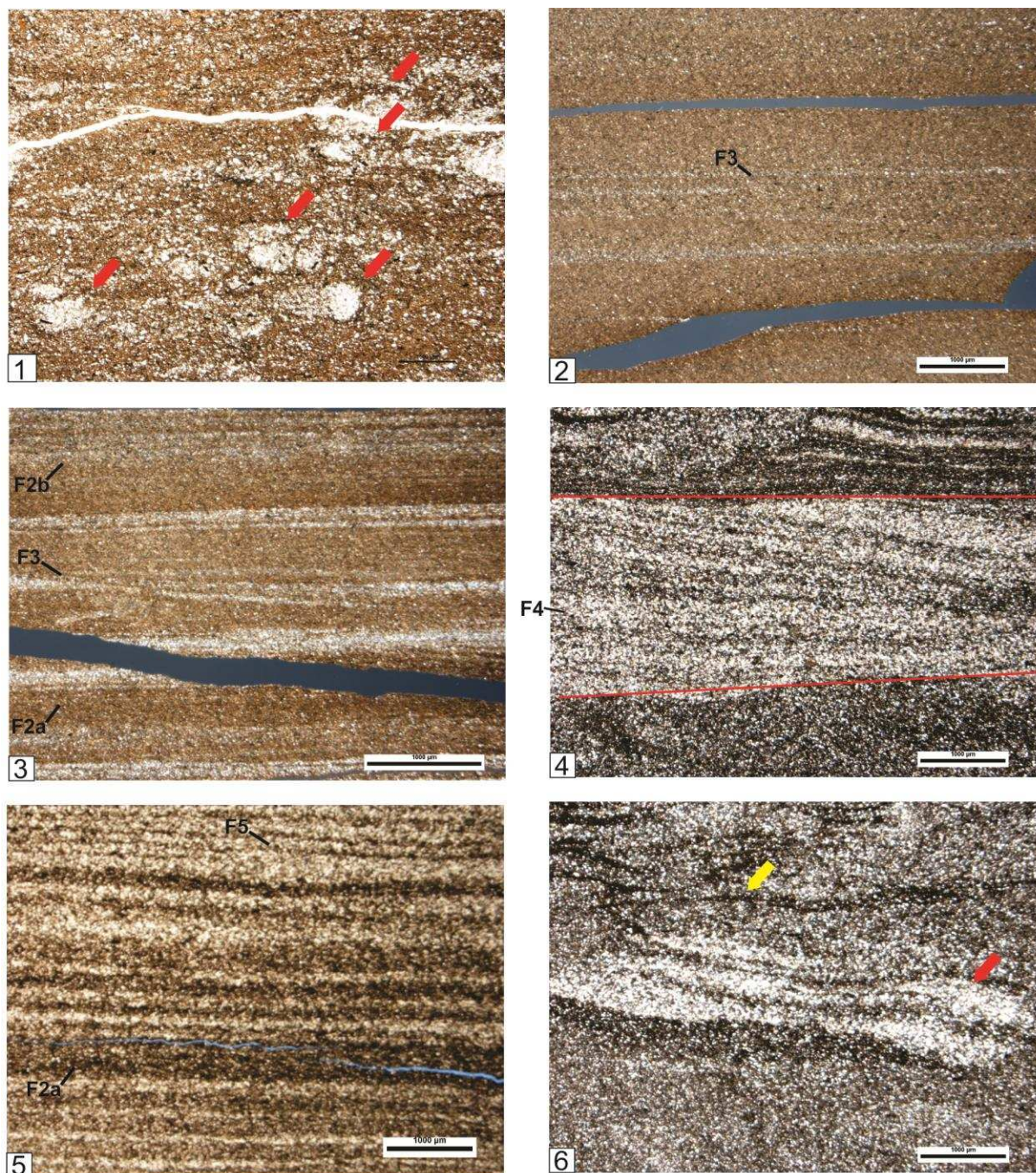


**Figure 5:** 1) Massive mudstone from Bellvue Dome (BD) at 5.83m showing Planolites burrows (facies 1) indicated by red arrows. 2) Downlapping laminae in a mudstone (facies 3) from Turkey Creek (TC) at 14.82m. 3) Mudstone containing regular laminae (facies 2a), irregular laminae (facies 2b), and downlapping laminae (facies 3); Dixon Dam section (DD) at 2.16m. 4) Siltstone consisting of downlapping laminae, outlined in red (facies 4). From TC at 20.66m. 5) Inversely graded planar laminated siltstone to mudstone facies 2a and 5) from Spring Canyon (SC) at 20.15m. 6) Siltstone containing a rip-up clasts (red arrow) and irregular mud clasts (indicated by yellow arrows) from section TC at 20.66m (facies 6).



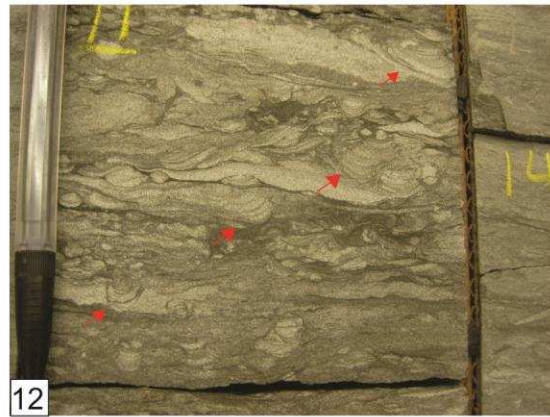
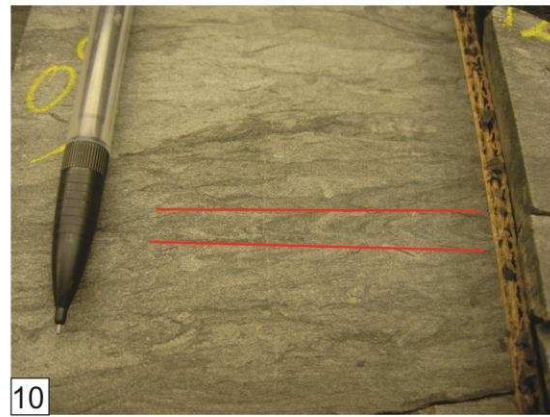
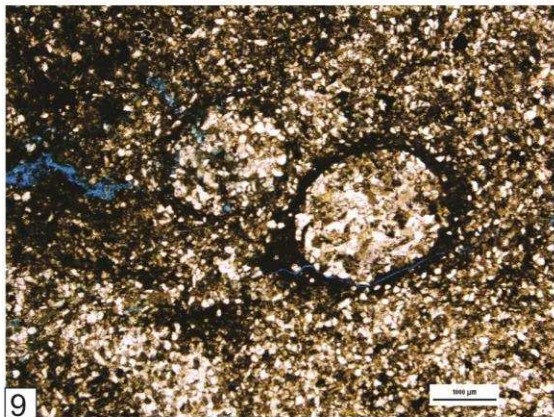
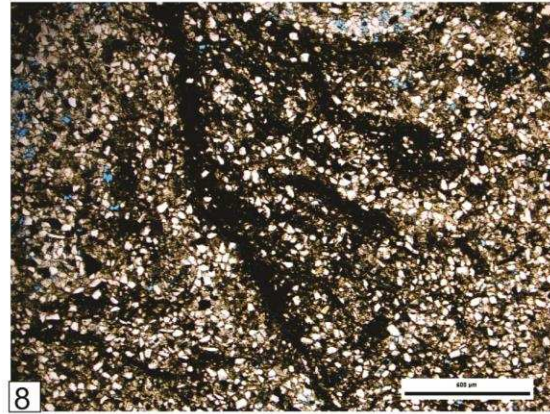
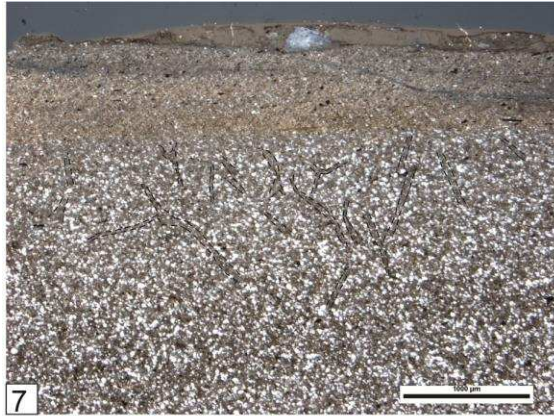


**Figure 5 (continued):** Photos showing bioturbated siltstone (facies 6): 7) Massive siltstone from TC at 10.6m that has been completely bioturbated by *Phycosiphon* isp. (some examples outlined in black). 8) *Chondrites* isp. from Turkey Creek at 32.11m. 9) *Schaubcylindrichnus freyi* isp. from Dixon Dam at 10.48m. 10) *Zoophycos*isp. from core D313 at 7909' 6.5" (11.37m) outlined in red. 11) *Skolithos* isp. from core D313 at 7924' 8", (6.78 m) indicated by red arrows. 12) *Teichichnus* isp. from D313 7911' 4" (10.84 m) indicated by red arrows.



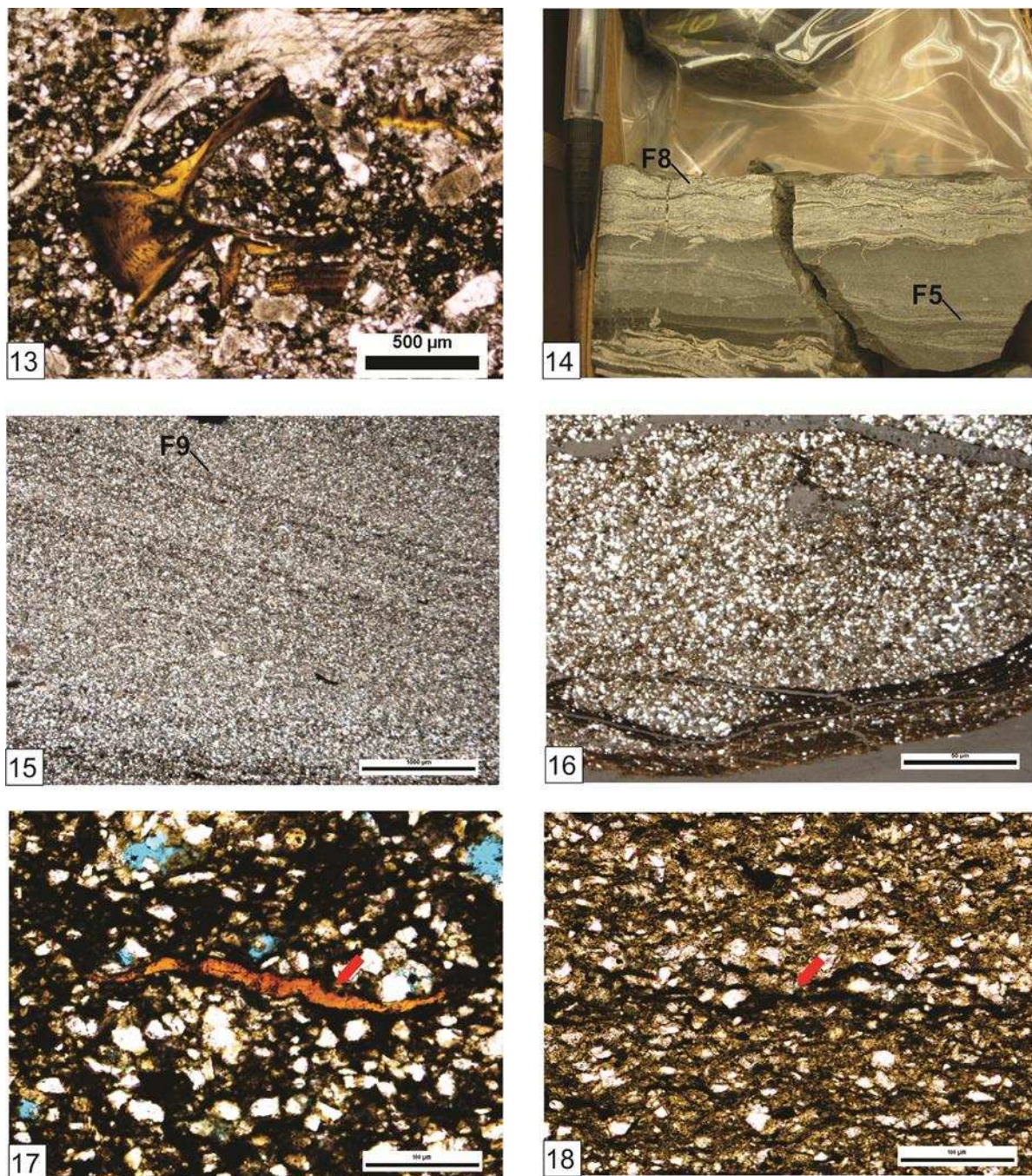


**Figure 5 (continued):** 13) Fish remains and Inoceramid shell debris from a lag deposit (facies 7), from D313 at 7911' 5.5" (10.74m). 14) Lag deposit from D313 at 7946' 4.7" (0.06m) showing contorted beds and shell debris (facies 7). 15) Thin section of the base of a hummock (facies 9) from D313 7932' (4.32m) 16) The bottom of a gutter cast from Dixon Dam at 15.895 m (facies 10). 17) Organic matter (Telalginite, indicated by a red arrow) from TC at 0.062m in massive siltstone (facies 7). 18) Bituminite (indicated by a red arrow) from TC at 14.61m preserved in a ripple-laminated mudstone to siltstone (facies 3 and 4).



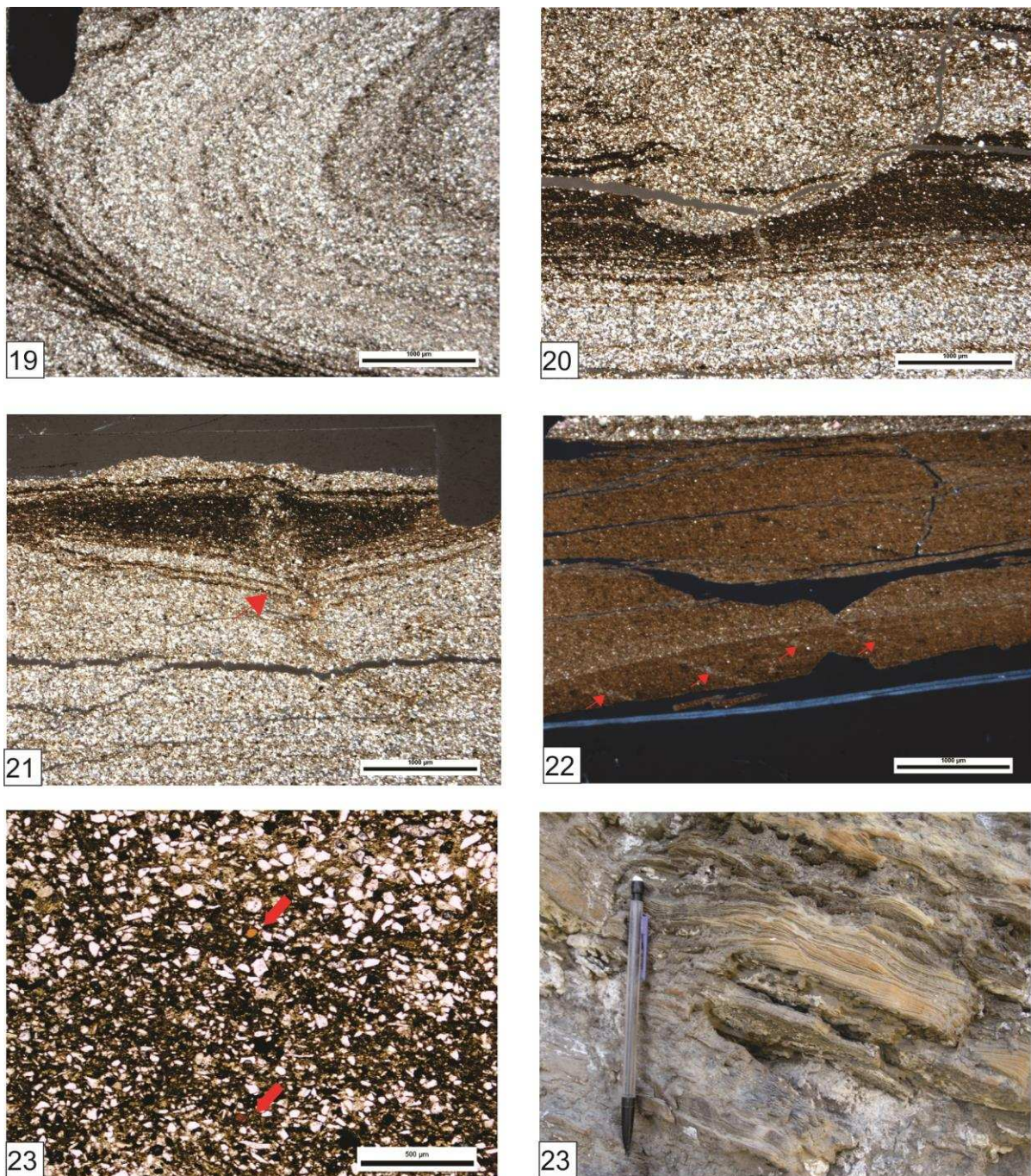


**Figure 5 (continued):** 19) Slump in planar to ripple laminated siltstone (facies 4 and 5). Sample taken from D313 at 7928' 4" (5.61m). 20) A scour eroding into a regular to irregular laminated mudstone (facies 2a and 2b) overlain by a massive siltstone (facies 6). Sample taken from DD 12.83m. 21) A Water escape structure (indicated by a red arrow) in a planar to ripple laminated siltstone (facies 5 and 4). Sample taken from DD at 11.47m. 22) Fractures preserved in a planar laminated mudstone (facies 2a), indicated by red arrows. Sample taken from D313 at 7942' (1.44m). 23) Two Vitrinite clasts (indicated by red arrows) from TC at 0.6m. 23) Rippled vfg sandstone (facies 8) found at TC (17.2m).

### 4.3 Facies Associations

Facies associations were defined by the co-occurrence of different facies in the same stratigraphic interval of the succession. The five facies associations of the Skull Creek are: (FA 1) Massive mudstone and siltstone, (FA 2) Laminated siltstone and mudstone, (FA 3) Ripple- to planar-laminated siltstone and mudstone, (FA 4) Mud-rich sandstone and siltstone, and (FA 5) Bioturbated siltstone to sandstone.

Facies Association	Facies Observed
Massive mudstone and siltstone (FA 1)	<ul style="list-style-type: none"> <li>• Massive mudstone (Facies 1)</li> <li>• Massive siltstone (Facies 6)</li> </ul>
Laminated siltstone and mudstone (FA 2)	<ul style="list-style-type: none"> <li>• Massive mudstone (Facies 1)</li> <li>• Regularly laminated mudstones (Facies 2a)</li> <li>• Irregularly laminated mudstones (Facies 2b)</li> <li>• Mudstones with downlapping laminae (Facies 3)</li> <li>• Fossil bearing siltstone (Facies 7)</li> </ul>
Ripple- to planar-laminated siltstone and mudstone (FA 3)	<ul style="list-style-type: none"> <li>• Massive mudstone (Facies 1)</li> <li>• Regularly laminated mudstones (Facies 2a)</li> <li>• Siltstones with downlapping laminae (Facies 4)</li> <li>• Laminated Siltstones (Facies 5)</li> <li>• Massive siltstone (Facies 6)</li> <li>• Fossil-bearing siltstone (Facies 7)</li> <li>• Fine-grained sandstone to siltstone with draping laminae (Facies 8)</li> <li>• Massive mud-rich sandstone to siltstone (Facies 9)</li> </ul>
Mud-rich sandstone and siltstone (FA 4)	<ul style="list-style-type: none"> <li>• Massive mudstone (Facies 1)</li> <li>• Regularly laminated mudstones (Facies 2a)</li> <li>• Siltstones with downlapping laminae (Facies 4)</li> <li>• Laminated siltstones (Facies 5)</li> <li>• Massive siltstone (Facies 6)</li> <li>• Fossil-bearing siltstone (Facies 7)</li> <li>• Fine-grained sandstone to siltstone with draping laminae (Facies 8)</li> <li>• Fine-grained sandstone to siltstone with HCS (Facies 9)</li> <li>• Massive mud-rich sandstone to siltstone (Facies 10)</li> </ul>

Bioturbated siltstone to sandstone (FA 5)	<ul style="list-style-type: none"> <li>• Bioturbated siltstone (Facies 6)</li> <li>• Massive mud-rich sandstone to siltstone (Facies 10)</li> </ul>
---	---

#### 4.3.1 Facies Association 1 – Massive mudstone and siltstone

FA 1 is composed of mudstone beds with intercalated bioturbated siltstone beds (facies 1 and 6). FA 1 appears massive in outcrop, yet in thin section, it contains mudstone and siltstone laminae that are 5 mm-10 mm thick with bioturbation intensities ranging from 1-5. Massive mudstone beds contain *Planolites* with *Phycosiphon* isp. The *Planolites* burrows are filled with coarser-grained material than the surrounding matrix, usually silt-size quartz grains, while *Phycosiphon* isp. are mud-filled. It is composed of silt-size quartz and carbonate grains (45%-25%), clay matrix (55%-75%), and contains minimal phosphate (~1%) and pyrite (~5%). Beds with high bioturbation intensities (BI=5) have the lowest TOC values of the facies associations (0.31- 0.40 wt. %). Organic matter types include vitrinite and some bituminite.

#### 4.3.2 Facies Association 2- Laminated siltstone and mudstone

FA 2 consists of massive to laminated mudstones (facies 1, 2a and 2b) that alternate with fossil-bearing siltstones (facies 7) and mudstones with downlapping laminae (facies 3). Regular- to irregularly-laminated mudstone beds (facies 2a and 2b) occur frequently within FA 2 and contain siltstone laminae (<1 mm thick). Occurring less frequently are mudstone beds that contain downlapping laminae (< 0.5 mm thick). Fossil-bearing siltstone beds are irregular in thickness (4 cm-0.4 cm thick). Bioturbation in FA 2 is minimal (BI= 0-2) with *Planolites* and *Phycosiphon* isp. traces. FA 2 is composed of silt-size carbonate and quartz grains (30-10%), clay (40-80%), pyrite (1-

5%), and organic matter (1-20%). TOC values are high within FA 2, ranging from 0.7 to 3.86 wt. % TOC. Organic matter types include vitrinite, telalginite, and bituminite.

#### **4.3.3 Facies Association 3 – Ripple to planar laminated siltstone**

FA 3 is composed of 1.5 m-0.02 m thick beds, alternating between planar-laminated siltstones and mudstones (facies 2a and 5), and siltstones containing downlapping laminae (facies 4). Within FA 3, there are some bioturbated siltstone beds (<2 cm thick) containing rip-up clasts (facies 6) with rippled siltstones (facies 8). Bioturbated beds contain *Cruziana* ichnofacies (specifically *Planolites* and *Chondrites*) ranging from a few traces (BI=1) to a thorough reworking of sediment (BI=5). Water-escape structures, slumps, and scour structures occur frequently at the bases of both mudstone and siltstone layers. FA 3 is composed of quartz and carbonate silt grains (60%-90%), clay (40%-10%), and pyrite (0-5%). TOC has a very large range of values, from 0.06 to 2.49 wt. %. The dominant organic matter type is vitrinite.

#### **4.3.4 Facies Association 4 – Mud-rich sandstone and siltstone**

Facies Association 4 is the coarsest-grained FA in the Skull Creek Fm. It is composed of HCS to combined-flow rippled sandstone and siltstone beds (facies 8 and facies 9) alternating with planar-laminated siltstones and mudstones (facies 2a and 5) and siltstones with downlapping laminae (facies 4). Siltstone and mudstone beds are normally and inversely graded. These beds can be capped by thin (<2cm) bioturbated siltstone beds (facies 6). Massive sandstones and siltstones (facies 10) can also contain rare traces of *Arencolites* (e.g. in the Dixon Dam outcrop). Shell debris is concentrated at the base of individual hummocks to form thin beds (0.5mm-0.1mm thick) (facies 7).

Very thin, massive mud layers (2cm-10cm) (facies 1) are interbedded, or overlie, HCS sandstones (facies 9) as mud drapes. Sampling from these mud-rich beds indicate overall low TOC values (0.11-1.37 wt. %). The dominant organic matter type is vitrinite.

#### **4.3.5 Facies Association 5 – Bioturbated siltstone and sandstone**

FA 5 is composed of massive, bioturbated siltstone beds (facies 6), which have very few remnants of bedding and contain rip-up clasts, and are interbedded with massive sandstone beds (facies 10). Siltstones within FA 5 are heavily bioturbated (BI=5-6) or have intermediate bioturbation (BI=3-4). The bioturbated siltstones contain the most diverse assemblage of ichnofossils within the Skull Creek Fm., including *Skolithos*, *Planolites*, *Chondrites*, *Teichichnus*, *Schaubcylichnus*, *Asterosoma*, and rare *Arencolites*, and *Zoophycos* traces. The most common trace fossils within this succession are *Planolites* and mud-filled *Chondrites*. TOC is very low within this facies association, with values ranging from 0-0.4 wt. %. Organic matter types include telalginite and AOM.



## 5.0 FACIES ARCHITECTURE

The Skull Creek Fm. is between 11 m and 35 m thick in the outcrops and cores studied in northern Colorado. However, its thickness changes do not display a clear thickening or thinning trend in any direction, but rather fluctuate between 11 m and 35 m along the N-S transect. Towards the east the formation seems to slightly increase in thickness, yet it remains unclear whether this reflects a general trend within the basin, or is just coincidental between the Turkey Creek section and Conoco Well A. In this study, the Skull Creek Fm. is subdivided into five stratigraphic intervals, here successively numbered “interval 1-5” from the base of the unit to the top (Figs. 6 and 7).

The succession consists of three intervals that are composed of mainly fining-upwards parasequences and two intervals with coarsening-upwards parasequences. The intervals composed of fining-upwards parasequences are between 0.5m-9m thick and comprise intervals 1, 2, and 5. Intervals 3 and 4 show distinct coarsening-upwards trends throughout all measured sections and are 4m-24m in thickness. Fining-upwards parasequences consist of basal laminated, wave-rippled, or bioturbated siltstones and sandstones (FA 3, FA 4, and FA 5) with massive to laminated mudstones at the top (FA 1 and 2). The opposite is true for coarsening-upwards parasequences. Parasequences range in thickness from 0.5m-4m and the only vertical trends within the succession are seen within intervals 3 and 4, where parasequences thicken upwards in both intervals. Sand content also increases upwards within interval 4. Laterally, there are no obvious trends in the number and thickness of parasequences. Contacts of parasequences are sharp and easily recognizable in each of the intervals. The bioturbated siltstone beds

(FA 5) of interval 1 are sharply overlain by the laminated or massive mudstones and siltstones (FA 1, FA 2 and FA 3) of interval 2. The top of interval 2 is picked at high TOC values, concretionary horizons, and where laminated siltstones (FA 3) become more prevalent (stratigraphic sections with TOC are found in Appendix 1). There is a sharp contact that separates the laminated to wave-rippled siltstones and sandstones (FA 3 and FA 4) of interval 3 and bioturbated siltstones and sandstones (FA 5) of interval 4. The laminated to massive mudstones and laminated siltstones (FA 1, FA 2, and FA 3) of interval 5 abruptly overlie the bioturbated siltstones and sandstones (FA 5) of interval 4.

Lag deposits only occur in intervals 2 and 3. The thickness of the lag deposits decreases up-section, and they are completely absent in the upper parts of interval 3. Bioturbation is generally restricted to the traces of *Chondrites*, *Planolites*, and *Phycosiphon*. However, in the middle to upper parts of interval 3 traces become more abundant in bioturbated siltstone to sandstone beds (FA 5) and comprise ichnospecies *Skolithos*, *Schaubcylindrichnus*, *Teichichnus*, *Asterosoma*, *Zoophycos* and *Arenocolites*. Bioturbation intensity reaches a maximum within interval 4 (BI= 3-6) where *Planolites* and *Chondrites* traces dominate, with minimal *Teichichnus*, *Schaubcylindrichnus*, *Skolithos*, *Arenocolites*, *Zoophycos*, *Asterosoma*, *Ophiomorpha*, *Thalassinoids* and *Cylindrichnus*. *Cruziana* ichnofacies is found throughout interval 4 with some traces of *Zoophycos* ichnofacies<sup>1</sup> in the lower to upper parts and *Skolithos* ichnofacies<sup>2</sup> in the middle parts. Within interval 5 bioturbation intensity shows a

---

<sup>1</sup> At 8519.2'-8521' (26.8m-26.3m), 8530.7'-8532' (23.1m-23.8m), and 8539.4'-8541.9' (20.1m-21.16m) in Well A

<sup>2</sup> At 8543.2'-8544.9' (19.7m-19.2m) and 8527'-8527.8' (24.4m-24.6m) in Well A

decrease up-section, and is minimal (BI=1-0) within the upper parts of interval 5. Traces are mostly *Cruziana* and *Zoophycos* ichnofacies with some *Cylindrichnus* and *Schaubcylindrichnus* concentrated in the siltstone beds.

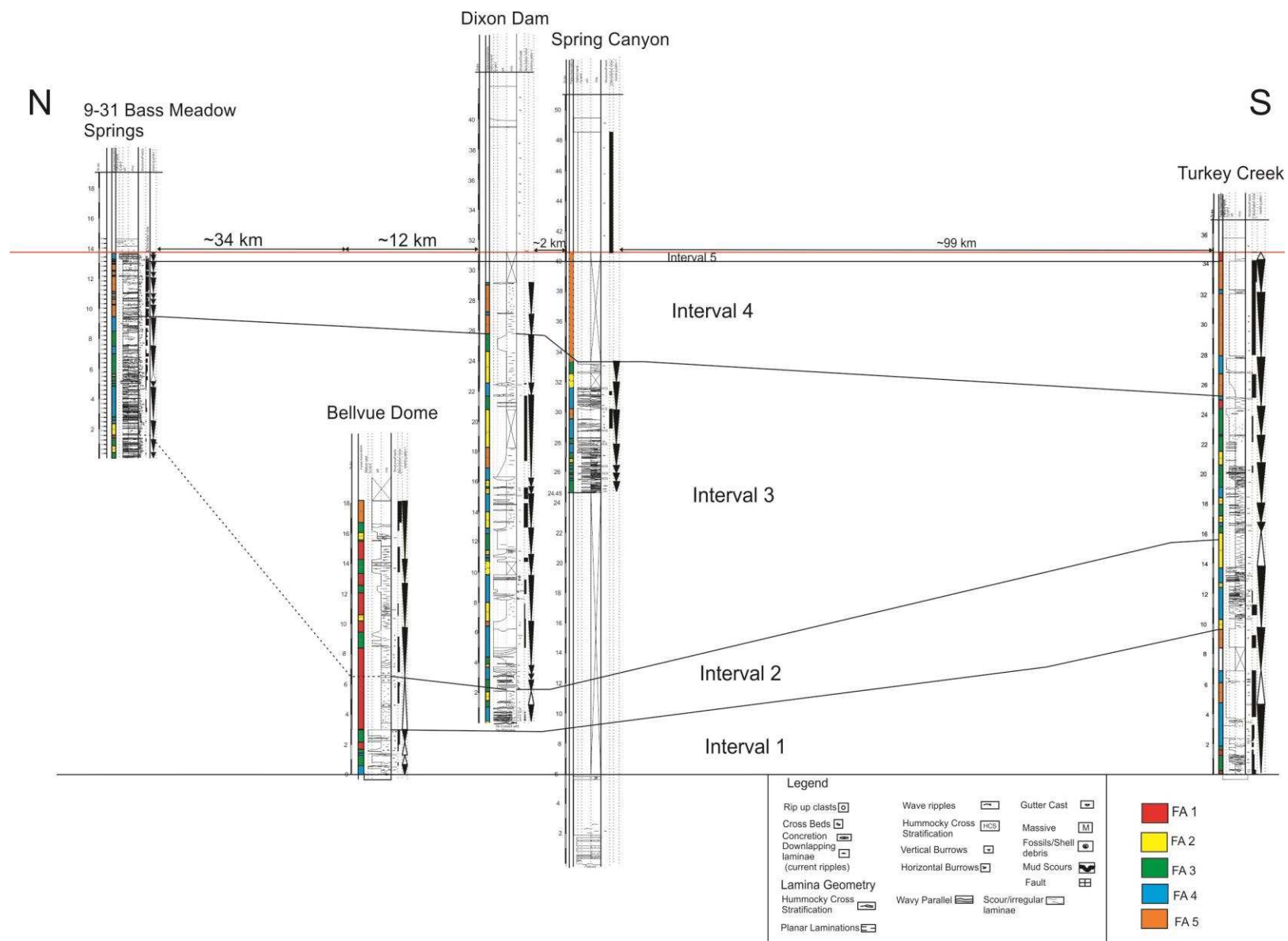


**Figure 6:** N-S transect of the Skull Creek Fm.

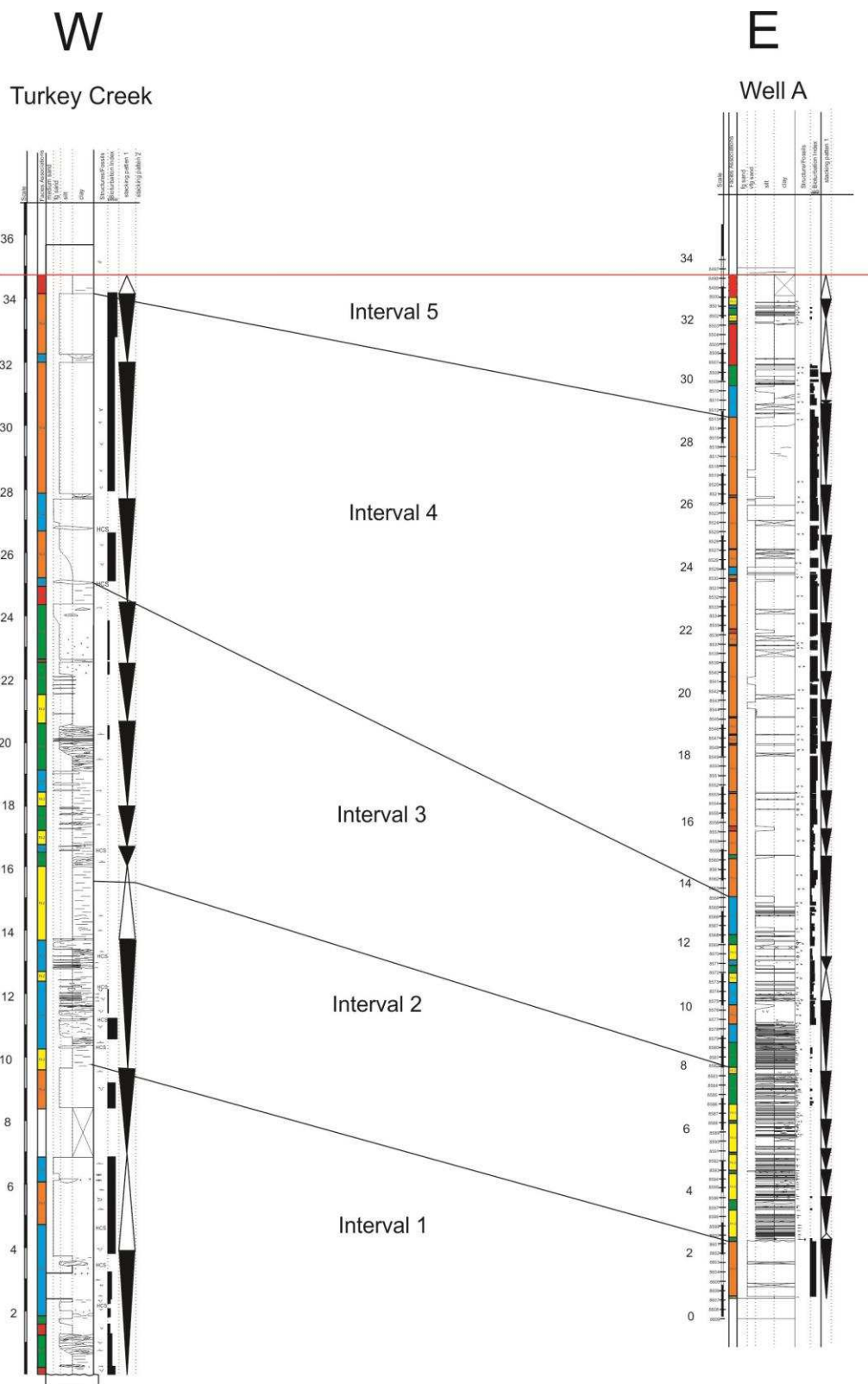


**Figure 7:** E-W transect for the Skull Creek Fm. Legend shown above.

## 6.0 INTERPRETATION

### 6.1 Depositional model

The Skull Creek Fm. represents a proximal-distal transect of a deltaic mudstone succession that was transported mainly as bed-load within hyperpycnal flows, with minimal deposition that occurred as a result of suspension settling. It is subdivided into five facies belts, which are equivalent to the five facies associations. Each facies association is characteristic of a distinct suite of sedimentary processes that vary between proximal and distal areas (Figs.8, 9 and 10). Sediment deposited in proximal areas along the continental shelf was transported by a combination of waves and currents to form HCS and combined flow ripples. More distal facies associations contain current ripples, planar laminations, and show no evidence of wave reworking, since most fine-grained sediments were deposited below storm wave base (Fig. 8). On top of laminated to wave-rippled beds, there can be bioturbated siltstone to mudstone beds that illustrate a break in sedimentation as a hyperpycnal flow wanes, and some fine-grained sediment will be deposited as a result of suspension during fairweather conditions.

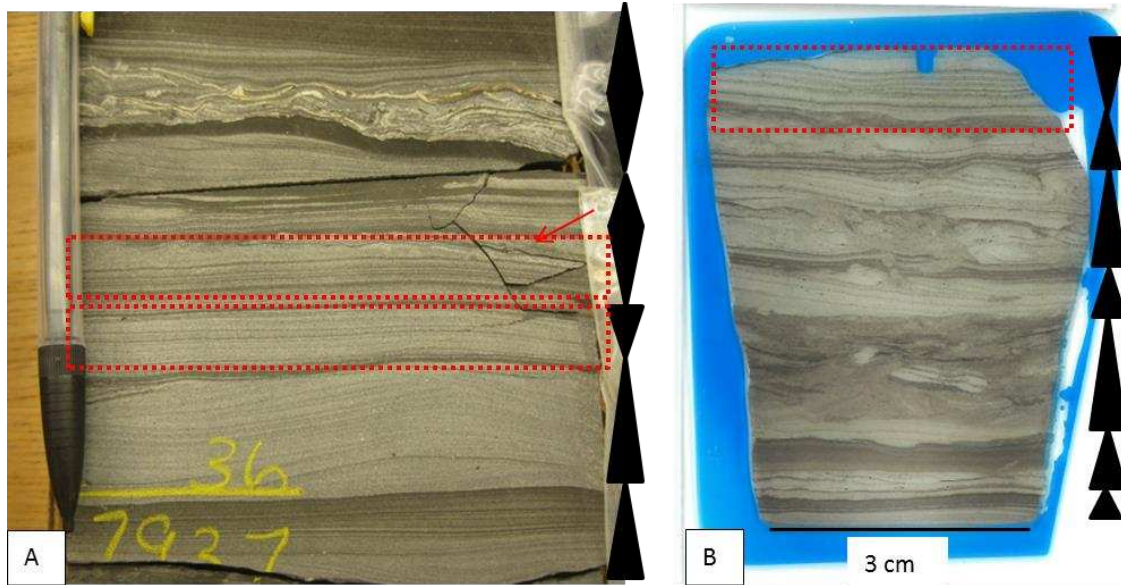


**Figure 8:** Core photo and thin section from FA 4 (left) and FA 3 (right) **(A)** The photo shows a basal wave-to combined flow rippled siltstone overlain by current and planar laminated beds. Inverse grading is shown by the upside-down triangles on the right and highlighted by the dashed red rectangles. The siltstone bed is slightly bioturbated at the top (red arrow). From 9-31 BMS core at 7936.9' **(B)** Normal to inversely graded siltstone with alternating current and planar laminated beds and bioturbated beds. From TC outcrop at 20.66 m.

The most proximal units are the bioturbated siltstones to sandstones of FA 5, which are found predominantly within interval 4. They are characteristic for an oxic, proximal environment since these sediments are heavily bioturbated and are composed of mainly coarse-grained sediments. Fine-grained sediments within FA 4 are preserved as mud filling in burrows or as faint mud laminae. The depositional environment can also be inferred from the ichnofossil suites present in these sediments that are divided into three different ichnofacies, *Skolithos*, *Zoophycos*, and *Cruziana*, which are characteristic for varying positions of the continental shelf. *Skolithos* is usually found along the upper to middle shoreface, *Cruziana* in a variety of environments, from the lower shoreface to the lower offshore, and *Zoophycos* is found in open marine environments (MacEachern et al. 2005). Most of the traces within FA 5 belong to the distal *Cruziana* ichnofacies, indicative of a lower offshore zone. Given the dominance of

*Cruziana* ichnofacies, along with the appearance of *Skolithos* and *Zoophycos* ichnofacies, FA 5 is envisioned to have been deposited in an overall oxic and proximal environment fluctuating from the middle shoreface to the lower offshore, which is supported by the coarse-grain size within FA 5 (MacEachern et al. 1999b).

FA 4 is composed of mainly wave-reworked siltstones and sandstones overlain by current-rippled to laminated siltstones and mudstones, with overlying bioturbated siltstone to mudstone beds. It is here interpreted that FA 4 sediments were deposited basinward, but adjacent to FA 5. Bioturbation diversity decreases from FA 5 to FA 4 and contains mostly *Cruziana* ichnofacies, specifically traces of *Planolites*, suggesting a stressed environment (Bann and Fielding, 2004). During high energy events, most likely induced by storms, sandstones and siltstones were transported offshore by both currents and wave action and are reworked above storm-wave base to form combined flow structures such as HCS sandstones and siltstones (Fig. 10.C.2) (Aigner and Reineck 1982; Duke et al. 1991; Mutti et al. 2003). Once the storm waves subsided, sediment was transported mainly by currents to produce structures like current-rippled to laminated siltstones and mudstones. Intercalated with current-rippled siltstones are siltstone beds that are slightly bioturbated, indicating a break in sedimentation between the high-energy event during fairweather conditions (Bann and Fielding, 2004).

The laminated to rippled siltstones of FA 3 are interpreted to represent a depositional environment that is located basinward of FA 4. Wave-rippled siltstones serve as indications of slight wave-reworking within FA 3; however, most of the prominent structures within FA 3 include cross-bedded to planar-laminated siltstones and mudstones. This suggests that while there must have been episodes of wave-



reworking, most of the sediment was transported as bed load by currents, and it was most likely deposited at times above and at times below storm-wave base as indicated by the partial presence or absence of wave- formed structures. Bioturbated siltstone beds overlie wave- or current-rippled siltstones and mudstones (similar to FA 4) and most likely represent fairweather conditions. Lag deposits are also common within FA 3 and represent the coarsest fraction of the material deposited in this setting that was concentrated into lags during events or from currents (Plint et al. 2012).

FA 2 is one of the most fine-grained units within the Skull Creek Fm. and is composed mainly of mudstone with thin, normally-graded planar and current-rippled siltstone beds interbedded with slightly bioturbated mudstones. The prevalence of planar-laminated to current-rippled beds suggests that sediments were transported in a fully turbulent to transitional flow (see facies 2a and facies 3 description) while bioturbated beds indicate fairweather conditions (Baas and Best 2002). These flows were introduced to the distal basin by high-energy events, which transported silt- and clay-size sediments offshore in relatively quiet-water conditions (indicated by bioturbated beds). FA 2 is located distally to FA 3 and was likely deposited below storm-wave base as bed-load because it lacks any evidence of wave reworking, and shows mainly current-generated structures.

FA 1 is composed of heavily bioturbated mudstones (BI=1-4) with silt-size grains that fill in burrows or are preserved as faint silt laminae. Rare remnant cross-bedding within FA 1 suggests that this unit was transported and deposited as bed-load from currents in a distal area of the basin, probably below storm wave-base since it lacks any wave generated structures. High levels of bioturbation indicate deposition in a sediment

starved zone where low levels of sediment input allow ample time for organisms to completely rework beds (Taylor and Gawthorpe 1993). This indicates that FA 1 was either deposited laterally or distally from FA 2, where sediment input was much less frequent, in overall quiet water conditions.

## **6.2 Sequence Stratigraphy**

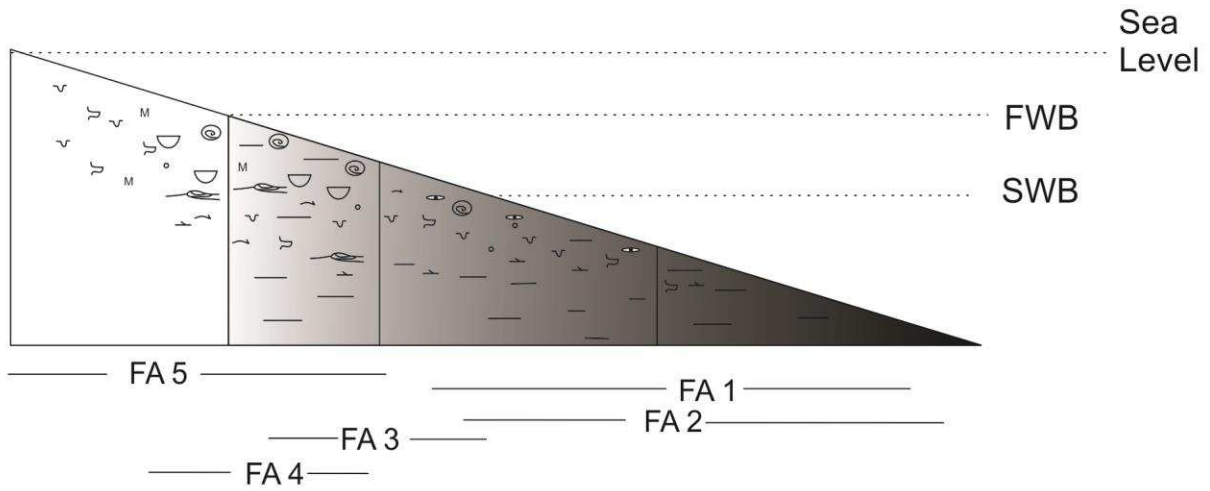
Once each interval was described and proximal versus distal facies belts were identified, the depositional environment for each interval was defined relating to either a rise or fall in energy conditions, which are linked to sea level fluctuations within the basin. Past studies have interpreted the Skull Creek as having a lower transgressive system tract (TST) and an upper highstand systems tract (HST) separated by a condensed section (Edwards 1999; Sutton et al. 2004). Based on new data from Well A where the upper part of the Skull Creek is well preserved, and the revised depositional model, the Skull Creek Fm. was divided into five different intervals instead of three. Each of these intervals is bounded by erosional or non-depositional surfaces that reflect the onset of changing environments.

Interval 1 is composed of mainly HCS to massive sandstones and siltstones (FA 4 and FA 5), which are interpreted to represent the most proximal facies associations within the Skull Creek Fm. The sand and silt content decreases upwards within this interval, which is caused by a decrease in energy, or a deepening of sea level, and is interpreted to be a transgression, or an early transgressive systems tract (TST). At the top of interval 1, a sharp contact separates the basal sandstone and siltstone beds (FA 5 and FA 4) and overlying fine-grained units (FA 2) of interval 2. This erosional contact

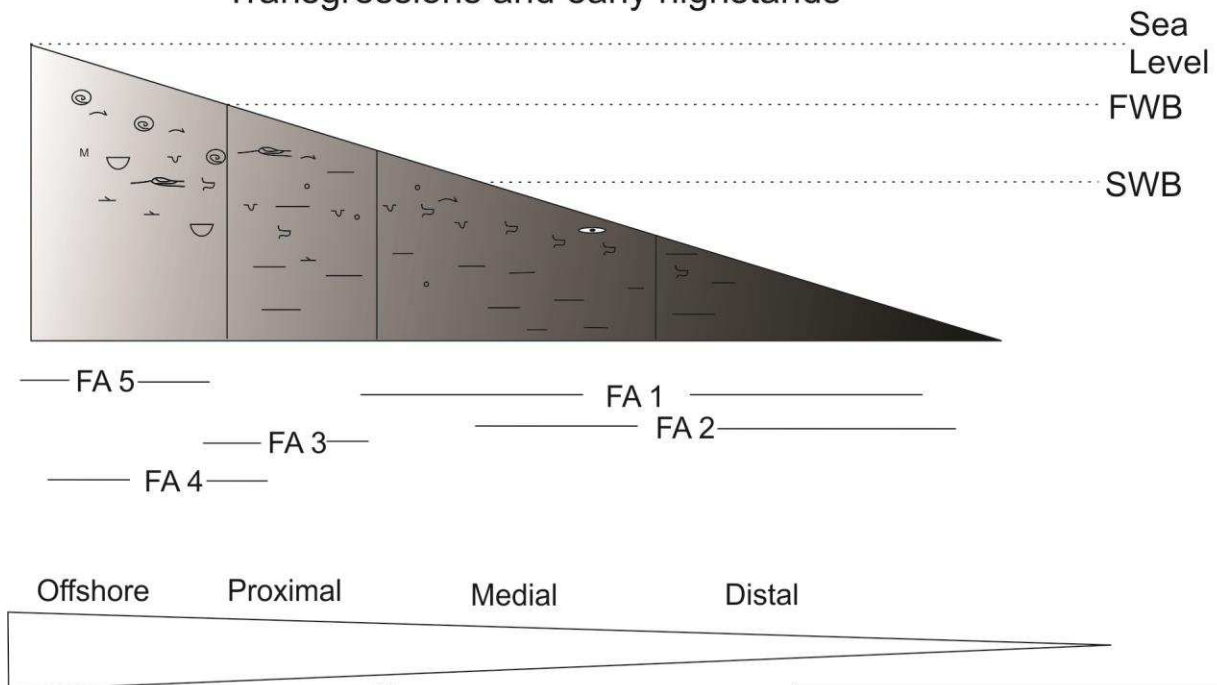
represents a decrease in accommodation space, possibly due to a short regression during an overriding high frequency cycle (Catuneanu et al. 2009). In relation to the siltstones and sandstones of interval 1, the overlying fine-grained sediments and fining-upward parasequences of interval 2 represent a decrease in energy within the basin due to sea level deepening, or a late TST (Bohacs et al. 2002). As sea level continued to rise, indicated by a decrease in silt content upwards, sediment accumulation decreased as accommodation space reached a maximum to form the MFS. The MFS is represented by the highest TOC values and along one distinct concretionary horizon, with the high TOC values formed due to sediment starvation and a greater intensity of localized, diagenetic reactions (Taylor and Macquaker 2000). The highest TOC values are associated with a MFS because sediment accumulation is low, and organic matter has a higher likelihood of being preserved in more sediment-starved environments (Creaney and Passey 1993). Interval 3 is composed of coarsening-upwards parasequences that thicken vertically. This indicates an overall decrease in accommodation space combined with a successively more proximal setting and higher sediment input, here interpreted to represent a highstand systems tract (HST). The erosional surface separating intervals 3 and 4 reflects a transition from a slightly stressed, offshore environment (interval 3) to a proximal, oxic environment (interval 4) with a shift from the wave-reworked sandstones and siltstones of interval 3 to bioturbated sandstones and siltstones of interval 4. Therefore, this erosional surface is interpreted to represent the sequence boundary (SB). Interval 4 is composed of proximal, bioturbated siltstones at the base and massive sandstone beds that become more common towards the top of the interval. The increase in grain size upwards within

interval 4 indicates an overall change to a more energetic environment due to a sea-level fall. Based on these observations, and since interval 4 is located directly above a SB, it is interpreted to be a LST. Between intervals 4 and 5, there is a gradual to sharp contact separating the coarsening-upwards units of interval 4 and fining-upwards sediments of interval 5. The contact is more gradual at the center of the basin, and is sharp along the edge of the basin. This unconformity is interpreted to represent a transgressive surface (TS) because it symbolizes the first stages of an increase in sea level, which results in minor erosion due to increased wave and storm activity in proximal areas, and a fining-upward trend in the deeper basin (Coe et al. 2002). Interval 5 shows a decrease in bioturbation intensity/diversity and grain-size from interval 4. The decrease in bioturbation intensity and switch to a more distal expression of *Cruziana* ichnofacies suggests that the environment is transitioning to a more open-marine environment, due to a rise in sea-level, while the fine grain size is interpreted to represent lessening energy conditions within the basin (Bann and Fielding 2004). Interval 5 is therefore interpreted to represent a transgression of the shoreline (TST). The HST is not preserved in the upper Skull Creek Fm. and may have been eroded during the formation of the Muddy (J) sandstones (Weimer 1996).

## Regressions late highstands and lowstands



## Transgressions and early highstands



Very Fine-Grained Sandstone

Silt

Clay

Grain Size

Legend		
Rip up clasts	Wave ripples	Gutter Cast
Cross Beds	Hummocky Cross Stratification	Massive
Concretion	Vertical Burrows	Fossils/Shell debris
Downlapping laminae (current ripples)	Horizontal Burrows	Mud Scours
<b>Lamina Geometry</b>		
Hummocky Cross Stratification	Wavy Parallel	Scour/irregular laminae
Planar Laminations		Fault

**Figure 9** Depositional model showing distribution of facies associations and their features.

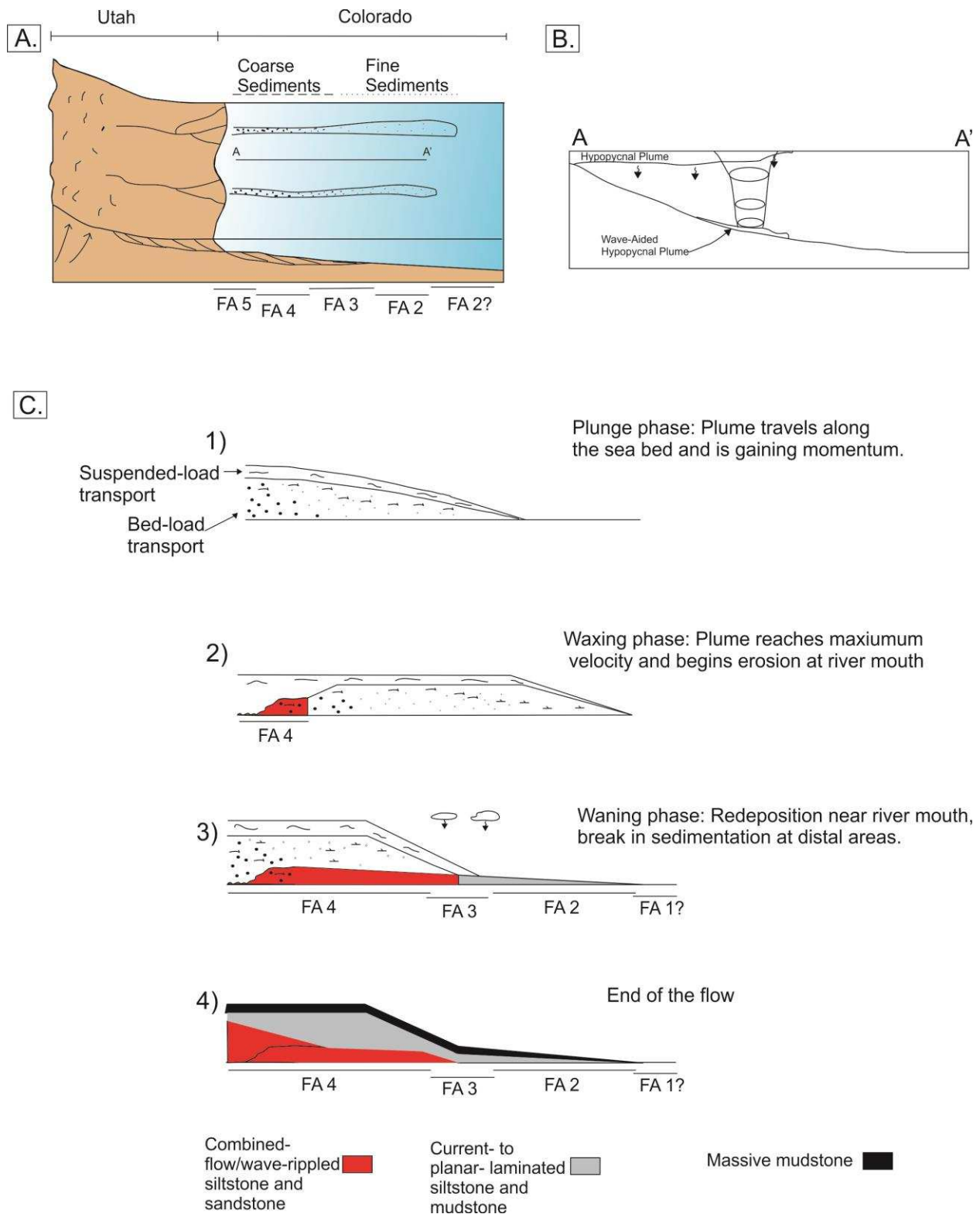


**Figure 10 (A)** This model illustrates the depositional environment of the Skull Creek Fm. Central Utah is experiencing regional uplift and crustal shortening and sediments are fed into the Cretaceous Interior Seaway by estuaries or along a prodelta. Modified from Wilson and Schieber (2014). **(B)** During major flooding events, a hyperpycnal plume is generated along the sea bottom and is transported with the help

of wave energy. Modified from Bhattacharya and MacEachern (2009). **(C)** Conceptual model showing the evolution of distal and proximal facies over time. At time 4, the colored blocks represent deposits in proximal and distal regions. As the flow becomes more dilute it will deposit current to planar laminated siltstones and mudstones. Modified from Mulder and Alexander 2001.

## 7.0 DISCUSSION

### 7.1 Transport mechanism of fine-grained sediments

In this study, the Skull Creek Fm. is interpreted to represent distal to proximal expressions of hyperpycnal flows (FA 1, FA 2, FA 3, and FA 4) and prodelta deposits (FA 5) as the shoreline first retrograded, and successively prograded. Sediments of fine-grained FAs (FA 1 and FA 2) are here envisioned to be mainly transported as bed-load in a turbulent flow. However, recent studies of modern mud-dominated continental shelves (e.g. Eel River delta) show that there is a possibility of transporting fine-grained sediments as fluid mud, due to the oscillatory wave motion during storm events (Traykovski et al. 2000). If sediments are transported as bed load, there should be at least some evidence of erosion of unconsolidated mud, as seen in other storm-generated density flows, as in the Cretaceous Kaskapau Fm. (Plint et al. 2012), or sedimentary structures indicative of bed load transport such as mudstone ripples (Schieber et al. 2007). Fluid mud layers, in contrast, look similar to the upper portion of wave enhanced sediment gravity flows (WESGFs), and can develop from turbulent flows as mud content increases and the flow becomes more laminar (Macquaker et al. 2010).

In order for hyperpycnal flows to be gravity-driven, slope gradients need to exceed  $0.7^{\circ}$ , and additional wave energy is needed to transport hyperpycnal flows along low-gradient slopes ( $<0.3^{\circ}$ ; Friedrichs et al. 2000; Wright and Friedrichs 2006). Wave-aided density flows can generate similar structures to wave-generated hyperpycnites,



such as lag deposits, wave and combined-flow-ripples, graded beds, and were described from the Kaskapau Formation (Plint et al. 2012). These fine-grained sediments originated as unconsolidated mud that was remobilized by storms and transported as bed-load, whereas sediments within the Skull Creek Fm. are interpreted to have been transported as bed load from river discharge events. The main argument for the remobilization of mud in the Kaskapau Fm. is the presence of intraclastic aggregates which are mixtures of clay, coccoliths, pyrite and organic carbon. These aggregates are a major distinguishing feature of wave-aided density flows, as intraclastic aggregates have not been identified within wave-aided hyperpycnites. Amorphous organic matter within the Skull Creek Fm. looks superficially similar to the Kaskapau intraclasts, but SEM examination indicates that Skull Creek organic matter does not exhibit the aggregate texture observed in the Kaskapau Fm. (Appendix 3). This would suggest that mud was not remobilized from proximal areas due to storm events, but was transported as bed load due to flooding events, possibly as fluid mud.

Within wave-aided hyperpycnal flows there are two subdivisions of the flow: an upper cohesive layer, or fluid mud layer, that is suspended by oscillatory motion of waves, and a turbulent basal layer where sediment is transported as bed load and contains both silt and mud grains (Traykovski et al 2000; Wilson and Schieber 2014). Similar structures may be produced by Wave Enhanced Sediment Gravity Flows (WESGFs), which show a tri-partite subdivision of facies that represent turbulent, transitional, and laminar flows (Maquaker et al., 2010). Within the Skull Creek Fm. the succession of these three different facies is rare but present, suggesting that similar conditions conducive to forming WESGFs persisted at least some of the time during

Skull Creek Fm. deposition. Within the distal laminated mudstones (FA 2), there are some thin (<1mm) normally graded siltstone laminae containing faint low-angle crossbeds that look similar to basal siltstone beds interpreted by Mulder and Alexander (2001) and Mulder et al. (2003) as turbulent flows with a high traction component. The irregularly-laminated mudstone beds that overlie some Skull Creek Fm. siltstones could represent mixing of lower coarse-grained sediments transported in a turbulent flow and fine-grained sediments that were held in suspension as fluid mud (Macquaker et al. 2010). The alternation between cross-bedded siltstone laminae and massive to irregularly-laminated mudstones within FA 2 suggests that these sediments could have been transported by hyperpycnal flows during intense flooding events when sediment on the continental shelf is remobilized as fluid mud and wave energy is high (Kinke et al. 1995; Friedrichs et al. 2000). However, the succession of these three different beds (basal siltstone beds, irregularly-laminated mudstones, and massive mudstone beds) does not necessarily have to be the product of WESGFs, and can be produced by the natural progression of hyperpycnal flows as they become more dilute of silt and sand particles (Baas and Best 2002). Flows with high clay concentrations can produce laminated mudstones that are overlain by massive mudstones due to the sediment interactions between the upper cohesive layer within a hyperpycnal flow and the lower turbulent layer. The succession of these different beds is commonly seen within FA 2 and it is more likely that massive and laminated mudstones are attributed to the natural evolution of a hyperpycnal flow and do not represent a succession formed by WESGFs.

Massive mudstones and siltstones of FA 1 contain abundant floating sand grains which could be an important indication of transport as fluid mud in these otherwise

heavily bioturbated mudstone units. Baas and Best (2011) found that similar “floating” clasts within massive mudstones were deposited from laminar flows that contained high sediment concentrations. These laminar flows are most common during high-discharge floods, when suspended sediment concentration will be the highest (Friedrichs and Scully 2007; Kinke et al. 1995). In contrast, the floating grains also could have originally formed siltstone laminae that were subsequently destroyed by bioturbation, which would support the interpretation that these sediments were transported as bed load in a turbulent flow. It is difficult to ascertain the depositional mechanism of the FA 1 mudstones because they are generally heavily bioturbated and most sedimentary structures have been destroyed. However, based on the presence of some crossbedding, FA 1 is speculated to have been deposited at least partially by turbulent flows.

## 7.2 Ichnofacies

Within FA 5, there are three major ichnofacies present, *Cruziana*, *Skolithos*, and *Zoophycos*, which co-occur through intervals 4 and 5. The identification and interpretation of different ichnofacies within this heavily bioturbated interval is very important to distinguish any fluctuations in sea level, since there are very few sedimentary structures that were preserved to help interpret the depositional environment. Beds that contain *Skolithos* co-occur with minimal *Planolites*, *Arenocolites* and *Schaubcylindrichnus*, but overall the beds are diminutive in other traces. The co-occurrence of *Skolithos* and *Cruziana* ichnofacies can indicate stressed environments, while *Cruziana* and *Zoophycos* indicate more normal marine conditions (Bhattacharya and MacEachern 2009; MacEachern and Gingras 2007). Because of the monospecific

trace fossil assemblage in the siltstone beds containing *Skolithos*, it is assumed that the hyperpycnal flows depositing these siltstone beds also brought in brackish water from the delta and therefore temporarily may have lowered salinity (MacEachern and Gingras 2007). The change in ichnofossil content within individual beds is therefore taken as a reflection of salinity changes from slightly brackish to fully marine, the latter indicated by *Zoophycos*, which is formed by environmentally sensitive organisms that do not thrive in brackish-water environments (MacEachern et al. 1999).

Beds containing *Skolithos*, *Zoophycos* and *Cruziana* ichnofacies regularly alternate in interval 4, with *Skolithos* and *Cruziana* being most prevalent in the middle part of interval 4. *Zoophycos* and *Cruziana* are found in the middle to upper part of interval 4 and the lower part of interval 5. A major shift in lithology and ichnofacies is noted at the beginning of interval 5, where beds transition from bioturbated siltstones and sandstones (FA 5) of interval 4 to laminated mudstones and siltstones (FA 2 and FA 3) in interval 5. Bioturbation intensity decreases upward within interval 5, and contains mainly *Zoophycos* and *Cruziana* ichnofacies. This change in trace fossil assemblages in the upper part of the Skull Creek Fm. therefore shows a change in depositional environments from proximal offshore to a distal offshore, more open-marine environment. This trend, best seen within the cores (9-31 BMS and Well A), indicates that relative sea-level must have been rising at the end of Skull Creek Fm. deposition. The lithology change from FA 5 siltstones of interval 4 to FA 3, FA 2, and FA 1 mudstones and siltstones of interval 5 is only reflected in Well A, Turkey Creek, and 9-31 BMS and are interpreted to reflect a rise in sea level. This interpretation is supported

by the ichnofossil assemblages that reflect the deepening sea level within the massive siltstones of FA 5, even though this interval is not exposed at all locations.

### **7.3 TOC Content**

Interval 2 at the Turkey Creek outcrop contains the highest TOC values (up to 3.84 wt.%) within the entire Skull Creek Fm. There are two possible explanations for these high TOC values: 1) the Turkey Creek outcrop is located close to the source of the hyperpycnal flows or 2) bioturbation intensity is much lower at Turkey Creek, so the preservation of organic matter is higher because of less burrowing activity.

In hyperpycnal flow deposits, high TOC values can reflect either a proximity to land, as most organic matter is derived from the terrestrial realm, or organic matter can be eroded from the sea bottom in proximal areas. Erosion is more common in relatively shallow rather than deep water on the shelf and is better preserved within fine-grained sediments (Bhattacharya and MacEachern 2009). The exact location of organic matter for the source of the Skull Creek Fm. is unknown, especially in Central Colorado, since the shoreline of the Skull Creek Seaway is not well constrained. However, possible paleodrainages of the Skull Creek Fm. can be estimated from the paleodrainages of the overlying Muddy (J) sandstones that were outlined by Weimer (1990, 1996). The paleodrainages of the Muddy (J) sandstones point to the SE of a paleohigh located near the Turkey Creek outcrop, suggesting that the sediment source for the Skull Creek Fm. was also close to the Turkey Creek outcrop. Therefore, sediments transported and deposited near the Turkey Creek outcrop are more likely to have higher concentrations of organic matter because they were not transported as far from the source compared

to other outcrop localities. The fine-grained sediments of interval 2 are especially prone to contain high TOC values since at proximal areas high sediment concentrations may dilute TOC values, leading to low TOC values within coarse-grained sediments (FA 4 and FA 5), while fine-grained sediments are deposited in more quiet water environments where the likelihood of preserving organic matter increases (Bohacs et al. 2005; Creaney and Passey 1993).

Favorable conditions for preserving organic matter are best met when sea level has reached its maximum height, around the MFS, which is where the highest TOC values are detected in the Turkey Creek section. Within the fine-grained sediments of the Skull Creek Fm., bioturbation intensities range in values from 2-0, and contain exclusively *Planolites* and *Phycosiphon* traces. At the Turkey Creek outcrop, the laminated mudstones (FA 2) at the MFS are not bioturbated any more intensely than similar samples taken from other outcrops. Therefore, if sediments were deposited in close proximity to the source, and in distal locations along the continental shelf, organic matter is more likely to be preserved and TOC values will be high.

#### **7.4 Gutter Casts**

At the Dixon Dam outcrop, gutter casts occur that are lined with massive mudstone (facies 1) at the base and filled with massive sandstone (facies 10). Gutter casts have been described by other authors as having a basal scour, come in a variety of irregular shapes, and can contain wave ripples, suggesting transport within an oscillatory flow (Aigner 1985; Myrow 1992). These structures are usually formed when a strong current erodes the sea bottom and storm sands carried from proximal areas fill in

these depressions. However, the presence of a basal shale layer has not been described in literature and suggests that the gutter casts within the Skull Creek Fm. formed in a different way.

Gutter casts in the Skull Creek Fm. originated when a strong current directed offshore scoured the sea bottom to create a depression (c.f. Aigner 1985). After the initial scour took place, there must have been a break in deposition during which mud was deposited, most likely by suspension, which is shown by the thin mud layer containing *Planolites* traces. The presence of *Planolites* traces suggests that there was enough time for the mud to be colonized by organisms before the depression was filled in with sand. The final event was infilling of the scour with very fine-grained sand, or silt, which was transported from proximal regions and deposited very quickly (indicated by the lack of structures or massive nature of the sand and silt) over the mud layers. An example of one of these gutter casts and a diagram highlighting its variable fill is shown below in Figure 11.

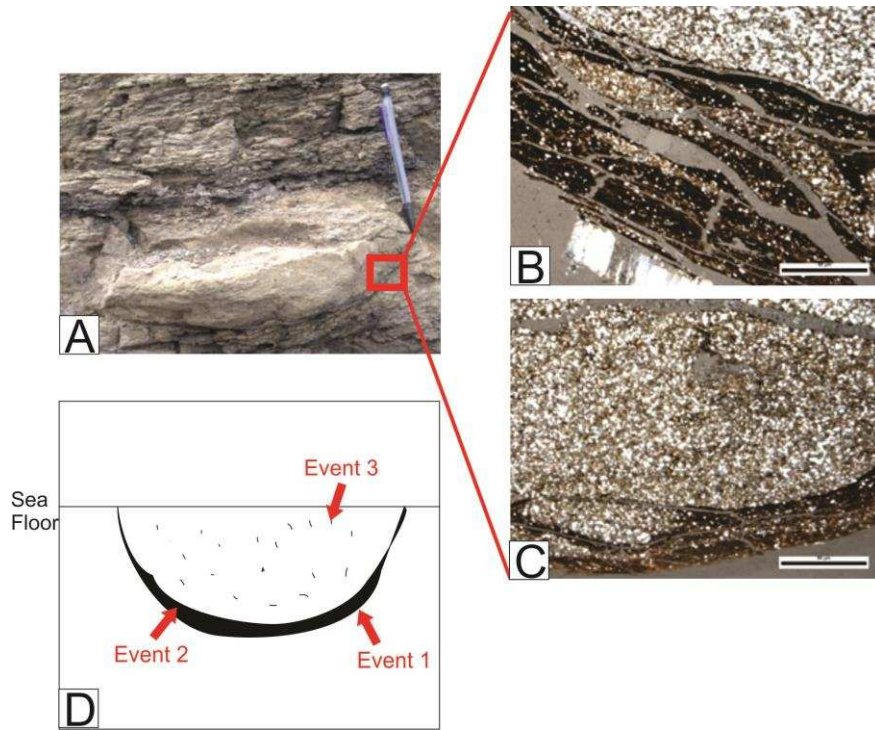


**Figure 11:** **A)** Gutter Cast at Dixon Dam that is lined with a thin mud layer (~0.5mm thick) at the base. The gutter cast was at 15.85m. **B) and C)** Thin sections of the mud layer below the gutter cast. The mud layer is fining upward (thin mud drape at the top) and is overlain with silt. **D)** Diagram showing the succession of events to form the gutter casts; Event 1: currents scour the sea bottom and create small depressions, Event 2: Mud was deposited from suspension in the depression as energy waned, Event 3: Very fine grained sand to silt is carried from the nearshore and deposited over the mud.



## 8.0 CONCLUSIONS

1. The Skull Creek Fm. consists of twelve different mudstone, siltstone and sandstone facies that were grouped into five facies associations (FAs). These are massive mudstone and siltstone (FA 1), fossiliferous mudstone and siltstone (FA 2), ripple to laminated siltstone and mudstone (FA 3), mud-rich sandstone and siltstone (FA 4), and bioturbated siltstone to sandstone (FA 5).

2. Sediments within the Skull Creek Fm. were deposited along the continental shelf in the distal portion of a delta system. They were transported as bed load within turbulent flows or as suspended load during river-flooding or storm events. FA 1 was deposited in a sediment starved-area along the continental shelf, either located distally or laterally to FA 2. FA 2 was deposited below storm-wave base and was transported as bed-load in a mostly turbulent flow. FA 3 and FA 4 are more medial to proximal deposits; FA 4 contains sand with minimal mud, while FA 3 is composed of silt. FA 3 was deposited at or below storm-wave base, contains mainly current-generated structures and shows minimal evidence of wave-reworking. FA 4 shows evidence of wave-reworking (HCS sandstones and siltstones and wave ripples) and was therefore deposited above storm wave base. FA 5 is the most proximal unit and was deposited along the middle shoreface to the lower offshore with intermittently stressed conditions, indicated by the presence of *Skolithos*.

3. By correlating the four outcrops and two cores along a N-S and E-W transect, the Skull Creek Fm. was subdivided into five stratigraphic intervals. Interval 1 is composed of proximal bioturbated to wave-rippled siltstones and sandstones (FA 4 and 5). Interval

2 is the most fine-grained unit and contains bioturbated mudstones or laminated and current-rippled mudstones which contain large concretions and lag deposits (FA 1, 2, and 3). Interval 3 contains wave- to current-rippled sandstones and siltstones with very thin bioturbated beds (FA 3 and 4). Interval 4 is composed of heavily bioturbated siltstones and massive sandstones (FA 5) with some very thin beds of massive mudstones or HCS sandstones (FA 1 and 4). Interval 5 is a fining-upwards unit that consists of bioturbated mudstones and siltstones at the base, and laminated to massive mudstones within the upper half (FA 1 and 2).

4. There are three transgressive cycles and one regressive cycle during the development of the Skull Creek Fm. Both interval 1 and interval 2 show an upwards decrease in grain size, which illustrates an overall decrease in energy within the basin. Therefore, interval 1 represents an early TST and interval 2 a late TST. Interval 3 and interval 4 are composed of the most proximal FAs and illustrate an overall decrease in accommodation space, consequently interval 3 is interpreted to be a HST and interval 4 is a LST. Interval 5 was deposited as sea level rose again (TST) and ends at the unconformity (or SB) between the Skull Creek Fm. and Muddy (J) sandstones.

5. TOC values within the Skull Creek Fm. are between 3.86 and 0.11 wt. %. Organic matter types are both terrestrial and marine in origin (Type II and III). Interval 2 contains the highest TOC values and the most oil-prone organic matter.

6. This study was accomplished by relating structures seen in the Skull Creek Fm. to structures observed by other researchers during flume experiments and along mud-dominated continental shelves. Mud-dominated successions deposited under humid

conditions along a tectonically active margin are conducive for producing flows with high-sediment concentrations and are transported by a combination of wave and current energy as wave-aided hyperpycnal flows. To identify formations that were deposited similarly to the Skull Creek Fm., coarse- to medium-grained sediments (siltstone and sandstone beds) should show a combination of wave-and current-generated structures and normally and inversely graded beds, while fine-grained sediments contain mainly current-generated structures and normally graded beds due to their more distal location along the continental shelf (below SWB).

## 9.0 BIBLIOGRAPHY

- Aigner, T., 1985, Storm Depositional Systems: Lecture Notes in Earth Sciences: New York, Springer-Verlag, v. 3, 174 p.
- Aigner, T. and Reineck, H., 1982, Proximity trends in modern storm sands from the Helgoland Bight (North Sea) and their implications for basin analysis: Errata zu Senckenbergiana marit, v.14, p. 183-215.
- Catuneanu O., Abreu, V., Bhattacharya, J.P., Blum, M.D., Dalrymple, R.W., Eriksson, P.G., Fielding, C.R., Fisher, W.L., Galloway, W.E., Gibling, M.R., Giles, K.A., Holbrook, J.M., Jordan, R., Kendall, C.G.St.C., Macurda, B., Martinsen, O.J., Miall, A.D., Neal, J.E., Nummedal, D., Pomar, L., Posamentier, H.W., Pratt, B.R., Sarg, J.F., Shanley, K.W., Steel, R.J., Strasser, A. Tucker, M.E., Winker, C., 2009, Towards the standardization of sequence stratigraphy: Elsevier, Earth-Science Reviews, v. 92, p. 1-33.
- Baas, J.H. and Best, J., 2002, Turbulence modulation in clay-rich sediment-laden flows and some implications for sediment deposition: Journal of Sedimentary Research, v. 72, no. 3, p. 336-340.
- Baas, J.H., Best, J.L. and Peakall, J., 2011, Depositional processes, bedform development and hybrid bed formation in rapidly decelerated cohesive (mud-sand) sediment flows: Sedimentology, v.58, p.1953- 1987.
- Bann, K.L. and Fielding, C.R., 2004, An Integrated ichnological and sedimentological comparison of non-deltaic shoreface and subaqueous delta deposits in Permian reservoir units of Australia: The Geological Society, London, Special Publication 228, p. 273-310
- Benton, M. J. and Harper, D.A., 1997, Basic Paleontology: University of California, Longman, 342 p.
- Bhattacharya, J.P. and Davies, R.K., 2001, Growth faults at the prodelta to delta front transition, Cretaceous Ferron Sandstone, Utah: Marine and Petroleum Geology, v. 18, p. 525-535.
- Bhattacharya, J.P. and Davies, R.K., 2004, Sedimentology and structure of growth faults at the base of the Ferron Member along Muddy Creek, Utah, *in* Chidsey, T.C, Jr, Adams, R.D., and Morris, T.H., eds., Regional to Wellbore Analog for Fluvial-Deltaic Reservoir Modeling: The Ferron Sandstone of Utah: American Association of Petroleum Geologists, Studies in Geology, co. 50, p. 279-304.
- Bhattacharya, J. P. and MacEachern, J., 2009, Hyperpycnal rivers and prodeltaic shelves in the Cretaceous Seaway of North America: Journal of Sedimentary Research, v. 79, p. 184-209, doi 10.2110/jsr.2009.026.

- Bhattacharya, J. P. and Willis, B.J., 2001, Lowstand deltas in the Frontier Formation, Powder River basin, Wyoming: Implications for sequence stratigraphic models: American Association of Petroleum Geologists Bulletin, v. 85, p. 261-294.
- Bohacs, K.M., Grabowski, G.J., Carroll, A.R., Mankiewicz, P.J., Miskell-Gerhardt, K.J., Schwalbach, J.R., Wegner, M.B., Simo, J.A., 2005, Production, destruction, and dilution—the many paths to source-rock development: SEPM Special Publication no.82, p. 61-101
- Bohacs, K.M., Neal, J.E. and Grabowski, G.J.Jr., 2002, Sequence stratigraphy in fine-grained rocks: Beyond the correlative conformity: 22<sup>nd</sup> Annual Gulf Coast Section SEPM Foundation Bob F. Perkins Research Conference, p. 321-347.
- Bohacs, K.M., Lazar, O., and Demko, T., 2014, Parasequence types in shelfal mudstone strata- Quantitative observations of lithofacies and stacking patterns, and conceptual link to modern depositional regimes: *Geology*, v. 42, no.2, p. 131-134, doi 10.1130/G35089.1.
- Bouma, A. H., 1962, *Sedimentology of some flysch deposits: a graphic approach to facies interpretation*, Amsterdam: Elsevier, 168p.
- Burtner, R.L., and Warner, M.A., 2009, Hydrocarbon generation in lower Cretaceous Mowry and Skull Creek shales of the Northern Rocky Mountain area: Rocky Mountain Association of Geologists, 20 p.
- Cobban, W.A., Merewether, E.A., Fouch, T.D., and Obradovitch, J.D., 1994, Some Cretaceous shorelines in the western interior of the United States: Mesozoic Systems of the Rocky Mountain Region, USA, p.393- 413.
- Creaney, S. and Passey, Q.R., 1993, Recurring patterns of total organic carbon and source rock quality within a sequences stratigraphic framework: The American Association of Petroleum Geologists Bulletin, v. 77, no. 3, p. 386-401.
- Curtis, C.D. and Coleman, M.L., 1986, Controls on the precipitation of early diagenetic calcite, dolomite, and siderite concretions in complex depositional sequences: The Society of Economic Paleontologists and Mineralogists, v. 38, p. 23-33.
- De Raaf, J.F.M., Boersma, J.R., and Gelder, A. Van, 1977, Wave-generated structures and sequences from a shallow marine succession, Lower Carboniferous, County Cork, Ireland: *Sedimentology*, v. 24, p. 451-483.
- Decelles, P.G., 2004, Late Jurassic to Eocene evolution of the Cordilleran thrust belt and foreland basin system, Western U.S.A: *American Journal of Science*, v. 304, p.105-168.
- Dechesne, M., Raynolds, R., G., Barkmann, P., E, and Johnson, K., R., 2011, Notes on the Denver Basin Geologic Maps: Bedrock Geology, Structure, and Isopach Maps of the Upper Cretaceous to Paleogene Strata between Greeley and Colorado Springs, Colorado: Colorado Geological Society.

- Dickinson, W. R., and Lawton, T. F., 2001, Carboniferous to Cretaceous assembly and fragmentation of Mexico: Geological Society of America Bulletin, v. 113, p. 1142–1160.
- Dolson, J.C., and Muller, D.S., 1994, Stratigraphic evolution of the Lower Cretaceous group, Western Interior, USA: Mesozoic Systems of the Rocky Mountain Region, USA, p.441- 456
- Dolson, J., Muller, D., Evetts, M.J., and Stein, J.A., 1991, Regional Paleotopographic trends and production, Muddy Sandstone (Lower Cretaceous), Central and Northern Rocky Mountains: The American Association of Petroleum Geologists Bulletin, v. 75, no. 3, p. 409-435
- Duke, W.L., Arnott, R.W.C., and Cheel, R.J., 1991, Shelf sandstones and hummocky cross-stratification: new insights on a stormy debate: Geology, v. 19, p. 625- 628.
- Edwards, K.K., 1999, Sequence stratigraphic framework for top seal development: Examples from the Skull Creek and Graneros shales, Denver basin: M.S. Thesis, Colorado State University, Fort Collins, Colorado, 473 p.
- Ethridge, F. and Holbrook, J., 1996, Sequence Stratigraphy of the Dakota Group and equivalents from North-Central Colorado to Northeastern New Mexico: Down-dip variations in sequence anatomy: A field trip guide for the 1996 GSA annual meeting, 43 p.
- Fishman, N.S., Hackley, P.C., Lowers, H.A., Hill, R.J., Egenhoff, S.O., Eberl, D.D., and Blum, A.E., 2012, The nature of porosity in organic-rich mudstones of the Upper Jurassic Kimmeridge Clay Formation, North Sea, offshore United Kingdom: International Journal of Coal Geology, v. 103, p. 32-50.
- Friedrichs, C.T. and Scully, M., 2007, Modeling deposition by wave-supported gravity flows on the Po River prodelta: From seasonal floods to prograding clinoforms: Continental Shelf Research, v. 27, p. 322-337.
- Friedrichs, C.T., Wright, L.D., Hepworth, D.A., and Kim, S.C., 2000, Bottom-boundary-layer processes associated with fine sediment accumulation in coastal seas and bays: Continental Shelf Research, v. 20, p. 807-841.
- Ghadeer, S. and MacQuaker, J., 2011, Sediment transport processes in an ancient mud-dominated succession: a comparison of processes operating in marine offshore settings and anoxic basinal environments: Journal of the Geological Society, London, v. 168, p. 1121-1132, doi 10.1144/0016-76492010-016.
- Graham, J., P. and Ethridge, G., 1995, Sequence Stratigraphic Implications of Gutter Casts in the Skull Creek Shale, Lower Cretaceous, Northern Colorado: The Mountain Geologist, v. 32, no. 4, p. 95-106.

- Jordan, T.E., 1981, Thrust loads and foreland basin evolution. Cretaceous, Western United States: The American Association of Petroleum Geologists Bulletin, v. 65, no.12, p. 2506-2520.
- Kineke, G.C., Sternberg, R.W., Trowbridge, J.H., and Geyer, W.R., 1996, Fluid-mud processes in the Amazon continental shelf: Continental Shelf Research, v. 16, no. 5/6, p. 667-696.
- Knepper, D.H., 2002, Planning for the Conservation and Development of Infrastructure Resources in Urban Areas— Colorado Front Range Urban Corridor: Things Planners, Decision-Makers, and the Public Should Know: Denver, U.S. Department of the Interior, U.S. Geological Survey, 32 p.
- MacEachern, J.A., Bann, K.L., Bhattacharya, J.P., and Howell, C.D. Jr., 2005, Ichnology of deltas: Organism responses to the dynamic interplay of rivers, waves, storms, and tides *in* River Deltas: Concepts, Models, and Examples: SEPM, Special Publications 83, p.49-85.
- MacEachern, J.A., Zaitlin, B.A., and Pemberton, G.S., 1999b, A sharp-based sandstone of the Viking Formation, Joffre Field, Alberta, Canada: criteria for recognition of transgressively incised shoreface complexes: Journal of Sedimentary Research, v. 69, no. 4, p. 876-892.
- MacEachern, J.A. and Gingras, M.K., 2007, Recognition of brackish-water trace-fossil suites in the Cretaceous Western Interior Seaway of Alberta, Canada *in* Sediment-Organism Interactions: A Multifaceted Ichnology: SEPM, Special Publication 89, p. 149-193.
- MacEachern, J.A., Pemberton, S.G., Raychaudhuri, I., and Vossler, S., 1991, Application of the *Glossifungites* ichnofacies to the recognition of sequence stratigraphic boundaries: examples from the Cretaceous of the Western Canada sedimentary basin, Alberta, Canada: American Association of Petroleum Geologist Bulletin, v.75, p. 625.
- MacEachern, J.A., Stelck, C.S., and Pemberton, S.G., Marine and marginal marine mudstone deposition: Paleoenvironmental interpretations based on the integration of ichnology, palynology and foraminiferal paleoecology: Society for Sedimentary Geology, SEPM Special Publication, no.64, p. 205-225.
- Macquaker, J., Bentley, S.J., and Bohacs, K.M., 2010, Wave-enhanced sediment-gravity flows and mud dispersal across continental shelves: Reappraising sediment transport processes operating in ancient mudstone successions: Geology, v.38, no.10, p. 947-950, doi 10.1130/G31093.1.
- Macquaker, J., Taylor, K., and Gawthorpe, R., 2007, High-resolution facies analyses of mudstones: Implications for paleoenvironmental and sequence stratigraphic interpretations of offshore ancient mud-dominated: Journal of Sedimentary Research, v. 77, p. 324-339, doi 10.2110/jsr.2007.029.

- Mulder, T. and Alexander, J., 2001, The physical character of subaqueous sedimentary density flows and their deposits: *Sedimentology*, v. 48, p. 269-299.
- Mulder, T., Syvitski, J., Migeon, S., Faugeres, J., and Savoye, B., 2003, Marine hyperpycnal flows: initiation, behavior and related deposits. A review: *Marine and Petroleum Geology*, v.20, p. 861-882.
- Mulder, T., Syvitski, J., and Skene, K. I., 1998, Modeling of erosion and deposition by turbidity currents generated at river mouths: *Journal of Sedimentary Research*, v. 68, no. 1, p. 124- 137.
- Mutti, E., Tinterri, R., Benevelli, G., di Biase, D., and Cavanna, G., 2003, Deltaic, mixed and turbidite sedimentation of ancient foreland basins: *Marine and Petroleum Geology*, v. 20, p. 733-755.
- Myrow, P.M., 1992, Pot and gutter casts from the Chapel Island Formation, southeast Newfoundland: *Journal of Sedimentary Research*, v. 62, no. 6, p. 992-1007
- Parsons, J.D., Bush, J.W.M., and Syvitski, P.M., 2001, Hyperpycnal plume formation from riverine outflows with small sediment concentrations: *Sedimentology*, v. 48, p. 465-478.
- Pattison, S., Ainsworth, R., and Hoffman, T., 2007, Evidence of across-shelf transport of fine- grained sediments: turbidite-filled shelf channels in the Campanian Aberdeen Member, Book Cliffs, Utah, USA: *Sedimentology*, v. 54, p. 1033-1063, doi 10.1111/j.1365-3091.2007.00871.x.
- Potsma, G., Wojciech, N., and Kleinspehn, K.L., 1988, Large floating clasts in turbidites: A mechanism for their emplacement: *Sedimentary Geology*, v. 58, p. 47-61.
- Potter, P.E., Maynard, J.B., and Pryor, W.A., 1980, *Sedimentology of shale*: New York, Springer-Verlag, p. 306.
- Plint, A.G, Macquaker, J., and Varban, B.L., 2012, Bedload transport of mud across a wide, storm-influenced ramp: Cenomanian-Turonian Kaskapau Formation, Western Canada, Foreland Basin: *Journal of Sedimentary Research*, v. 82, p. 801-822, doi 10.2110/jsr.2012.64.
- Schieber, J., 2002, The Role of an Organic Slime Matrix in the Formation of Pyritized Burrow Trails and Pyrite Concretions: *PALAIOS*, v. 17, p.104-109.
- Schieber, J. and Southard, J., 2009, Bedload transport of mud by floccule ripples- direct observation of ripple migration processes and their implications: *Geology*, v.37, no. 6, p. 483-486, doi 10.1130/G25319A.1.

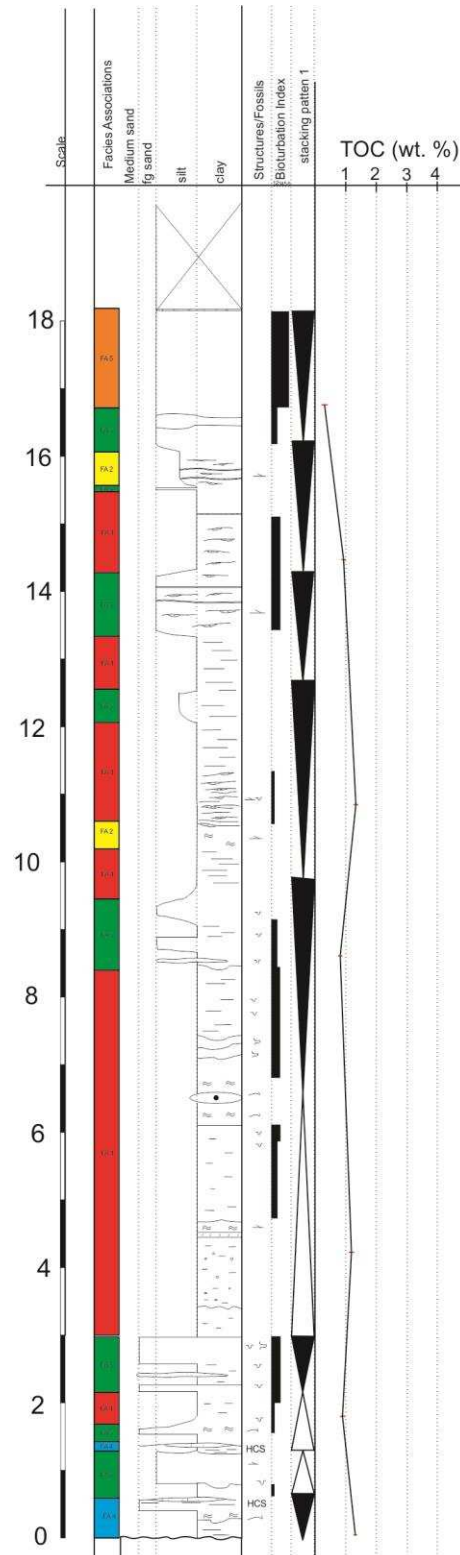


- Schieber, J., Southard, J., and Thaisen, K., 2007, Accretion of mudstone beds from migrating floccule ripples: *Science*, v. 318, p.1760- 1763, doi 10.1126/science.1147001.
- Stauffer, P.F., 1967, Grain-flow deposits and their implications, Santa Ynez Mountains, California: *Journal of Sedimentary Petrology*, v. 37, no. 2, p.487- 508.
- Sutton, S.J., Ethridge, F.G., Almon, W.R., Dawson, W.C., and Edwards, K.J., 2004, Textural and sequence-stratigraphic controls on sealing capacity of Lower and Upper Cretaceous shales, Denver Basin, Colorado: *AAPG Bulletin*, v. 88, no. 8, p. 1185-1206.
- Taylor, A.M. and Gawthorpe, R.L., 1993, Application of sequence stratigraphy and trace fossil analysis to reservoir description: examples from the Jurassic of the North Sea: *The Geological Society, London*, p. 317- 335.
- Taylor, A.M. and Goldring, R., 1993, Description and analysis of bioturbation and ichnofabric: *Geological Society of London, Journal*, v. 150, p.141-148.
- Taylor, K. and MacQuaker, J., 2000, Spatial and temporal distribution of authigenic minerals in continental shelf sediments: Implications for sequence stratigraphic analysis: *Marine Authigenesis: From Global to Microbial*, SEPM Special Publication, no. 66, p. 309- 323.
- Trappe, J., 2001, A nomenclature system for granular phosphate rocks according to depositional texture: *Sedimentary Geology*, v. 145, no. 1, p.135-150.
- Traykovski, P., Geyer, W., Irish, J., and Lynch, J., 2000, The role of wave-induced density- driven fluid mud flows for cross-shelf transport on the Eel River continental shelf: *Continental Shelf Research*, v. 20, p. 2113-2140.
- U.S. Geological Survey, 2003, 2002 USGS assessment of oil and gas resource potential of the Denver Basin Province of Colorado, Kansas, Nebraska, South Dakota, and Wyoming: USGS Fact Sheet FS-002-03.
- Weimer, R., J., 1996, Guide to the Petroleum Geology and Laramide Orogeny, Denver Basin and Front Range, Colorado: *Colorado Geological Society*, p. 1-121.
- Wilson, R.D. and Schieber, J., 2014, Muddy prodeltaic hyperpycnites in the lower Genesee Group of Central New York, USA: Implications for mud transport in epicontinental seas: *Journal of Sedimentary Research*, v. 84, p. 866-874, doi <http://dx.doi.org/10.2110/jsr.2014.70>.
- Wright, L.D. and Friedrichs, C.T., 2006, Gravity-driven transport on continental shelves: A status report: *Continental Shelf Research*, v. 26, p. 2092-2107.

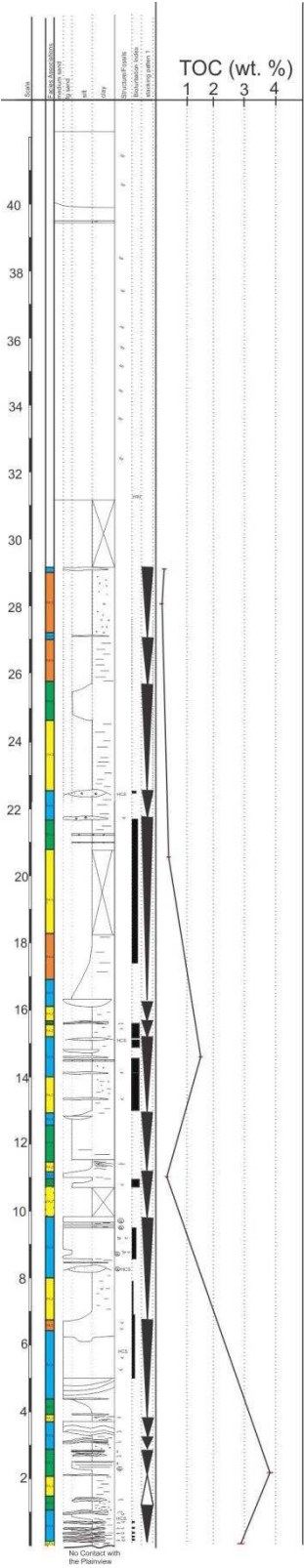
## 10.0 APPENDICES

## Appendix 1: TOC data

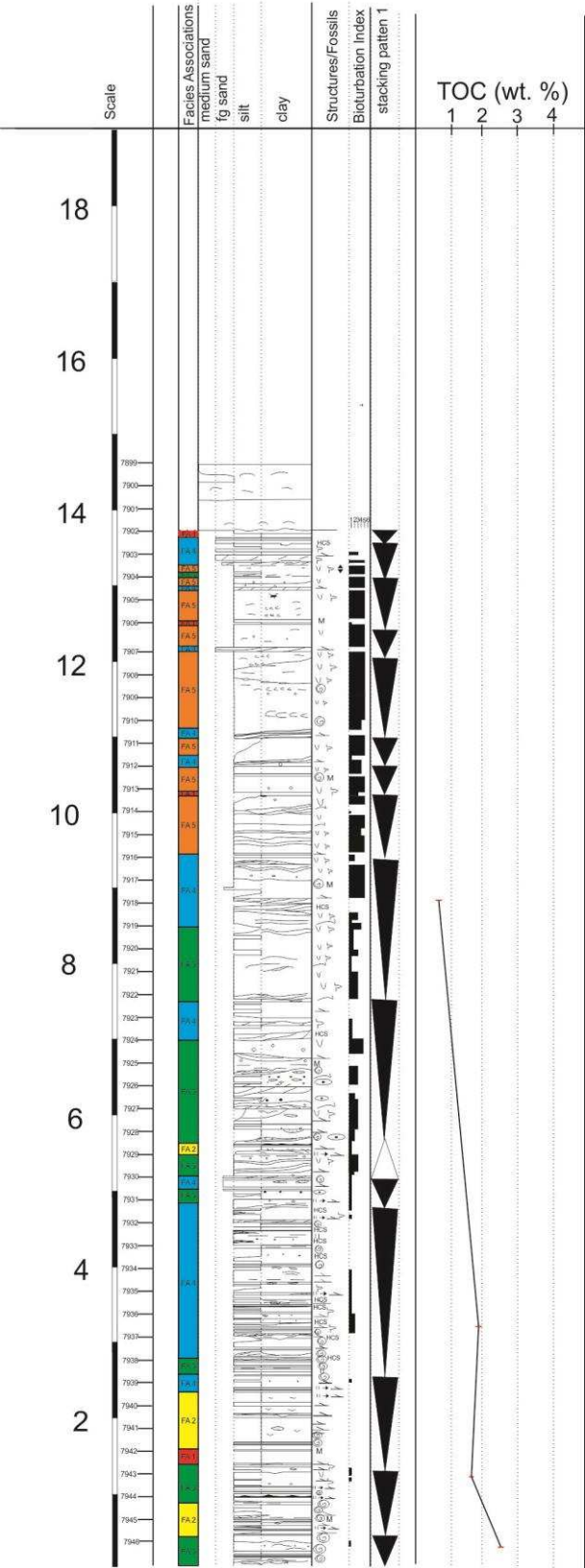
### Bellvue Dome



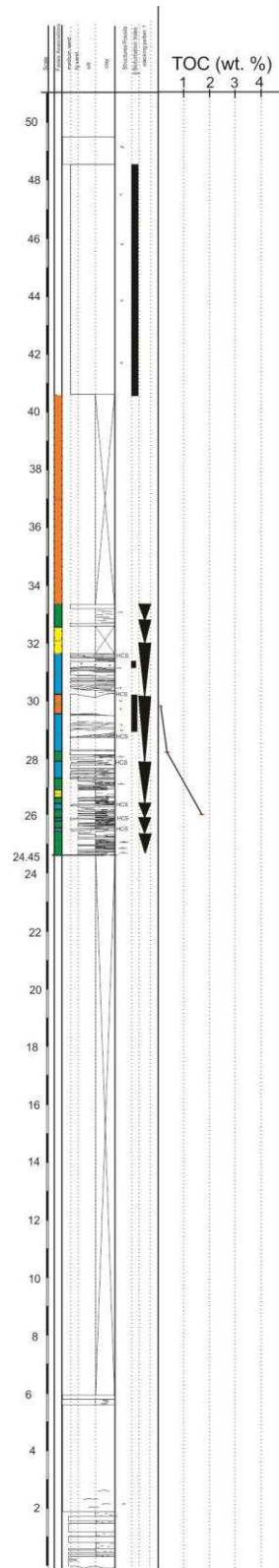
Dixon Dam



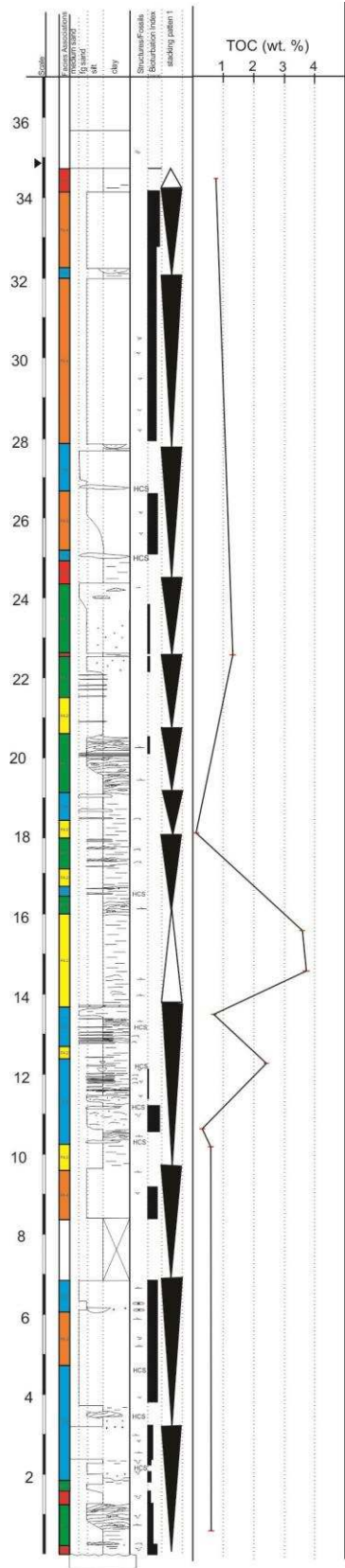
9-31 Bass Meadow Springs



## Spring Canyon Dam



Turkey Creek





# TOTAL ORGANIC CARBON, PROGRAMMED PYROLYSIS DATA

Company : CSU

Project No : BH-74590 / BH-74590

Well Name	Depth (Top)	Formation	Sample Type	Sample Prep	*	Leco TOC	RE S1	RE S2	RE S3	Tmax (°C)	**	Ro, %	HI	OI	S2/S3	S1/TOC *100	PI	Notes Checks	Pyrogram	LAB ID
BD-0.6-14			Rock	NOPR		1.13														3403774651
BD-1.70-14			Rock	NOPR		0.93														3403774655
BD-10.96-14			Rock	NOPR		1.43												TOC		3403774657
BD-14.26-14			Rock	NOPR		0.91												TOC		3403774653
BD-16.86-14			Rock	NOPR		0.39												TOC		3403774639
BD-4.20-14			Rock	NOPR		1.39														3403774637
BD-8.66-14			Rock	NOPR		0.92	0.13	0.71	0.33	438			77	36	2.2	14	0.16	RE	n:ls2sh:hts2sf	3403774663
D313	7917		Chunk	NOPR		0.60												TOC		3403795658
D313	7936.9		Chunk	NOPR		1.82												TOC		3403795660
D313	7942		Chunk	NOPR		1.63												TOC		3403795662
D313	7946		Chunk	NOPR		2.45												TOC		3403795656
DD-0.05-14			Rock	NOPR		2.97	0.98	5.90	0.89	434			199	30	6.6	33	0.14	RE	n:ls2sh:hts2sf	3403774711
DD-10.48-14			Rock	NOPR		0.39														3403774707
DD-14.47-14			Rock	NOPR		0.53														3403774709
DD-2.16-14			Rock	NOPR		3.75												TOC		3403774703
DD-20.5-14			Rock	NOPR		0.40												TOC		3403774705
DD-28.02-14			Rock	NOPR		0.21														3403774701
DD-29.12-14			Rock	NOPR		0.29												TOC		3403774737
SC-25.65-14			Rock	NOPR		1.73	0.26	2.52	0.84	435			146	49	3.0	15	0.09	RE	n:ls2sh:hts2sf	3403774735
SC-27.85-14			Rock	NOPR		0.44												TOC		3403774667
SC-29.52-14			Rock	NOPR		0.11												TOC		3403774699
TC-0.5-14			Rock	NOPR		0.66														3403774625
TC-10.21-14			Rock	NOPR		0.61												TOC		3403774623
TC-10.6-14			Rock	NOPR		0.31														3403774631
TC-12.23-14			Rock	NOPR		2.49												TOC		3403774627
TC-13.49-14			Rock	NOPR		0.70														3403774629
TC-14.71-14			Rock	NOPR		3.86	0.58	18.67	0.66	416			484	17	28.3	15	0.03	TOC RE	n:ls2sh	3403774619
TC-15.66-14			Rock	NOPR		3.56	0.34	13.89	0.64	420			390	18	21.7	10	0.02	RE	n:ls2sh	3403774733
TC-18.2-14			Rock	NOPR		0.11												TOC		3403774633
TC-22.66-14			Rock	NOPR		1.37												TOC		3403774621
TC-34.5-14			Rock	NOPR		0.72												TOC		3403774635

## Notes:

"-1" - not measured or invalid value for Tmax  
TOC - Total Organic Carbon, wt. %  
S1 - volatile hydrocarbon (HC) content, mg HC/ g rock  
S2 - remaining HC generative potential, mg HC/ g rock  
S3 - carbon dioxide content, mg CO<sub>2</sub>/ g rock

\* - comments regarding contamination  
\*\* - low S2, Tmax is unreliable  
Meas. %Ro - measured vitrinite reflectance  
HI - Hydrogen index = S2 x 100 / TOC, mg HC/ g TOC  
OI - Oxygen Index = S3 x 100 / TOC, mg CO<sub>2</sub>/ g TOC  
PI - Production Index = S1 / (S1+S2)

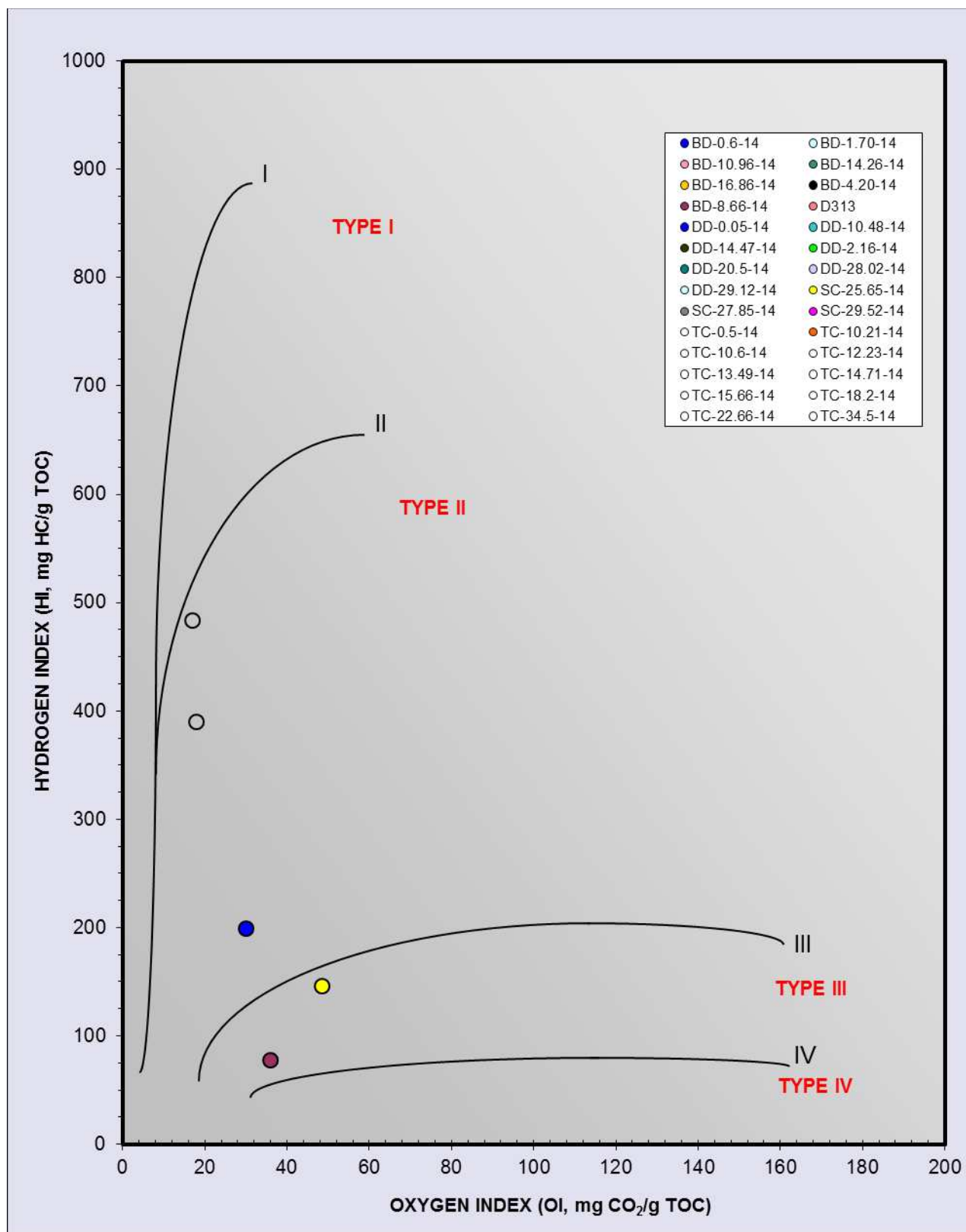
## Pyrogram:

f - flat S2 peak  
n - normal  
hts2sh - low temperature S2 shoulder  
hts2sh - high temperature S2 shoulder  
hts2p - low temperature S2 peak  
hts2p - high temperature S2 peak

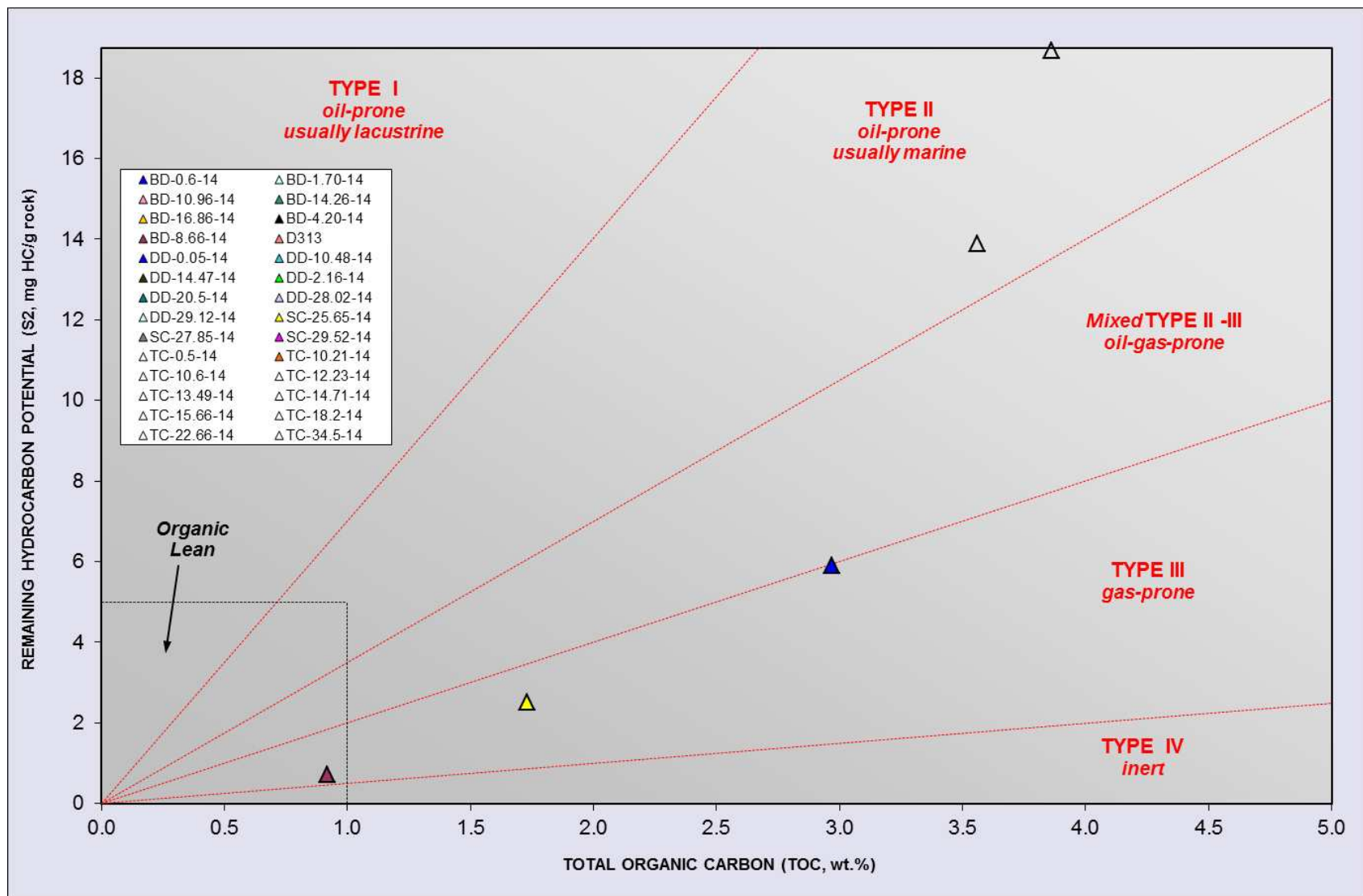
LECO - TOC on Leco Instrument  
RE - Programmed pyrolysis or  
TOC on Rock-Eval instrument  
SRA - Programmed pyrolysis by SRA  
Instrument  
EXT - Extracted Rock  
NOPR - Normal Preparation



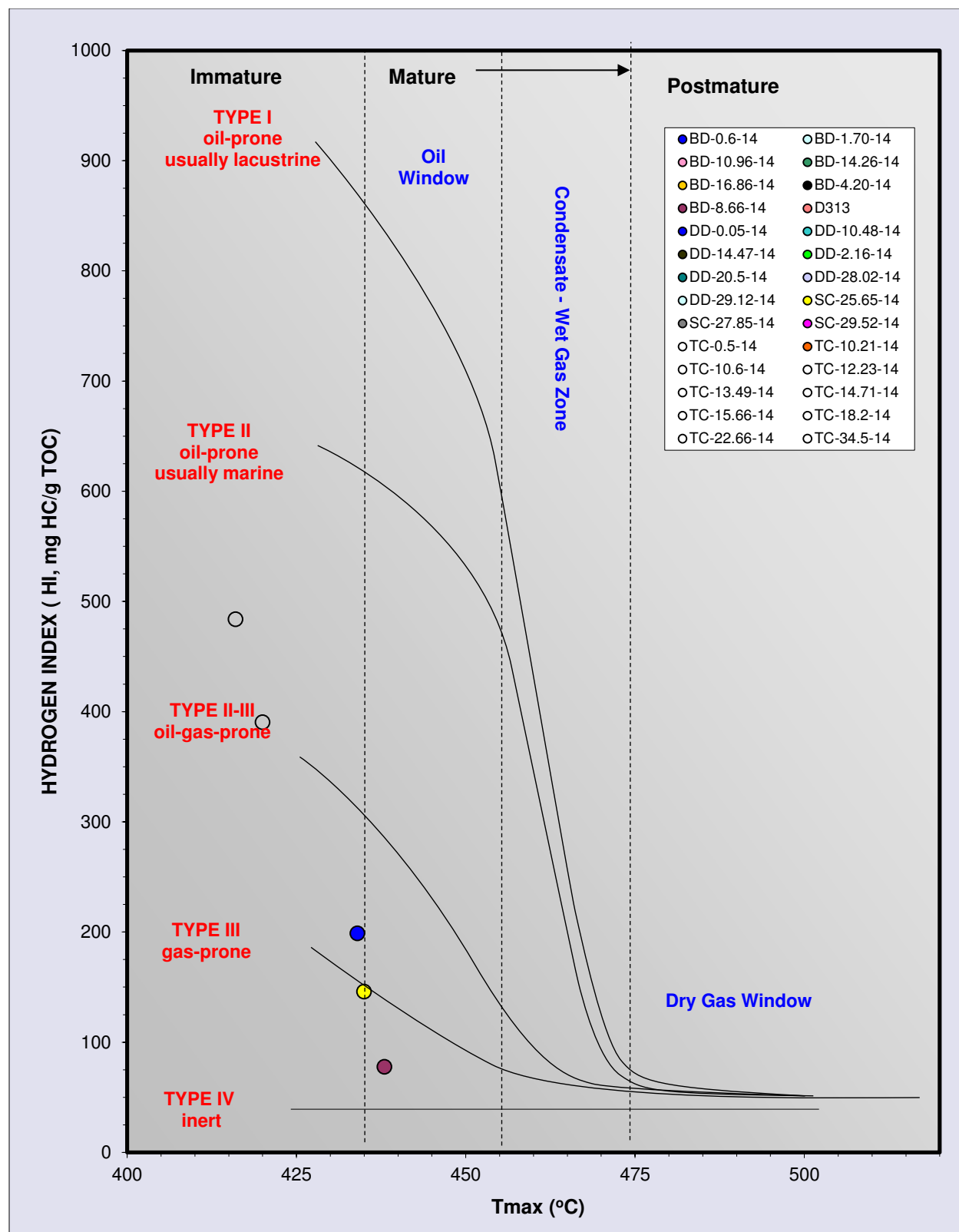
## Kerogen Type



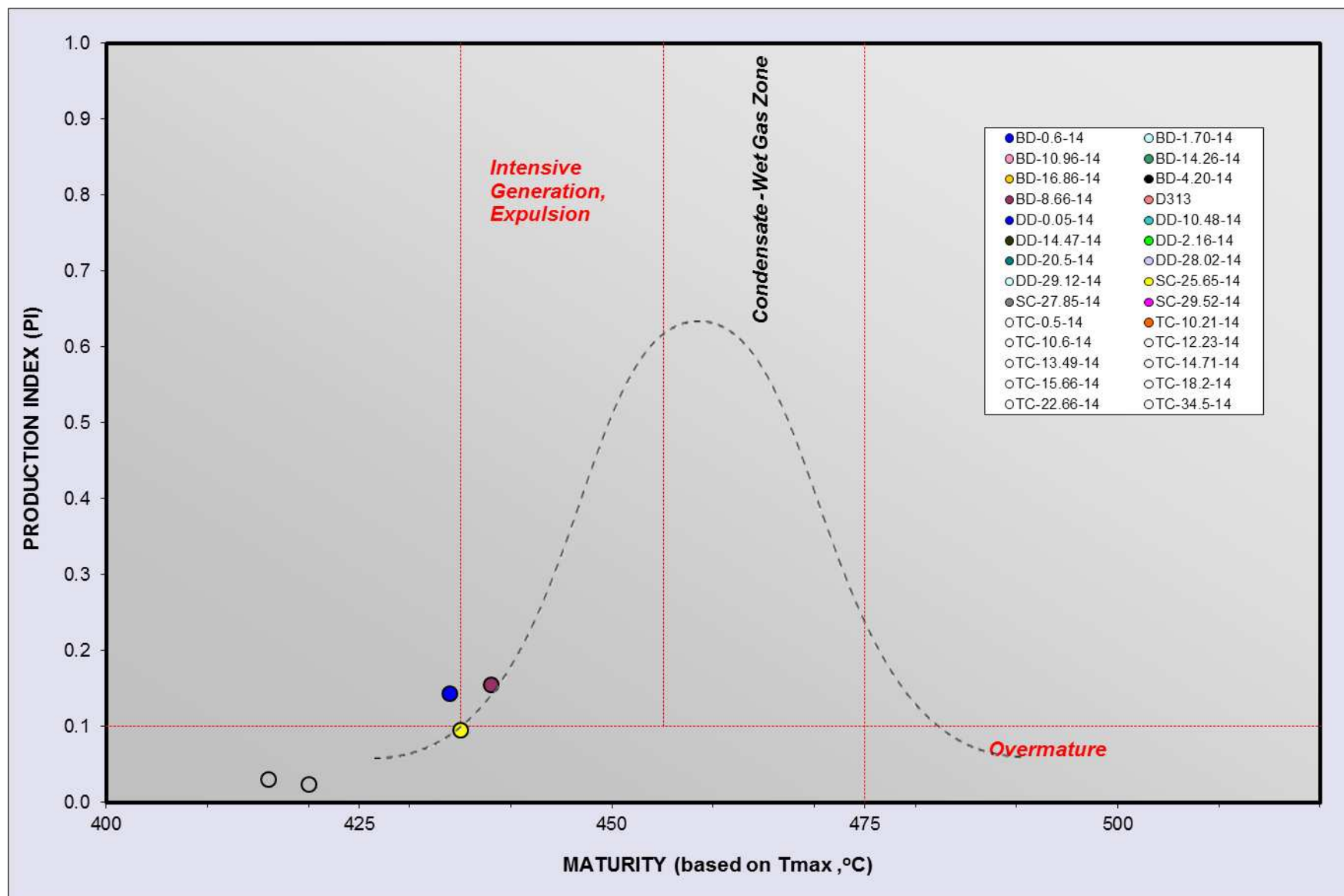
## Kerogen Quality Plot



## Kerogen Type and Maturity (Tmax)



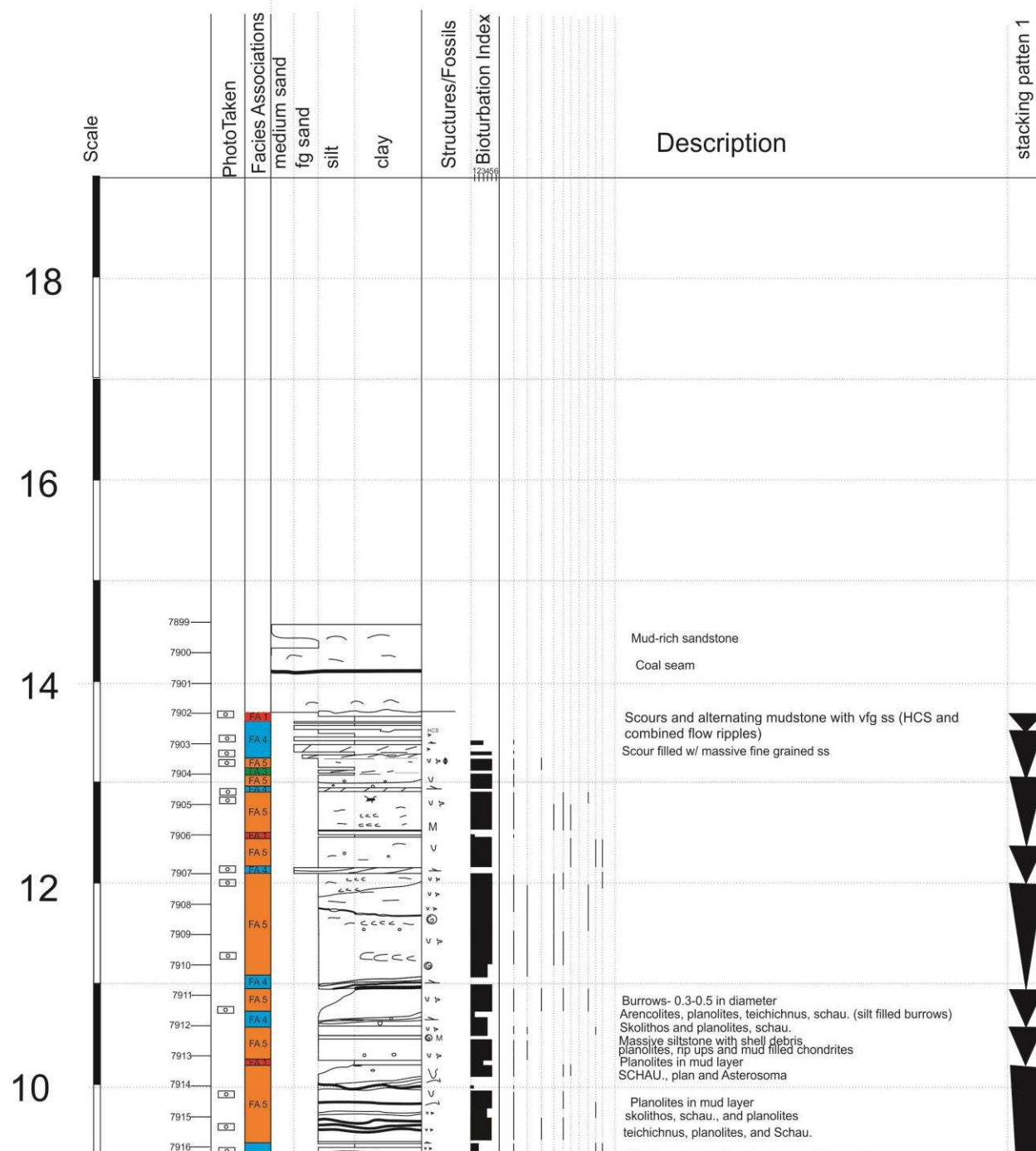
## Kerogen Conversion and Maturity (Tmax)



## Appendix 2: Stratigraphic sections

### 9-31 Bass Meadow Springs

Well: 9-31 Bass Meadow Springs County: Larimer State: Colorado  
 Stratigraphic Interval: Skull Creek-Muddy J. Logged By: Kathleen Masterson Date: 11/11/2014

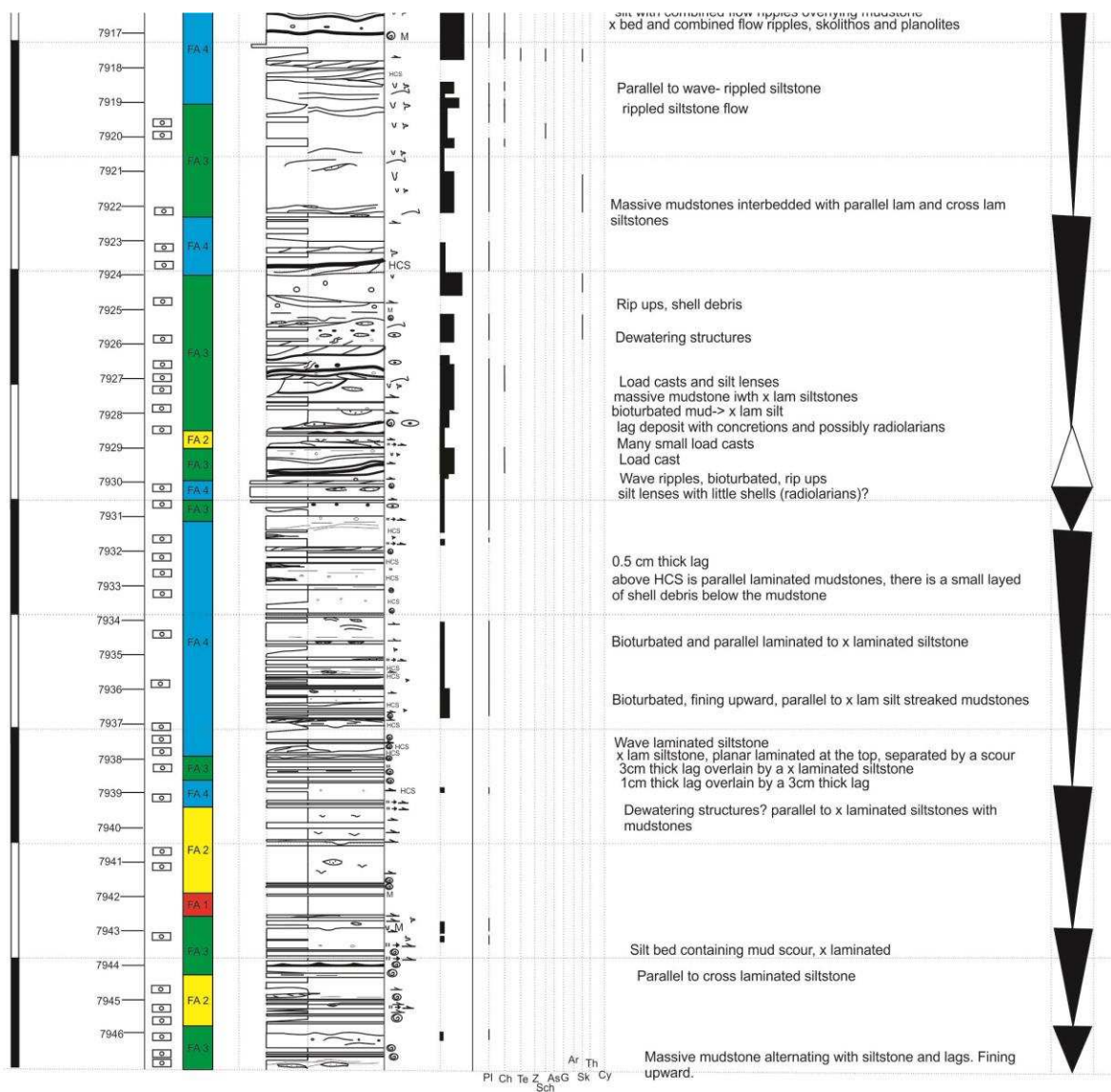


8

6

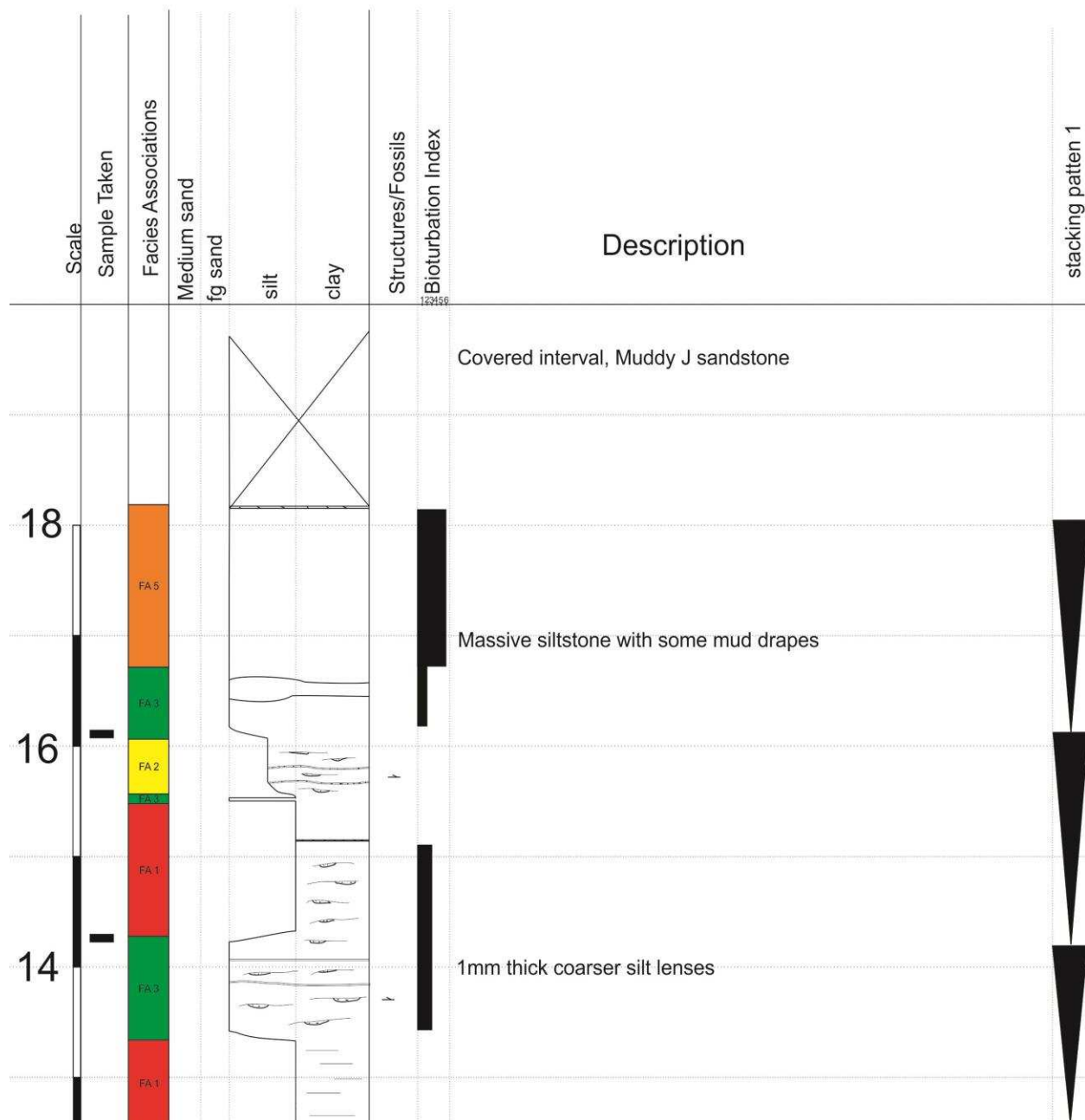
4

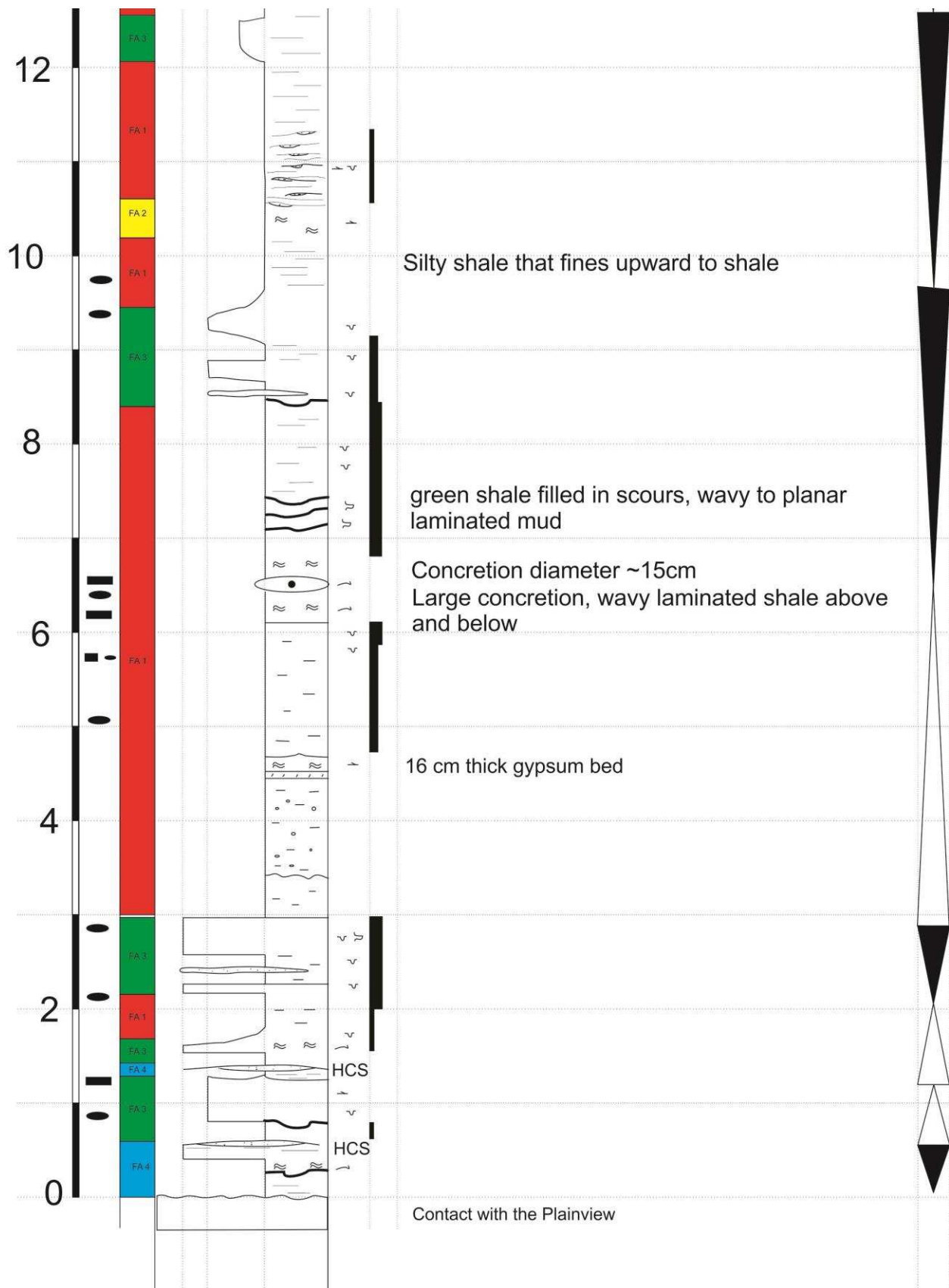
2





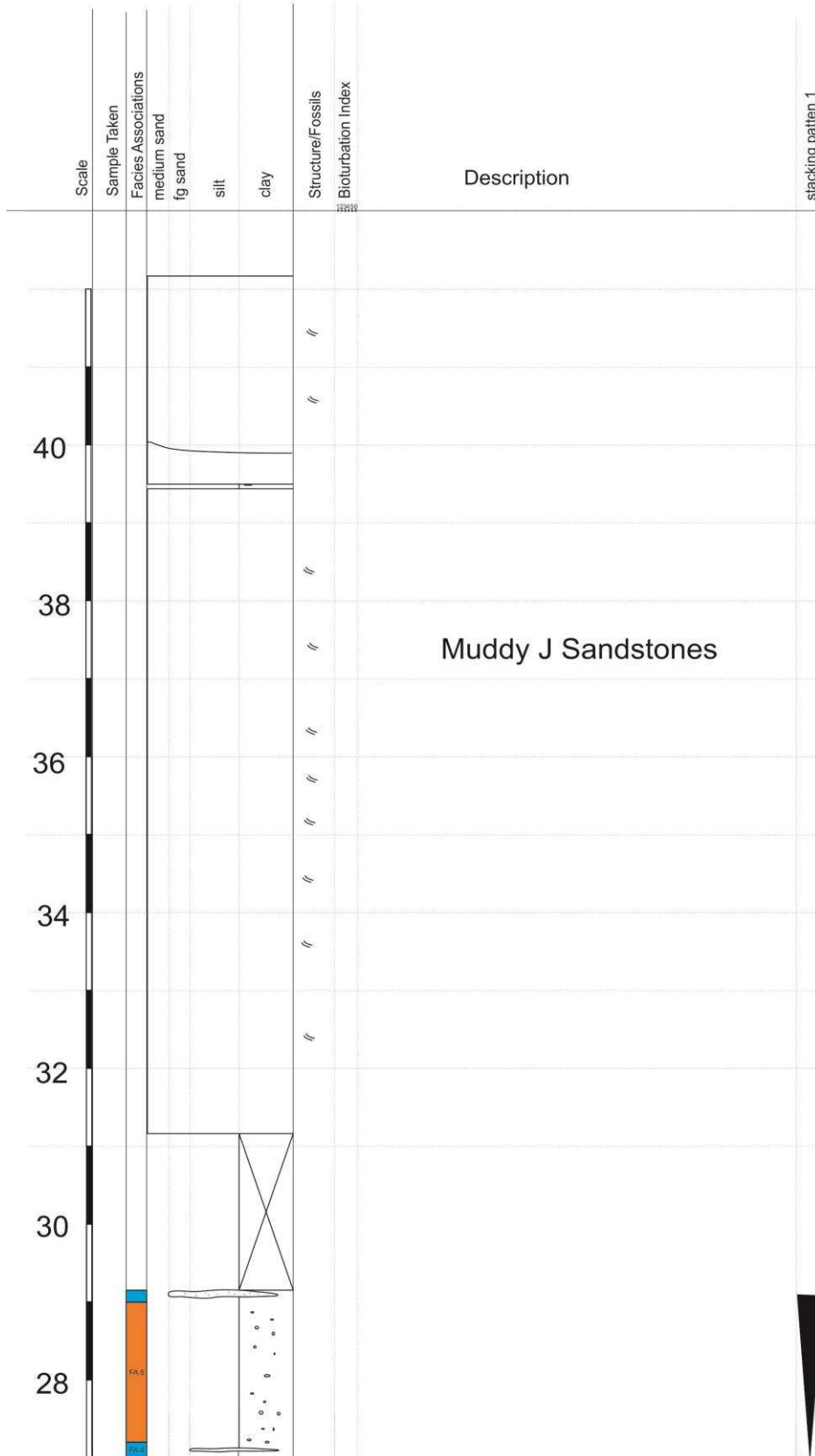
Well: Bellvue Dome County: Larimer State: Colorado  
 Stratigraphic Interval: Plainview-Skull Creek-Muddy J Logged By: Kathleen Masterson Date: 4/16/2014

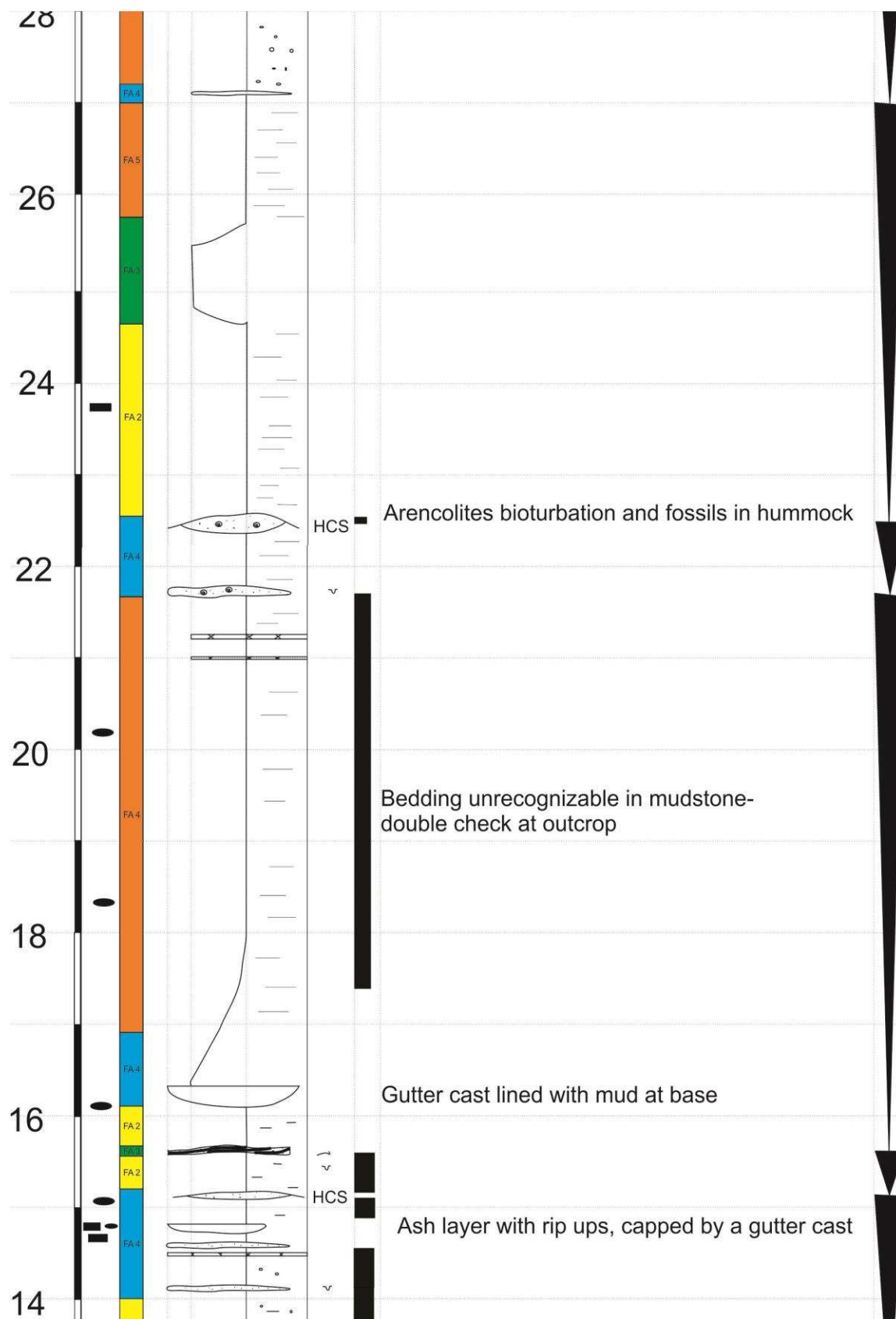


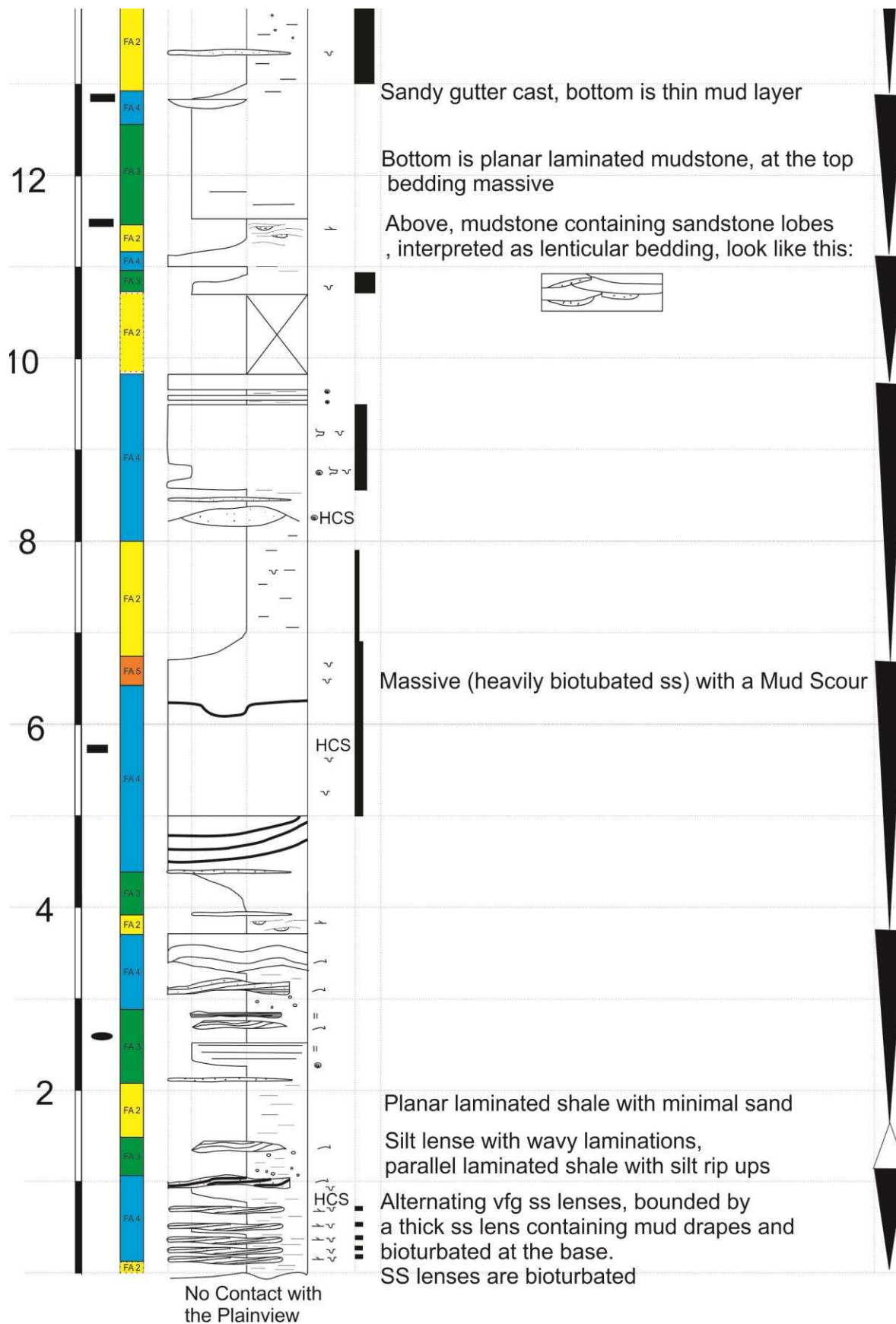




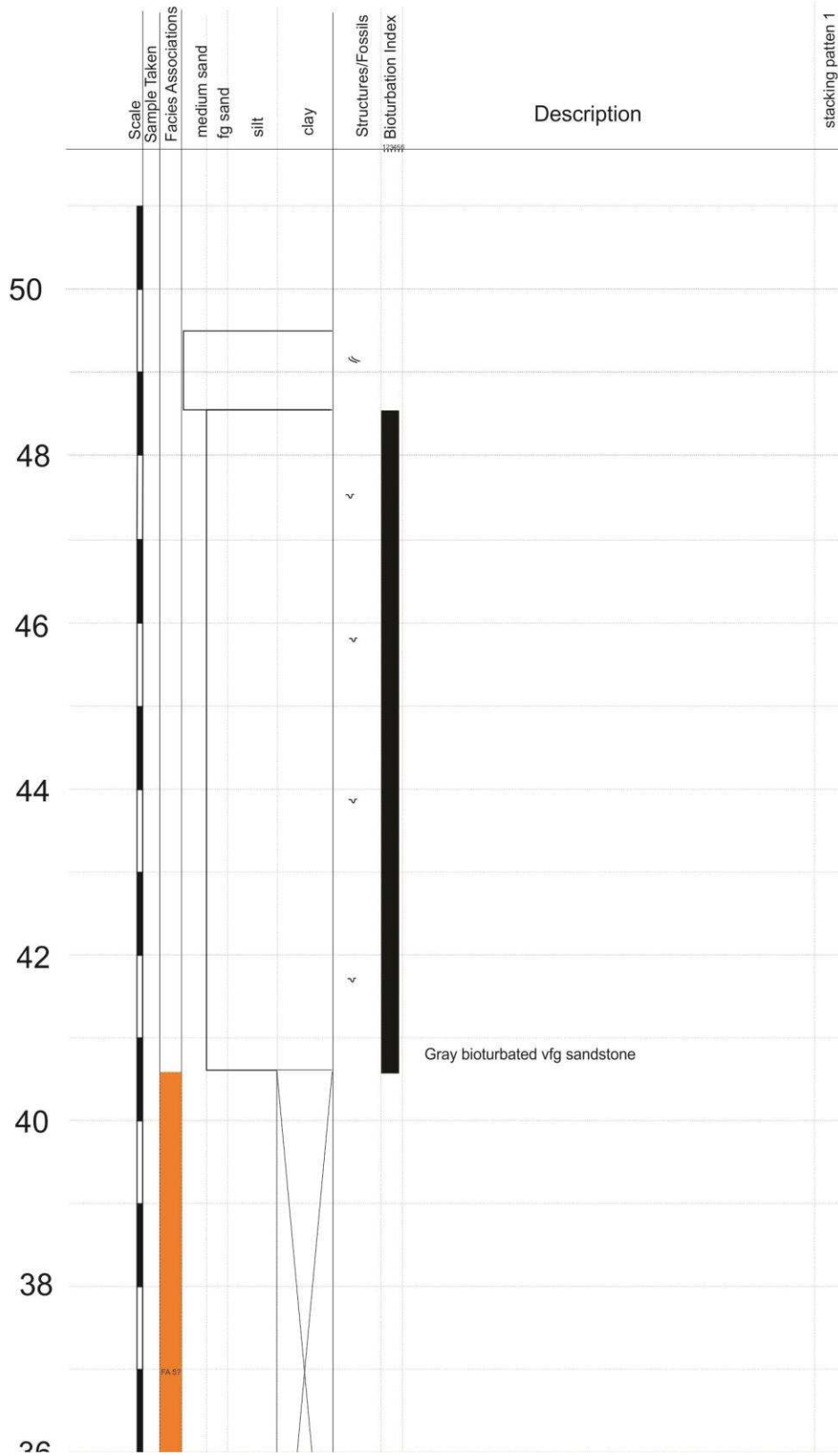
Well: Dixon Dam..... County: Larimer..... State: Colorado.....  
 Stratigraphic Interval: Plainview-Skull Creek-Muddy J Logged By: Kathleen Masterson..... Date: 4/2/2014.....

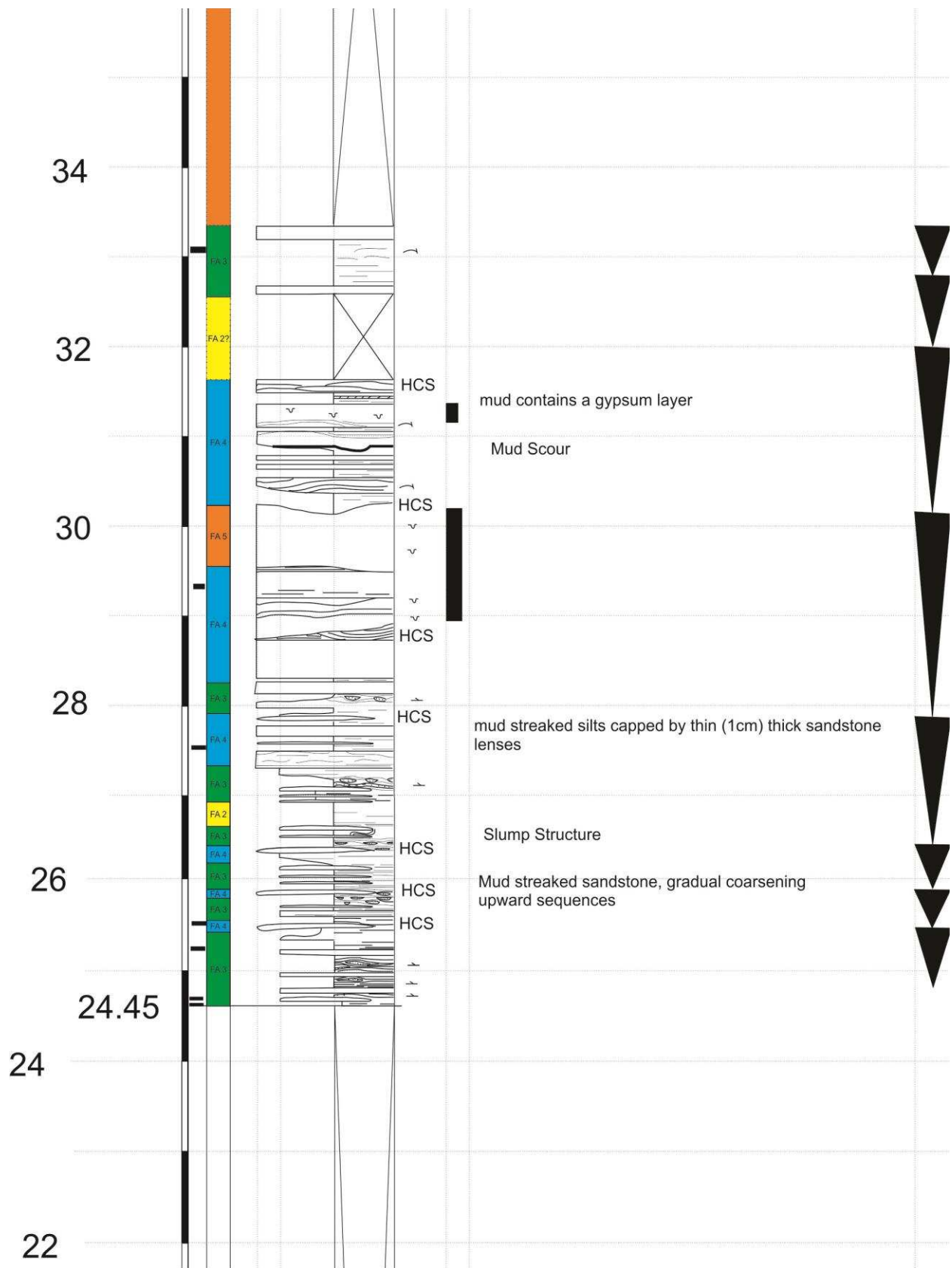


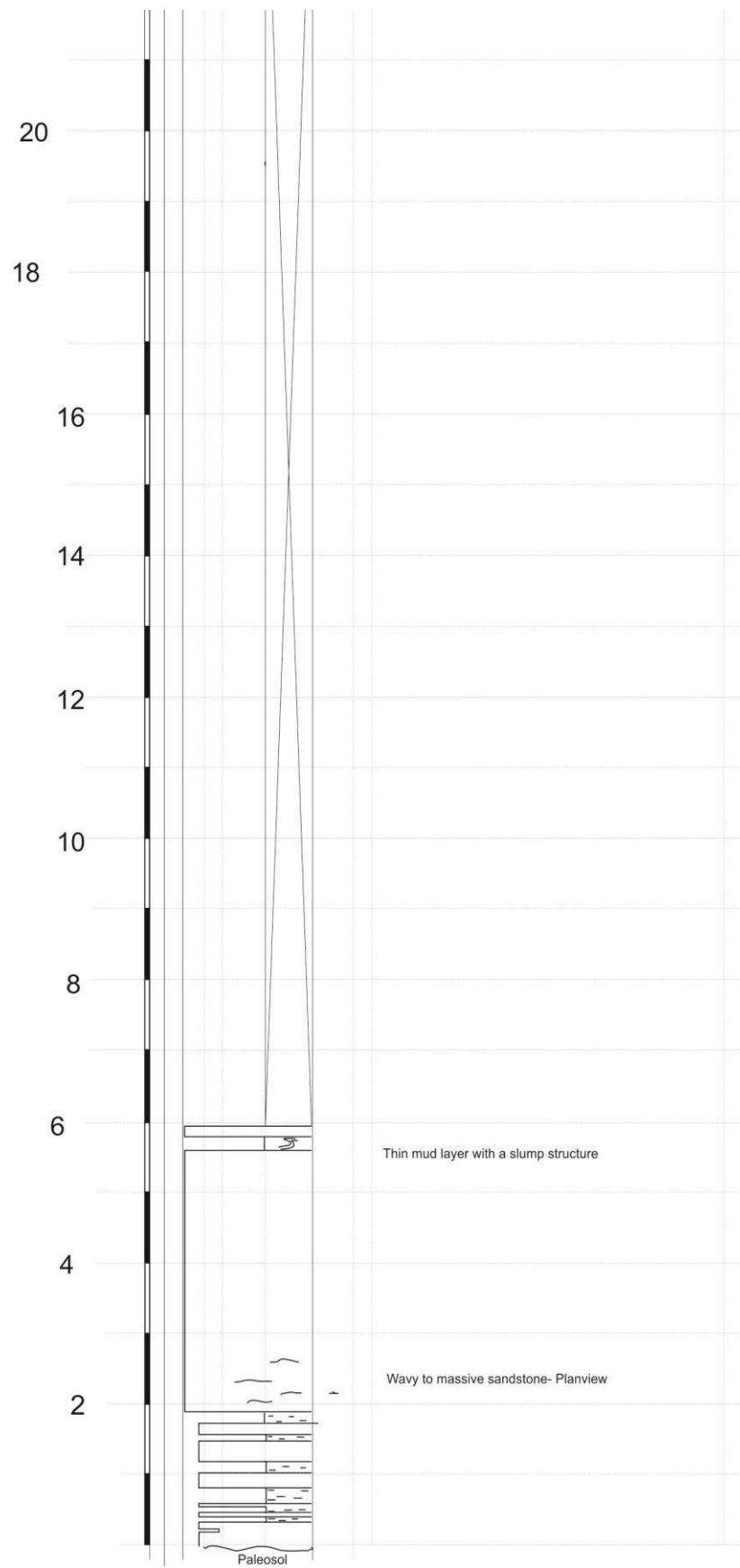




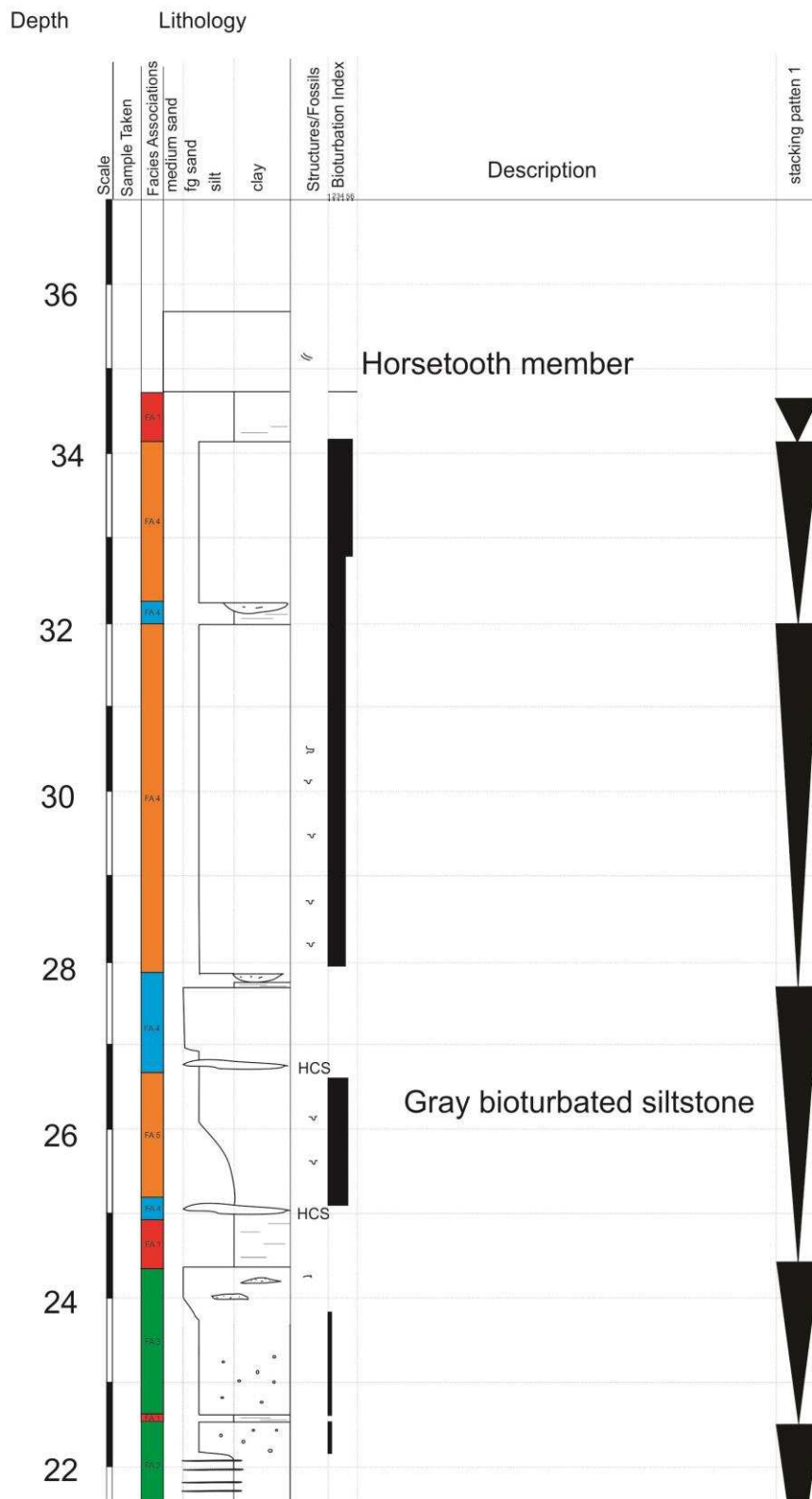
Well: Spring Canyon Dam..... County: Larimer..... State: Colorado.....  
Stratigraphic Interval: Plainview-Skull Creek-Muddy J..... Logged By: Kathleen Masterson..... Date: 9/12/2014.....

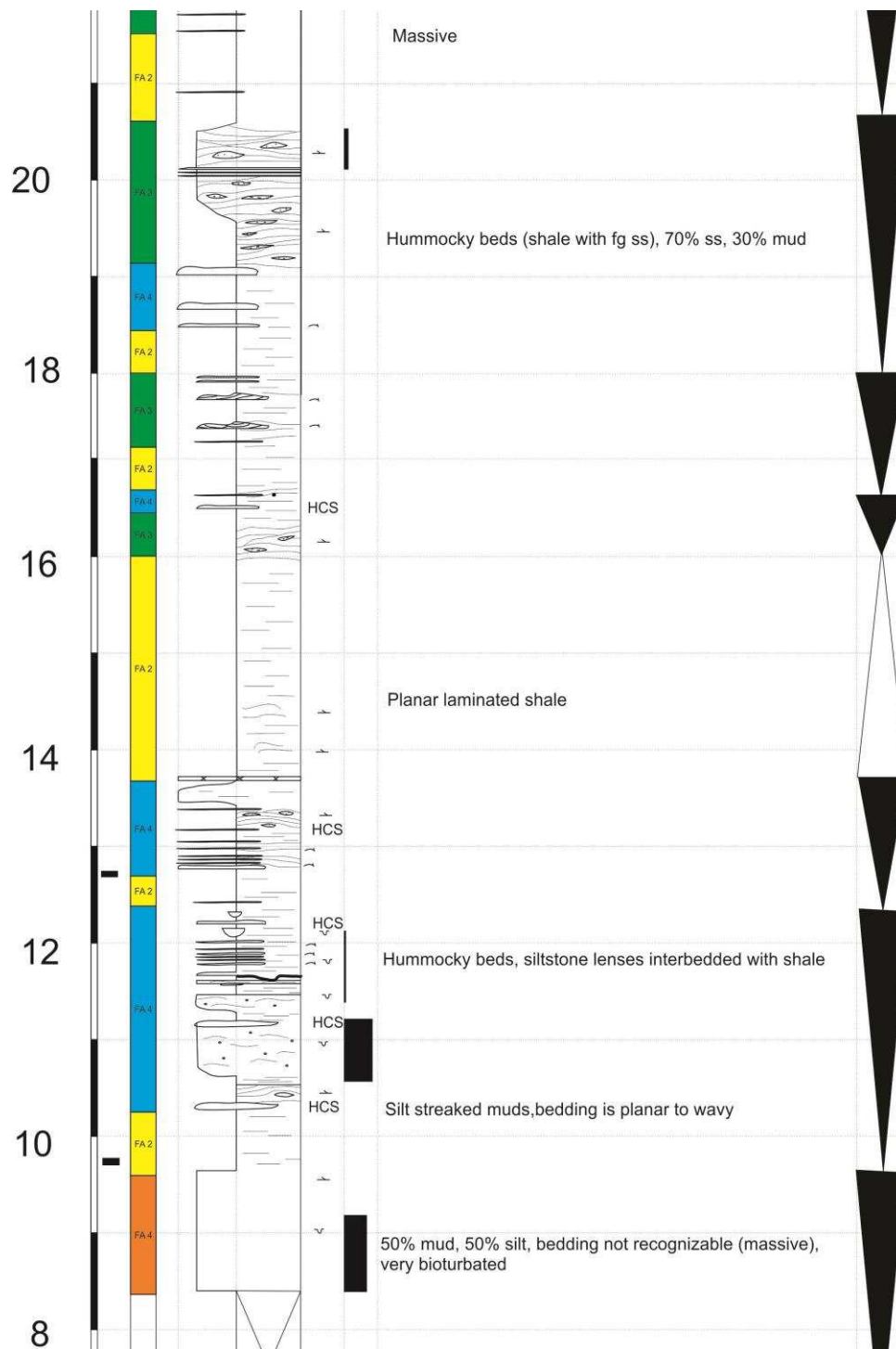




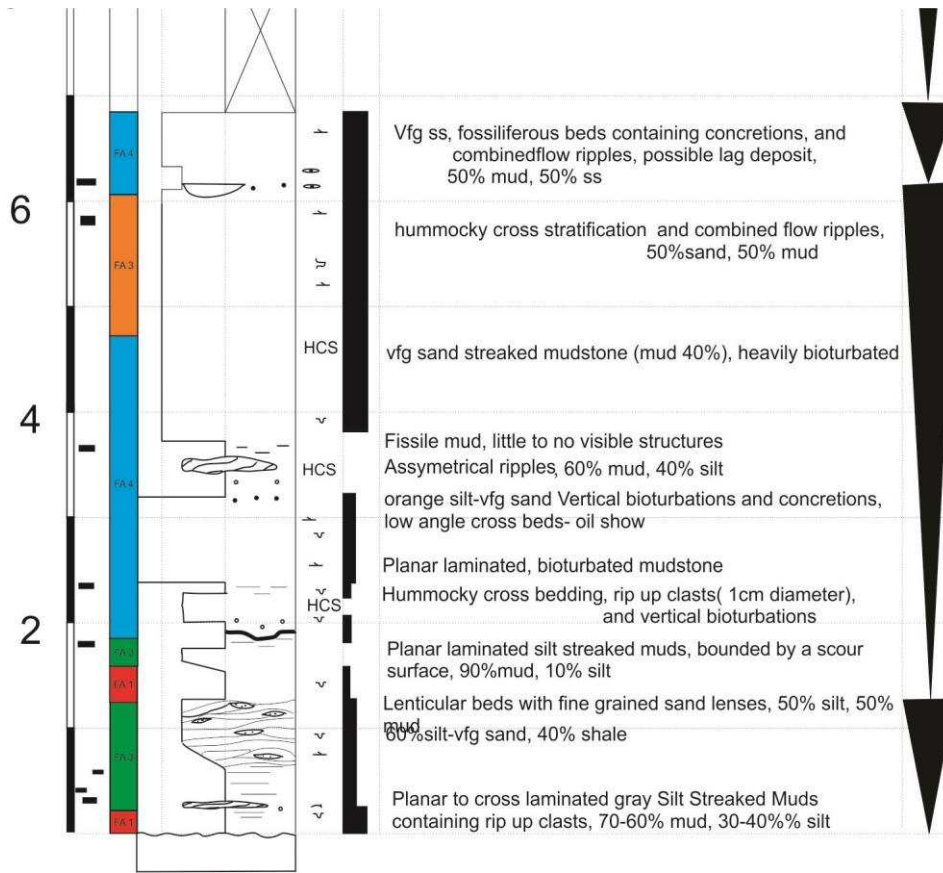


Well: Turkey Creek County: Jefferson State: Colorado  
 Stratigraphic Interval: Plainview-Skull Creek-Muddy J Logged By: Kathleen Masterson Date: 9/4/2014

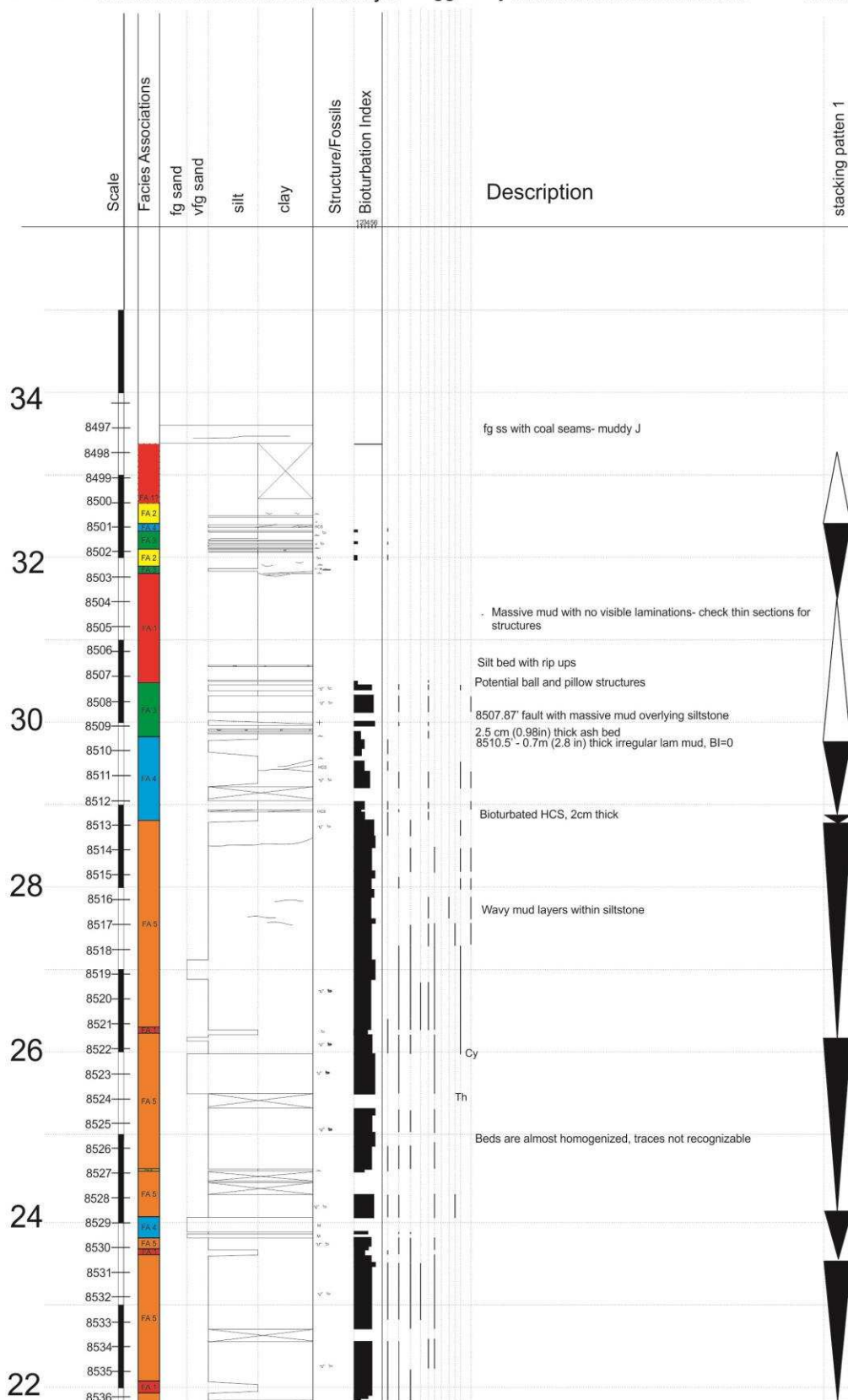


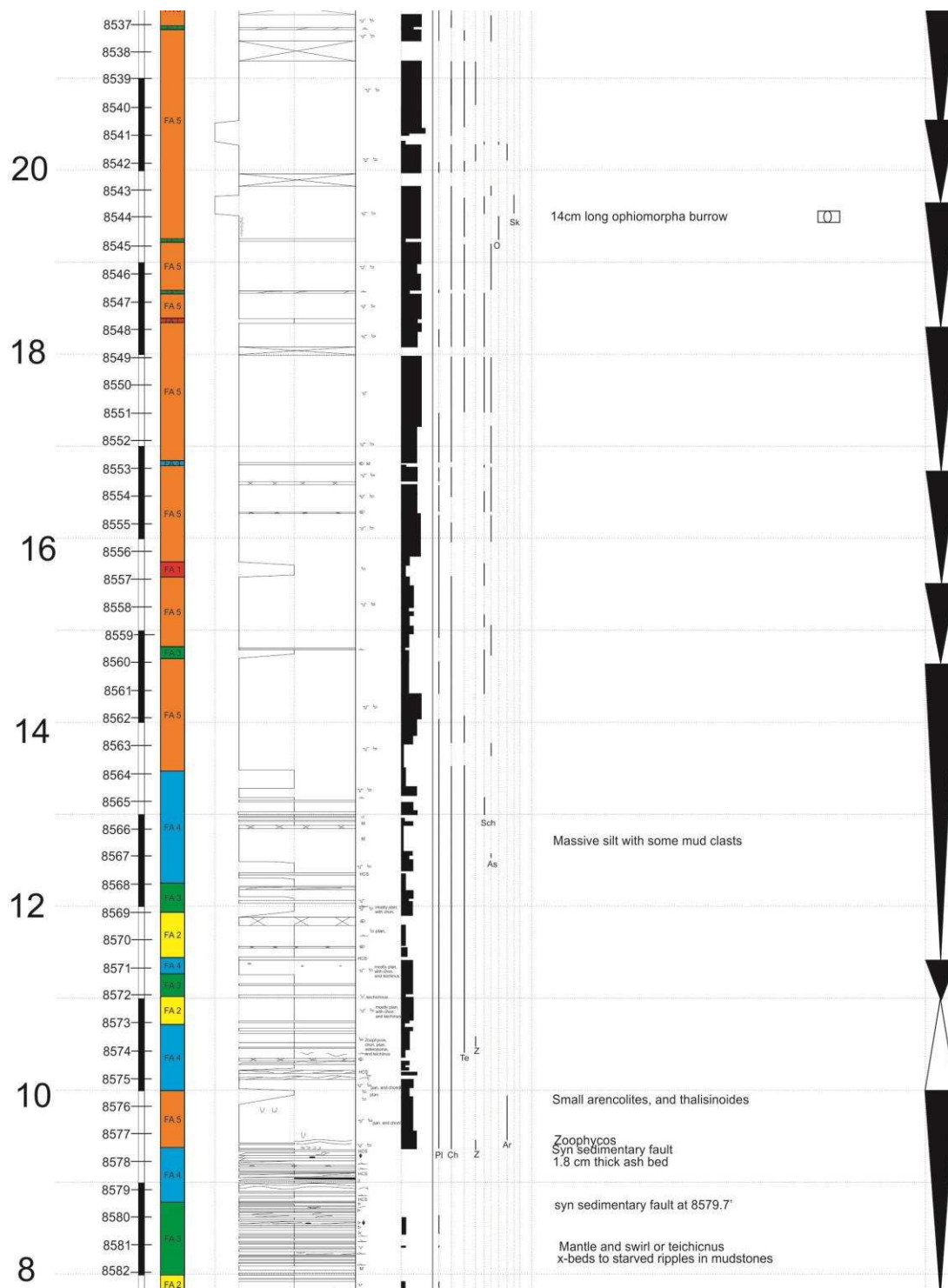


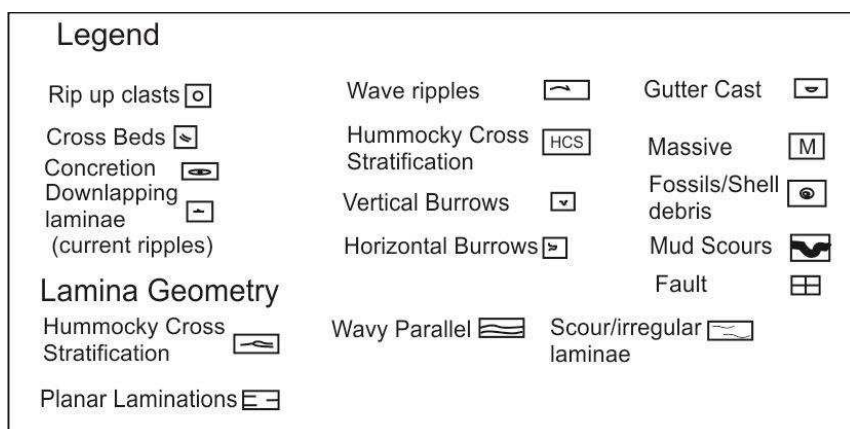
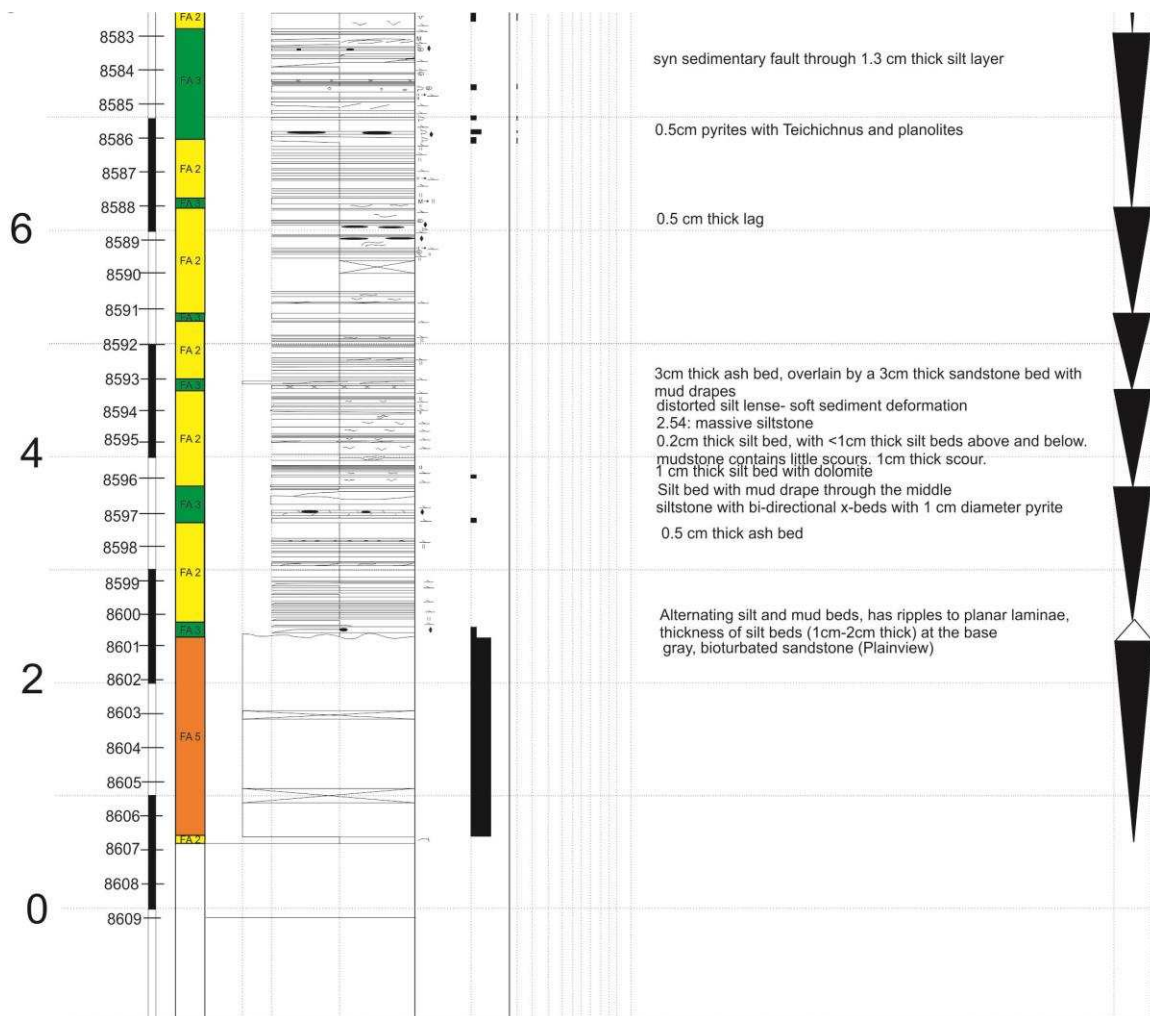




Well: Well A County: State: Colorado  
 Stratigraphic Interval: Plainview-Skull Creek-Muddy J Logged By: Kathleen Masterson Date: 2/27/2015







## Appendix 3: Scanning Electron Microscope (SEM) Report

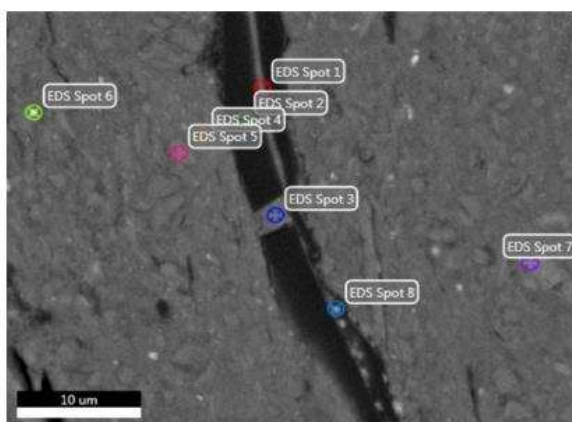
EDAX TEAM

Page 1

Masterson

Author: segenhoff  
Creation: 3/4/2015  
Sample Name: BD-6.12-14

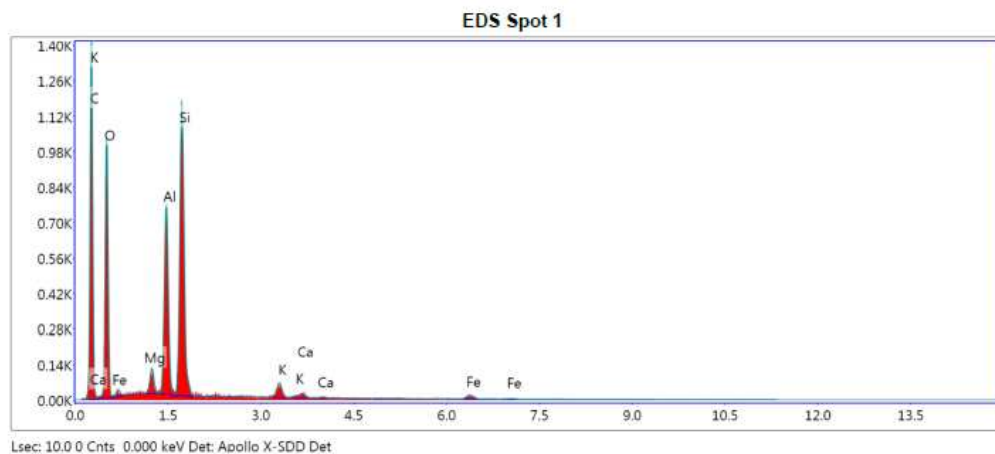
### Area 2



Notes:

## EDS Spot 1

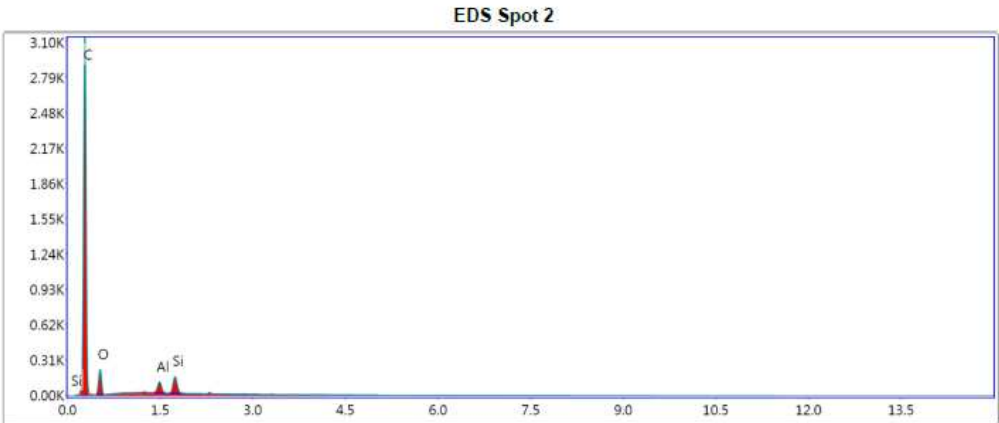
kV: 15      Mag: 3539      Takeoff: 35.5      Live Time(s): 10      Amp Time(μs): 12.8      Resolution:(eV) 126.7

**eZAF Smart Quant Results**

Element	Weight %	Atomic %	Net Int.	Error %	Kratio	Z	R	A	F
C K	49.71	61.88	643.17	9.61	0.16	1.05	0.98	0.31	1
O K	29.26	27.35	552.98	10.41	0.07	1	1	0.24	1
MgK	0.92	0.57	73.30	10.54	0.01	0.91	1.03	0.72	1.01
AlK	6.43	3.57	551.94	4.73	0.05	0.88	1.03	0.83	1.01
SiK	10.56	5.62	894.52	3.96	0.08	0.9	1.04	0.86	1
K K	1.19	0.45	57.45	14.29	0.01	0.83	1.06	0.99	1
CaK	0.47	0.17	18.61	29.56	0.00	0.84	1.06	1	1
FeK	1.46	0.39	20.38	24.15	0.01	0.74	1.07	1.01	1

EDS Spot 2

kV: 15      Mag: 3539      Takeoff: 35.5      Live Time(s): 10      Amp Time(μs): 12.8      Resolution(eV) 126.7



Lsec: 10.0 0 Cnts 0.000 keV Det: Apollo X-SDD Det

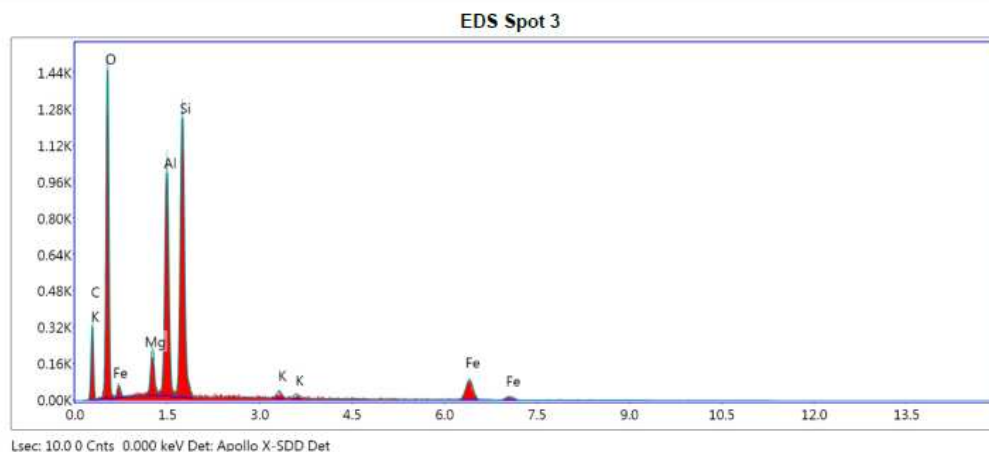
**eZAF Smart Quant Results**

Element	Weight %	Atomic %	Net Int.	Error %	Kratio	Z	R	A	F
C K	82.63	87.33	1,471.75	5.00	0.59	1.01	1	0.7	1
O K	14.05	11.15	118.60	13.44	0.02	0.96	1.01	0.17	1
Al K	1.32	0.62	72.99	8.88	0.01	0.85	1.04	0.88	1
Si K	2.00	0.90	112.77	7.53	0.02	0.86	1.05	0.94	1



## EDS Spot 3

kV: 15      Mag: 3539      Takeoff: 35.5      Live Time(s): 10      Amp Time(μs): 12.8      Resolution(eV) 126.7

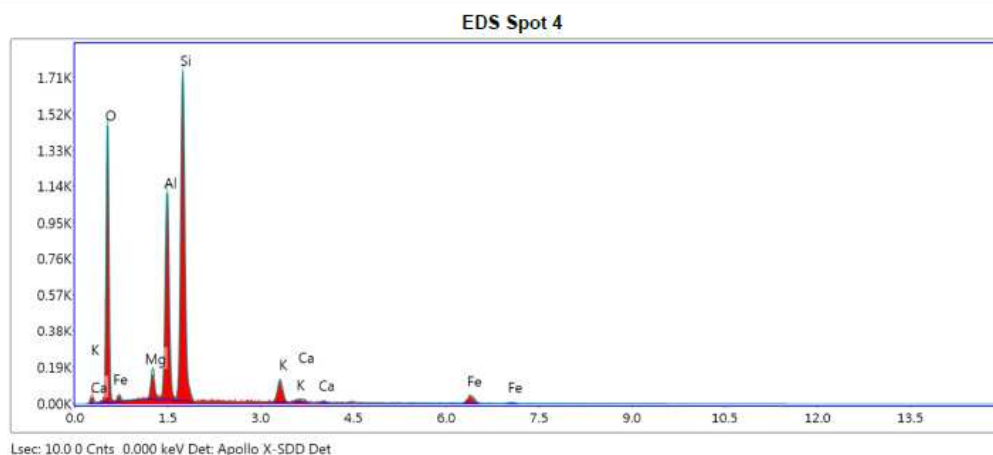
**eZAF Smart Quant Results**

Element	Weight %	Atomic %	Net Int.	Error %	Kratio	Z	R	A	F
C K	22.60	34.72	155.56	12.58	0.05	1.1	0.96	0.2	1
O K	35.24	40.65	804.90	8.94	0.13	1.05	0.98	0.34	1
MgK	2.52	1.92	150.80	8.56	0.02	0.96	1.01	0.65	1.01
AlK	12.07	8.26	784.87	5.15	0.08	0.92	1.02	0.75	1.01
SiK	16.00	10.52	1,009.20	4.74	0.12	0.94	1.02	0.77	1
K K	0.85	0.40	33.43	13.68	0.01	0.87	1.05	0.96	1.01
FeK	10.72	3.54	124.82	7.45	0.08	0.78	1.06	1.01	1



## EDS Spot 4

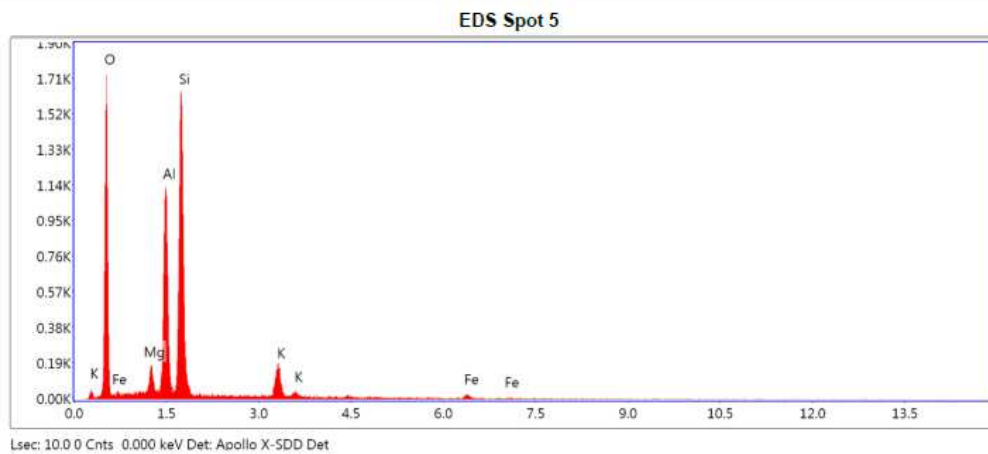
kV: 15      Mag: 3539      Takeoff: 35.5      Live Time(s): 10      Amp Time(μs): 12.8      Resolution:(eV) 126.7

**eZAF Smart Quant Results**

Element	Weight %	Atomic %	Net Int.	Error %	Kratio	Z	R	A	F
O K	40.16	55.60	797.60	8.38	0.17	1.08	0.97	0.4	1
MgK	2.51	2.28	117.17	9.23	0.02	0.99	1	0.67	1.02
AlK	16.46	13.51	827.15	4.93	0.12	0.95	1.01	0.77	1.02
SiK	29.49	23.26	1,365.76	4.75	0.22	0.97	1.01	0.75	1
K K	4.26	2.41	121.09	8.69	0.04	0.9	1.04	0.93	1.01
CaK	0.70	0.39	16.59	36.67	0.01	0.91	1.04	0.94	1.01
FeK	6.42	2.55	55.63	15.55	0.05	0.8	1.06	1	1

## EDS Spot 5

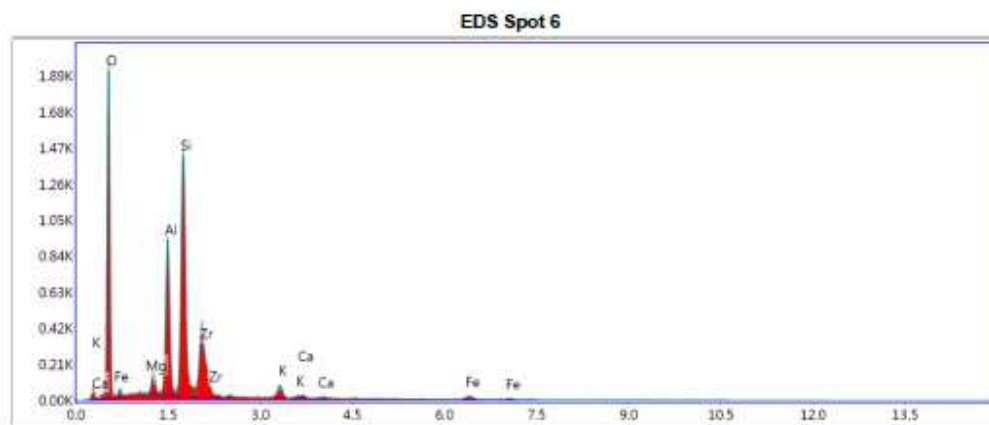
kV: 15      Mag: 3539      Takeoff: 35.5      Live Time(s): 10      Amp Time(μs): 12.8      Resolution(eV) 126.7

**eZAF Smart Quant Results**

Element	Weight %	Atomic %	Net Int.	Error %	Kratio	Z	R	A	F
O K	45.09	59.96	967.05	8.26	0.19	1.07	0.97	0.4	1
MgK	2.50	2.19	127.99	8.94	0.02	0.98	1	0.68	1.02
AlK	16.68	13.15	914.17	4.69	0.12	0.94	1.01	0.78	1.02
SiK	26.76	20.27	1,344.76	4.71	0.20	0.96	1.02	0.76	1
K K	6.27	3.41	192.77	5.97	0.05	0.89	1.04	0.93	1
FeK	2.70	1.03	25.22	25.95	0.02	0.8	1.06	1	1

## EDS Spot 6

kV: 15 Mag: 3539 Takeoff: 35.5 Live Time(s): 10 Amp Time(μs): 12.8 Resolution:(eV) 126.7



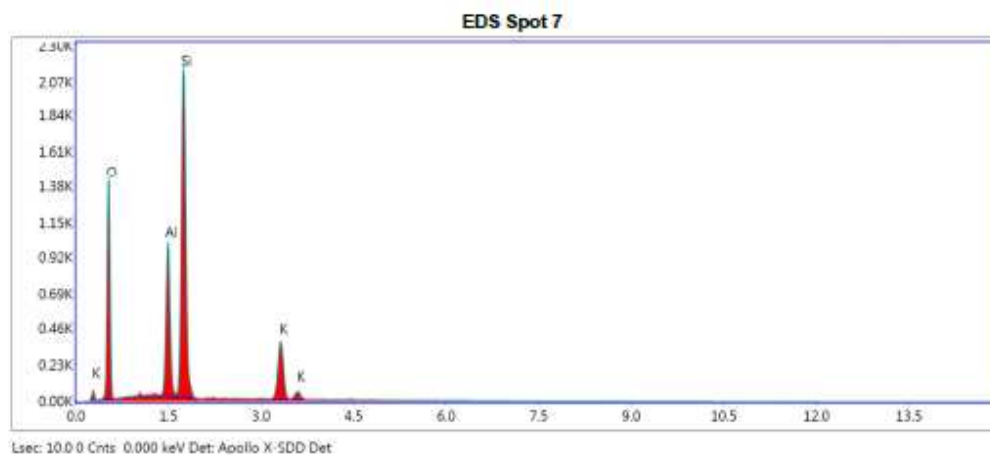
Lsec: 10.0 0 Cnts: 0.000 keV Det: Apollo X-SDD Det

eZAF Smart Quant Results

Element	Weight %	Atomic %	Net Int.	Error %	Kratio	Z	R	A	F
O K	47.27	66.99	1,063.38	8.60	0.19	1.1	0.95	0.36	1
MgK	1.78	1.66	98.37	9.92	0.01	1.01	0.99	0.64	1.01
AlK	11.25	9.45	685.72	5.38	0.08	0.97	0.99	0.75	1.01
SiK	19.04	15.37	1,132.13	4.67	0.15	0.99	1	0.77	1
ZrL	14.86	3.69	357.60	5.98	0.10	0.75	1.18	0.88	1
K K	2.19	1.27	76.02	14.12	0.02	0.92	1.03	0.9	1
CaK	0.70	0.40	20.40	27.25	0.01	0.93	1.03	0.93	1
FeK	2.92	1.15	31.65	24.67	0.02	0.82	1.05	1	1

## EDS Spot 7

kV: 15      Mag: 3539      Takeoff: 35.5      Live Time(s): 10      Amp Time(μs): 12.8      Resolution(eV) 126.7

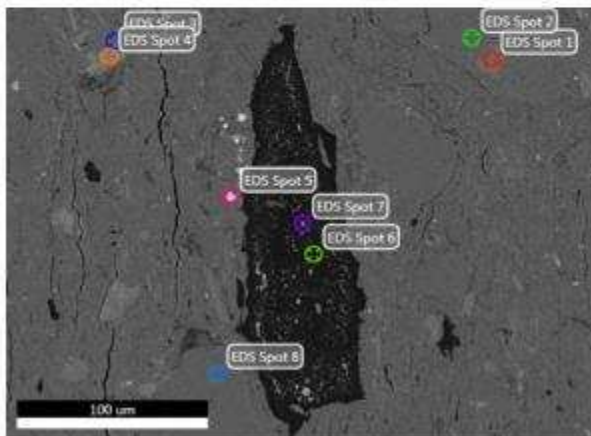
**eZAF Smart Quant Results**

Element	Weight %	Atomic %	Net Int.	Error %	Kratio	Z	R	A	F
O K	43.06	58.33	765.60	9.24	0.15	1.07	0.97	0.33	1
Al K	12.82	10.30	737.80	4.74	0.10	0.94	1.01	0.81	1.02
Si K	31.82	24.55	1,702.26	4.16	0.25	0.96	1.02	0.8	1
K K	12.30	6.82	379.02	4.51	0.10	0.89	1.04	0.93	1

## Masterson

Author: segenhoff  
Creation: 3/4/2015  
Sample Name: BD-6.12-14

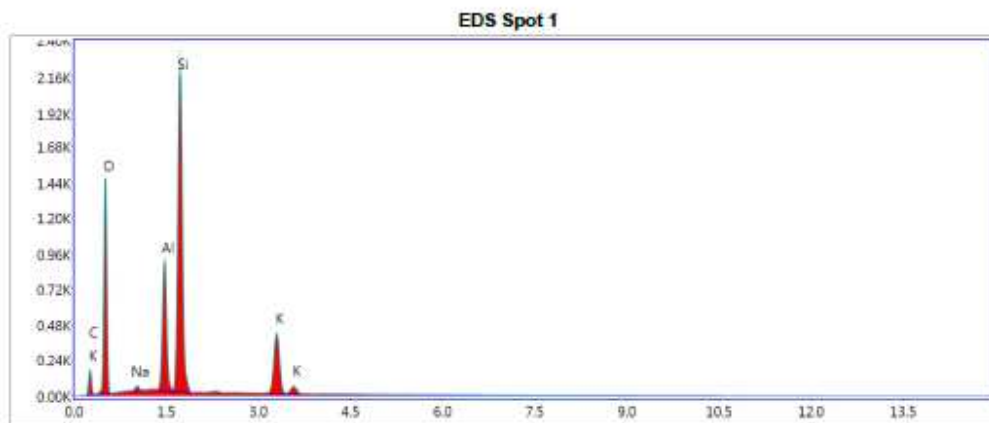
## Area 3



Notes:

## EDS Spot 1

kV: 15 Mag: 526 Takeoff: 35.5 Live Time(s): 10 Amp Time(μs): 12.8 Resolution:(eV) 126.7

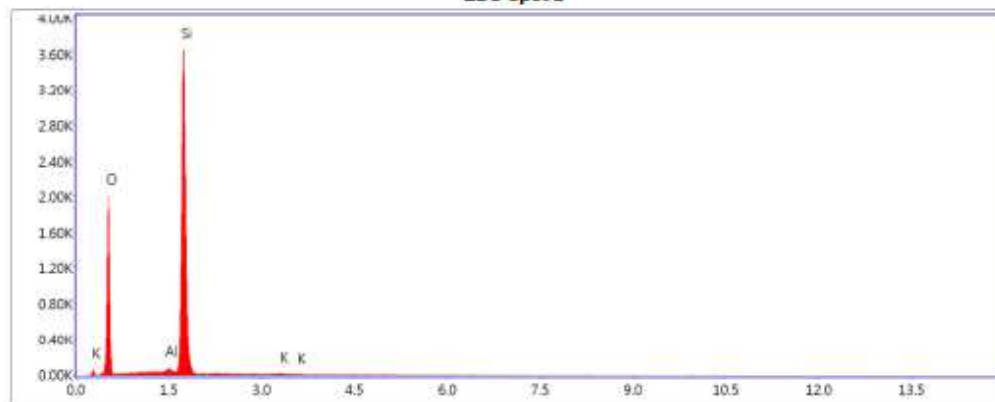
eZAF Smart Quant Results

Element	Weight %	Atomic %	Net Int.	Error %	Kratio	Z	R	A	F
C K	11.52	18.79	68.02	15.87	0.02	1.1	0.95	0.18	1
O K	40.43	49.53	781.94	9.56	0.13	1.05	0.98	0.3	1
Na K	0.60	0.51	23.44	22.49	0.00	0.95	1	0.54	1.01
Al K	9.46	6.87	655.84	4.82	0.07	0.93	1.01	0.61	1.02
Si K	26.71	18.64	1,775.97	3.92	0.21	0.95	1.02	0.82	1
K K	11.27	5.65	426.60	4.24	0.09	0.87	1.05	0.95	1

## EDS Spot 2

kV: 15      Mag: S25      Takeoff: 35.5      Live Time(s): 10      Amp Time(μs): 12.8      Resolution(eV) 126.7

EDS Spot 2



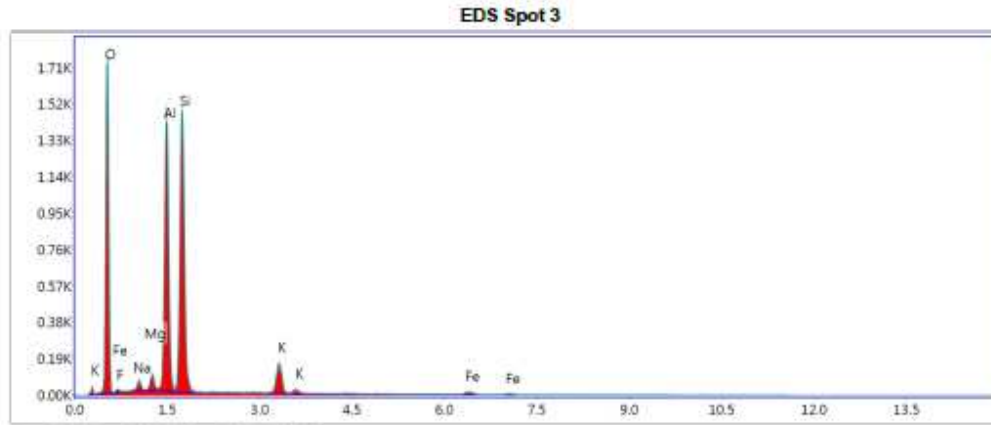
Lsec: 10.0.0 Cnts: 0.000 keV Det: Apollo X-SDD Det

eZAF Smart Quant Results

Element	Weight %	Atomic %	Net Int.	Error %	Kratio	Z	R	A	F
O K	48.48	62.36	1,137.66	7.81	0.22	1.05	0.97	0.44	1
Al K	0.86	0.66	51.21	13.06	0.01	0.93	1.01	0.82	1.04
Si K	50.00	36.63	2,970.03	2.97	0.42	0.95	1.02	0.89	1
K K	0.66	0.35	19.91	31.99	0.01	0.87	1.05	0.92	1

## EDS Spot 3

kV: 15      Mag: 526      Takeoff: 35.5      Live Time(s): 10      Amp Time(μs): 12.8      Resolution(eV) 126.7



Lsec: 10.0 0 Cnts: 0.000 keV Det: Apollo X-SDD Det

eZAF Smart Quant Results

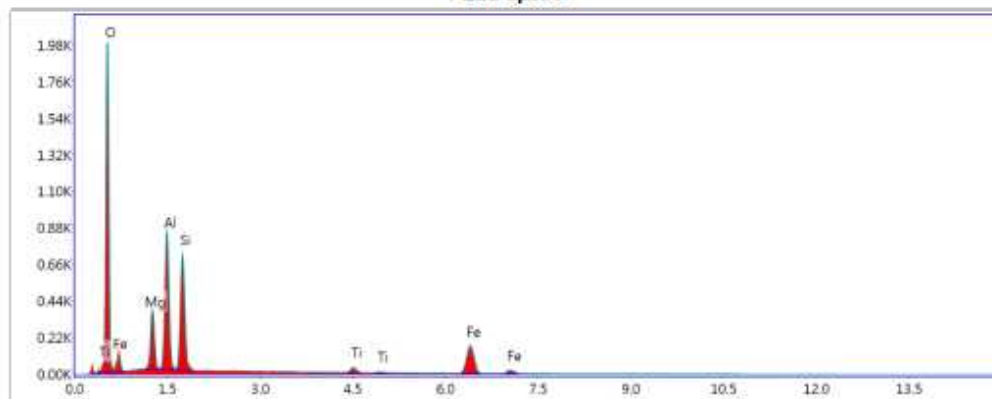
Element	Weight %	Atomic %	Net Int.	Error %	Kratio	Z	R	A	F
O K	44.50	59.00	948.28	6.18	0.20	1.07	0.97	0.41	1
F K	0.38	0.42	5.70	84.28	0.00	0.99	0.98	0.24	1
NaK	1.24	1.14	38.41	15.73	0.01	0.97	1	0.53	1.01
MgK	1.30	1.13	64.02	12.38	0.01	0.98	1	0.68	1.02
AlK	20.42	16.05	1,092.79	4.51	0.15	0.94	1.01	0.79	1.01
SiK	24.33	18.38	1,156.83	4.96	0.17	0.96	1.02	0.74	1
K K	5.50	2.99	164.08	6.75	0.05	0.89	1.04	0.93	1
FeK	2.34	0.89	21.19	27.61	0.02	0.8	1.06	1	1



## EDS Spot 4

kV: 15      Mag: 526      Takeoff: 35.5      Live Time(s): 10      Amp Time(us): 12.6      Resolution:(eV) 126.7

EDS Spot 4



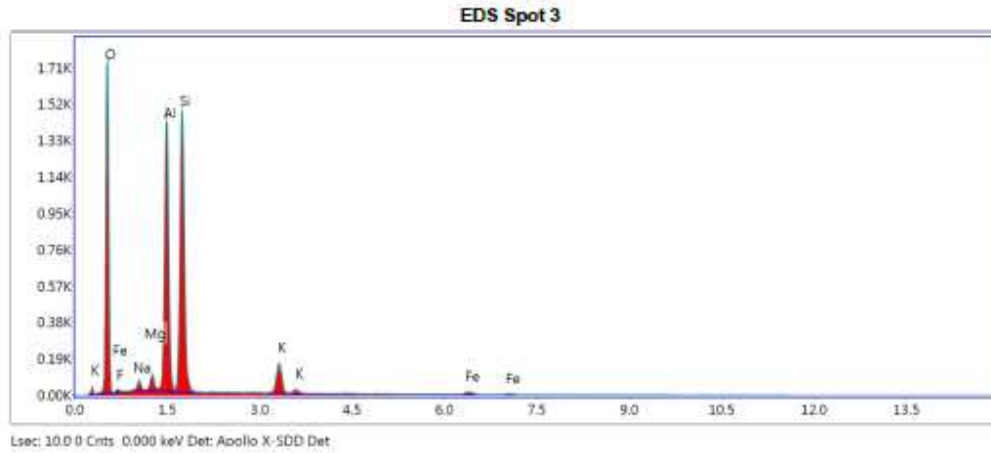
Lsec: 10.0 0 Cnts: 0.000 keV Det: Apollo X SDD Det

eZAF Smart Quant Results

Element	Weight %	Atomic %	Net Int.	Error %	Kratio	Z	R	A	F
O K	39.46	58.71	1,061.17	7.12	0.22	1.11	0.95	0.51	1
MgK	6.55	6.41	262.48	8.40	0.04	1.02	0.99	0.55	1.01
AlK	14.36	12.67	628.78	6.50	0.09	0.98	0.99	0.64	1.01
SiK	12.33	10.46	543.62	6.32	0.08	1	1	0.67	1
TiK	1.66	0.82	35.55	23.27	0.01	0.85	1.04	0.99	1.07
FeK	25.64	10.93	237.52	5.81	0.21	0.83	1.05	1	1

## EDS Spot 3

kV: 15      Mag: 526      Takeoff: 35.5      Live Time(s): 10      Amp Time(μs): 12.8      Resolution(eV) 126.7

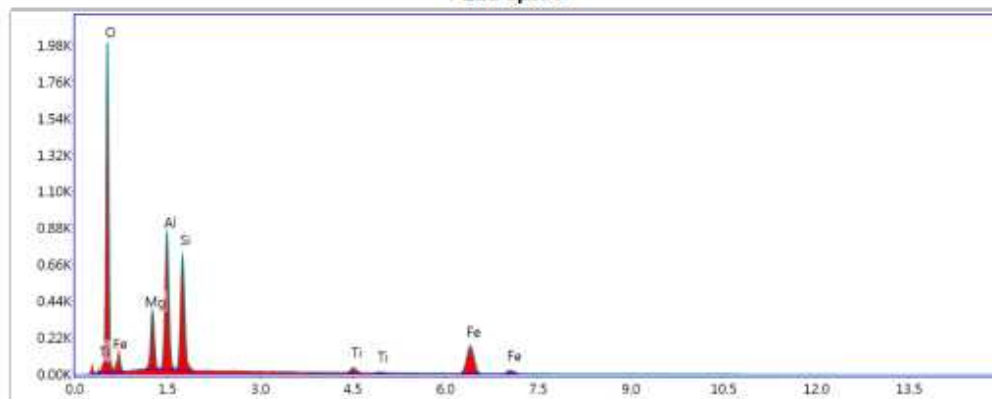
eZAF Smart Quant Results

Element	Weight %	Atomic %	Net Int.	Error %	Kratio	Z	R	A	F
O K	44.50	59.00	948.28	6.18	0.20	1.07	0.97	0.41	1
F K	0.38	0.42	5.70	84.28	0.00	0.99	0.98	0.24	1
NaK	1.24	1.14	38.41	15.73	0.01	0.97	1	0.53	1.01
MgK	1.30	1.13	64.02	12.38	0.01	0.98	1	0.68	1.02
AlK	20.42	16.05	1,092.79	4.51	0.15	0.94	1.01	0.79	1.01
SiK	24.33	18.38	1,156.83	4.96	0.17	0.96	1.02	0.74	1
K K	5.50	2.99	164.08	6.75	0.05	0.89	1.04	0.93	1
FeK	2.34	0.89	21.19	27.61	0.02	0.8	1.06	1	1

## EDS Spot 4

kV: 15      Mag: 526      Takeoff: 35.5      Live Time(s): 10      Amp Time(us): 12.6      Resolution:(eV) 126.7

EDS Spot 4



Lsec: 10.0 0 Cnts: 0.000 keV Det: Apollo X SDD Det

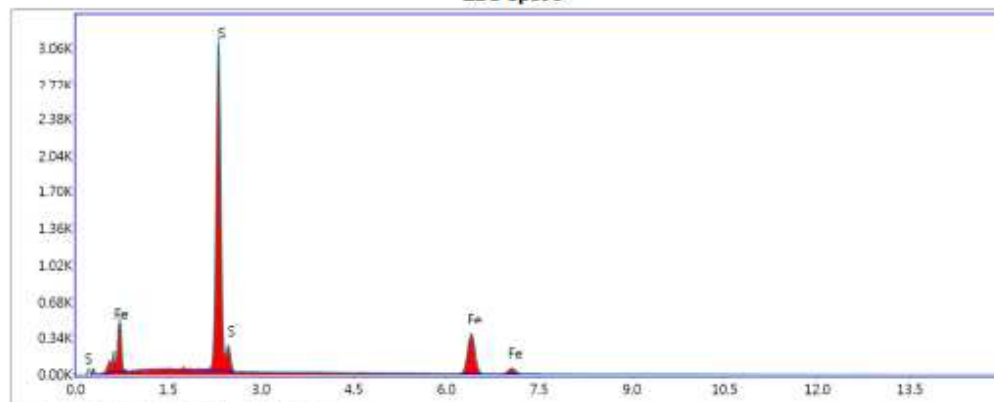
eZAF Smart Quant Results

Element	Weight %	Atomic %	Net Int.	Error %	Kratio	Z	R	A	F
O K	39.46	58.71	1,061.17	7.12	0.22	1.11	0.95	0.51	1
MgK	6.55	6.41	262.48	8.40	0.04	1.02	0.99	0.55	1.01
AlK	14.36	12.67	628.78	6.50	0.09	0.98	0.99	0.64	1.01
SiK	12.33	10.46	543.62	6.32	0.08	1	1	0.67	1
TiK	1.66	0.82	35.55	23.27	0.01	0.85	1.04	0.99	1.07
FeK	25.64	10.93	237.52	5.81	0.21	0.83	1.05	1	1

## EDS Spot 5

kV: 15      Mag: 526      Takeoff: 35.5      Live Time(s): 10      Amp Time(μs): 12.8      Resolution:(eV) 126.7

## EDS Spot 5



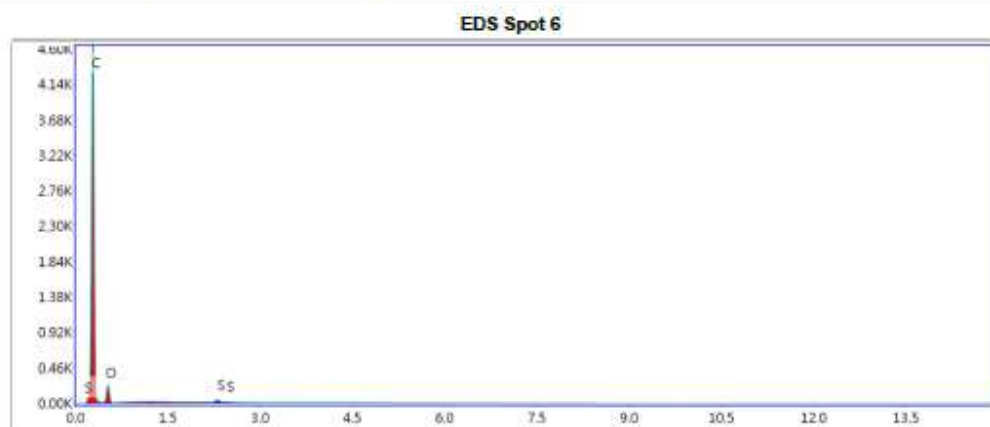
Lsec: 10.0 0 Cnts: 0.000 keV Det: Apollo X-SDD Det

eZAF Smart Quant Results

Element	Weight %	Atomic %	Net Int.	Error %	Kratio	Z	R	A	F
S K	53.00	66.26	2,802.41	3.13	0.51	1.07	0.97	0.89	1
FeK	47.00	33.74	520.59	4.28	0.42	0.92	1.02	0.99	1

## EDS Spot 6

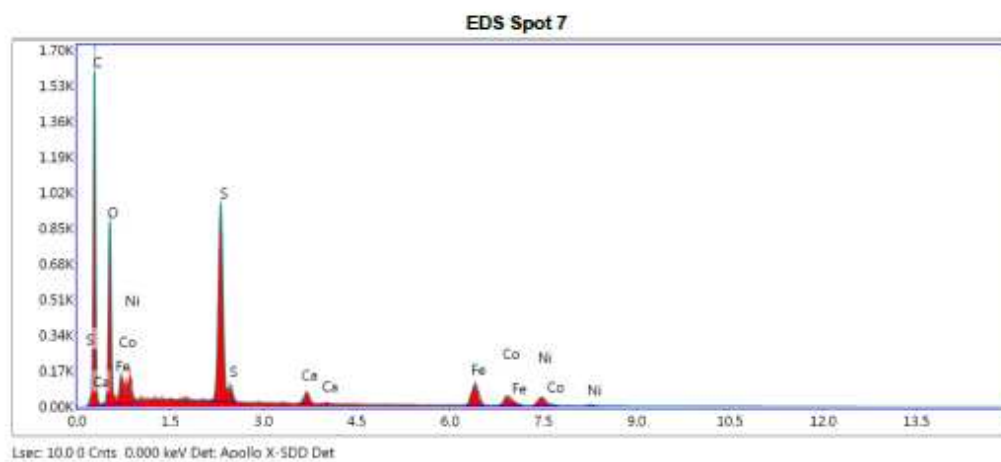
kV: 15      Mag: 525      Takeoff: 35.5      Live Time(s): 10      Amp Time(μs): 12.8      Resolution:(eV) 126.7

**eZAF Smart Quant Results**

Element	Weight %	Atomic %	Net Int.	Error %	Kratio	Z	R	A	F
C K	86.88	90.02	2,201.39	3.52	0.73	1.01	1	0.83	1
O K	12.53	9.75	121.87	13.43	0.02	0.96	1.01	0.17	1
S K	0.59	0.23	32.27	20.56	0.00	0.84	1.06	1.01	1

## EDS Spot 7

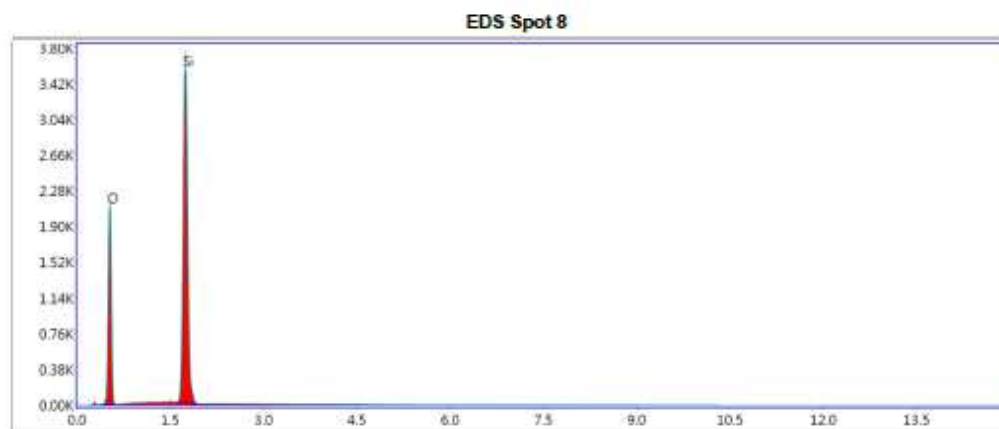
KV: 15      Mag: 526      Takeoff: 35.5      Live Time(s): 10      Amp Time(μs): 12.8      Resolution:(eV) 126.7

**eZAF Smart Quant Results**

Element	Weight %	Atomic %	Net Int.	Error %	Kratio	Z	R	A	F
C K	50.47	68.39	775.23	9.51	0.16	1.08	0.96	0.29	1
O K	20.87	21.23	482.50	10.79	0.05	1.03	0.96	0.23	1
S K	9.49	4.82	846.86	3.24	0.08	0.9	1.03	0.94	1
CaK	1.17	0.47	59.85	14.34	0.01	0.87	1.05	0.99	1.02
FeK	7.84	2.26	146.36	8.04	0.06	0.77	1.06	1.01	1.05
CoK	4.80	1.33	87.80	14.48	0.04	0.75	1.06	1.01	1.01
NIK	5.37	1.49	62.15	14.69	0.04	0.77	1.06	1	1

## EDS Spot 8

kV: 15      Mag: 526      Takeoff: 35.5      Live Time(s): 10      Amp Time(μs): 12.8      Resolution(eV) 126.7

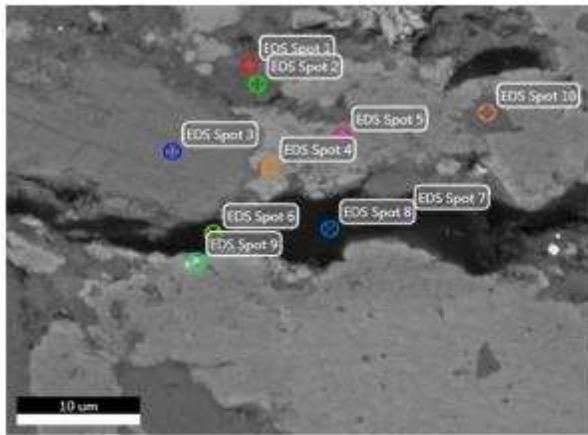
**eZAF Smart Quant Results**

Element	Weight %	Atomic %	Net Int.	Error %	Kratio	Z	R	A	F
O K	49.77	63.50	1,163.88	7.67	0.24	1.05	0.98	0.45	1
Si K	50.23	36.50	2,907.75	2.92	0.43	0.95	1.02	0.9	1

## Masterson

Author: segenhoff  
Creation: 3/4/2015  
Sample Name: TC-14.61-14

## Area 3

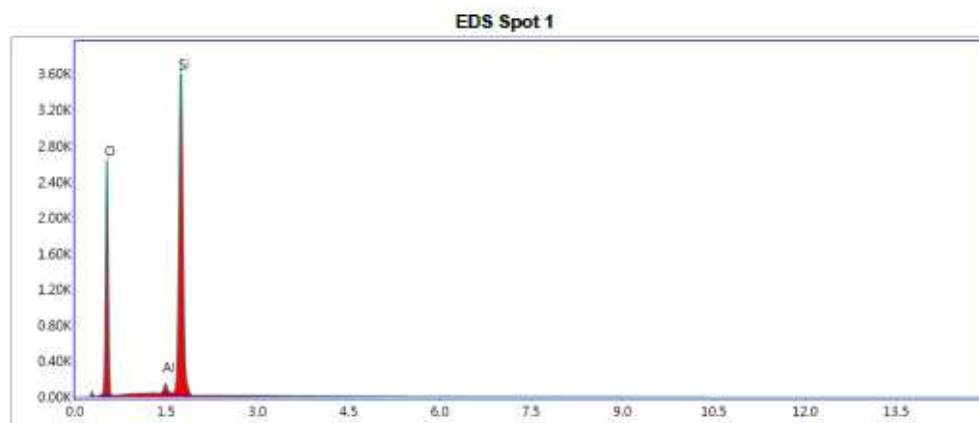


Notes:



## EDS Spot 1

kV: 15      Mag: 3405      Takeoff: 35.5      Live Time(s): 10      Amp Time(μs): 12.8      Resolution(eV) 126.7

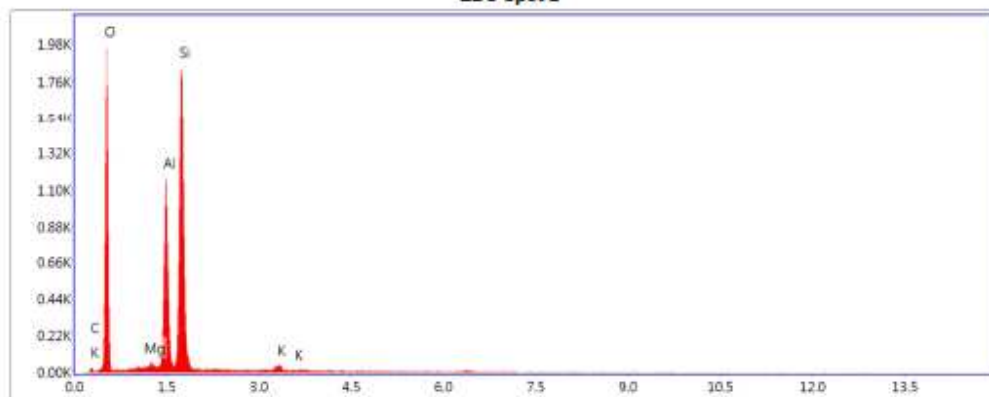
**eZAF Smart Quant Results**

Element	Weight %	Atomic %	Net Int.	Error %	Kratio	Z	R	A	F
O K	52.56	66.02	1,418.42	7.39	0.26	1.05	0.98	0.47	1
Al K	1.44	1.07	90.14	9.36	0.01	0.92	1.02	0.81	1.04
Si K	46.00	32.91	2,897.98	3.11	0.38	0.94	1.02	0.88	1

## EDS Spot 2

kV: 15      Mag: 3406      Takeoff: 35.5      Live Time(s): 10      Amp Time(μs): 12.8      Resolution:(eV) 126.7

## EDS Spot 2



Lsec: 10.00 Cnts: 0.000 keV Det: Apollo X-SDD Det

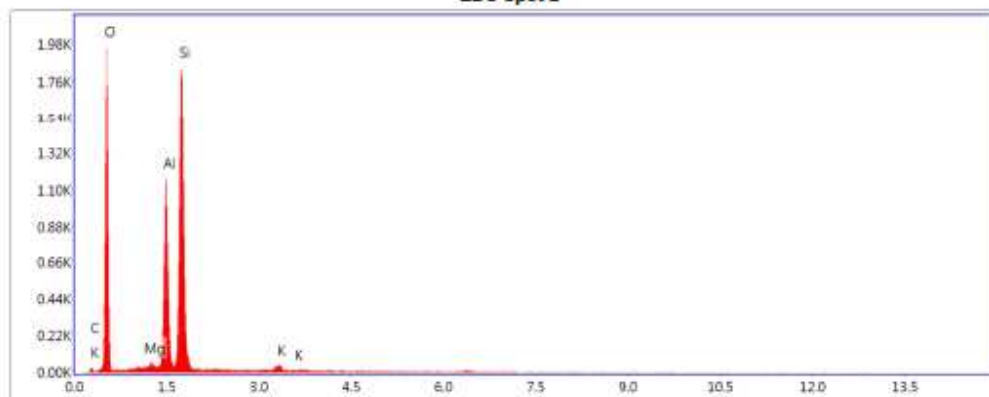
eZAF Smart Quant Results

Element	Weight %	Atomic %	Net Int.	Error %	Kratio	Z	R	A	F
C K	2.70	4.48	10.10	38.62	0.00	1.1	0.96	0.14	1
O K	48.65	60.70	1,083.94	7.82	0.22	1.05	0.98	0.44	1
MgK	0.54	0.44	26.96	18.73	0.00	0.97	1.01	0.7	1.02
AlK	16.01	11.85	672.67	4.43	0.12	0.93	1.02	0.82	1.02
SiK	30.63	21.77	1,510.92	4.38	0.23	0.95	1.02	0.78	1
K K	1.48	0.75	42.98	15.01	0.01	0.87	1.05	0.93	1

## EDS Spot 2

kV: 15      Mag: 3406      Takeoff: 35.5      Live Time(s): 10      Amp Time(μs): 12.8      Resolution:(eV) 126.7

## EDS Spot 2



Lsec: 10.00 Cnts: 0.000 keV Det: Apollo X-SDD Det

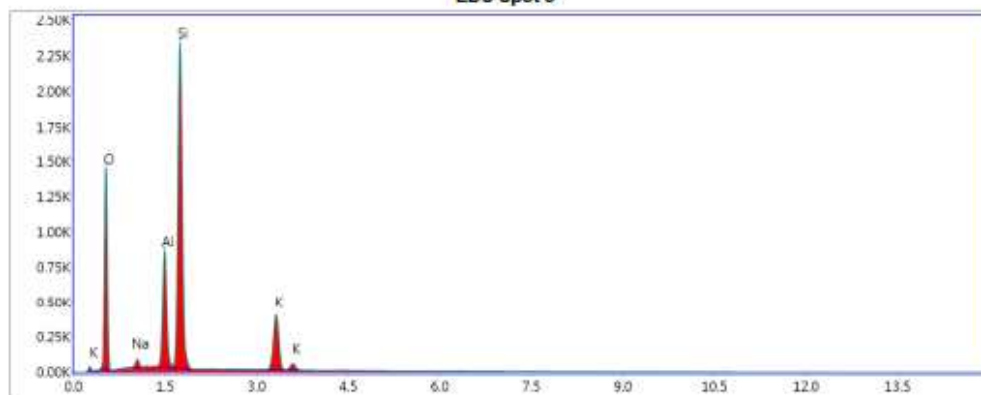
eZAF Smart Quant Results

Element	Weight %	Atomic %	Net Int.	Error %	Kratio	Z	R	A	F
C K	2.70	4.48	10.10	38.62	0.00	1.1	0.96	0.14	1
O K	48.65	60.70	1,083.94	7.82	0.22	1.05	0.98	0.44	1
MgK	0.54	0.44	26.96	18.73	0.00	0.97	1.01	0.7	1.02
AlK	16.01	11.85	672.67	4.43	0.12	0.93	1.02	0.82	1.02
SiK	30.63	21.77	1,510.92	4.38	0.23	0.95	1.02	0.78	1
K K	1.48	0.75	42.98	15.01	0.01	0.87	1.05	0.93	1

## EDS Spot 3

kV: 15      Mag: 3406      Takeoff: 35.5      Live Time(s): 10      Amp Time(μs): 12.8      Resolution(eV) 126.7

## EDS Spot 3



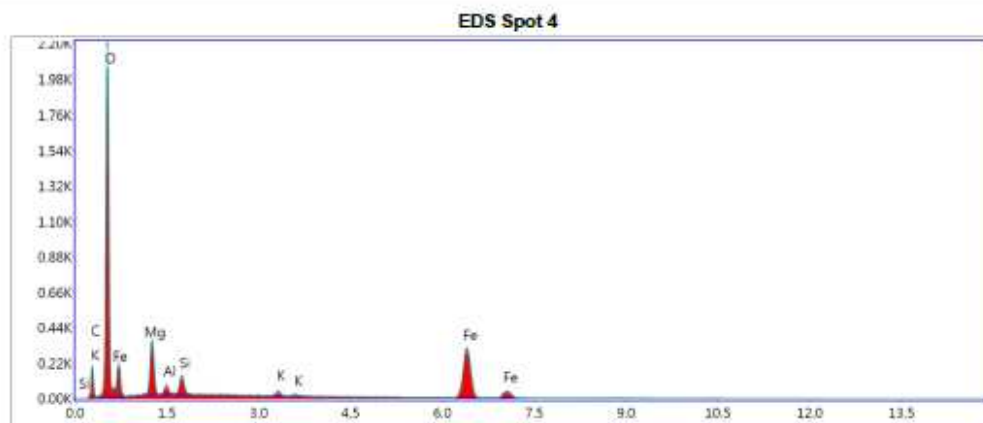
Lsec: 10.00 Cnts: 0.000 keV Det: Apollo X SDD Det

## eZAF Smart Quant Results

Element	Weight %	Atomic %	Net Int.	Error %	Kratio	Z	R	A	F
O K	42.93	58.18	791.28	9.24	0.15	1.07	0.97	0.33	1
NaK	1.09	1.03	36.67	18.23	0.01	0.97	0.99	0.53	1.01
AlK	10.81	8.69	642.27	4.92	0.08	0.94	1.01	0.8	1.02
SiK	32.47	25.07	1,829.42	4.05	0.25	0.96	1.02	0.81	1
K K	12.69	7.04	407.88	4.66	0.11	0.89	1.04	0.93	1

## EDS Spot 4

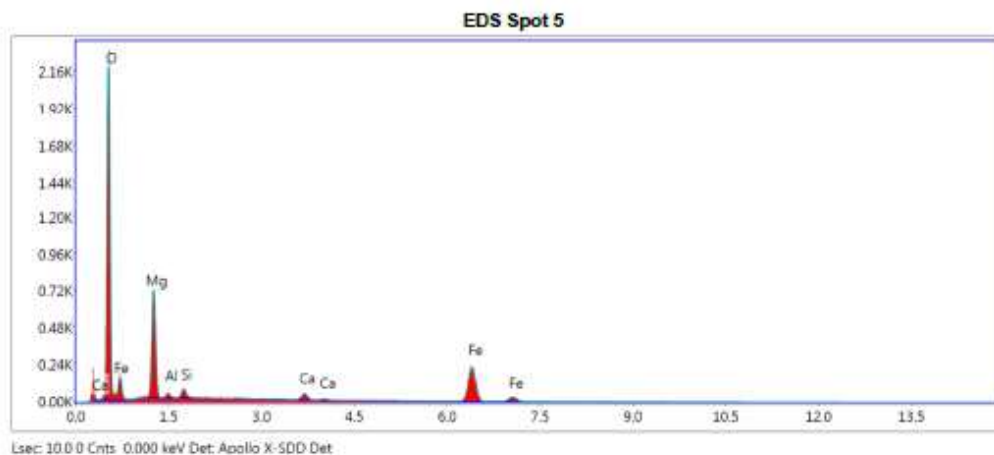
kV: 15      Mag: 3406      Takeoff: 35.5      Live Time(s): 10      Amp Time(μs): 12.6      Resolution(eV) 126.7

eZAF Smart Quant Results

Element	Weight %	Atomic %	Net Int.	Error %	Kratio	Z	R	A	F
C K	10.51	19.87	94.51	14.27	0.04	1.16	0.92	0.29	1
O K	38.60	54.77	1,176.06	7.08	0.22	1.11	0.95	0.51	1
MgK	6.36	5.94	246.11	9.31	0.03	1.02	0.98	0.47	1
AlK	1.00	0.84	44.52	16.71	0.01	0.98	0.99	0.57	1
SiK	1.84	1.49	94.83	12.11	0.01	1	1	0.69	1
K K	0.86	0.50	31.95	21.96	0.01	0.93	1.03	0.96	1.04
FeK	40.83	16.60	433.76	4.28	0.34	0.83	1.05	1.01	1

## EDS Spot 5

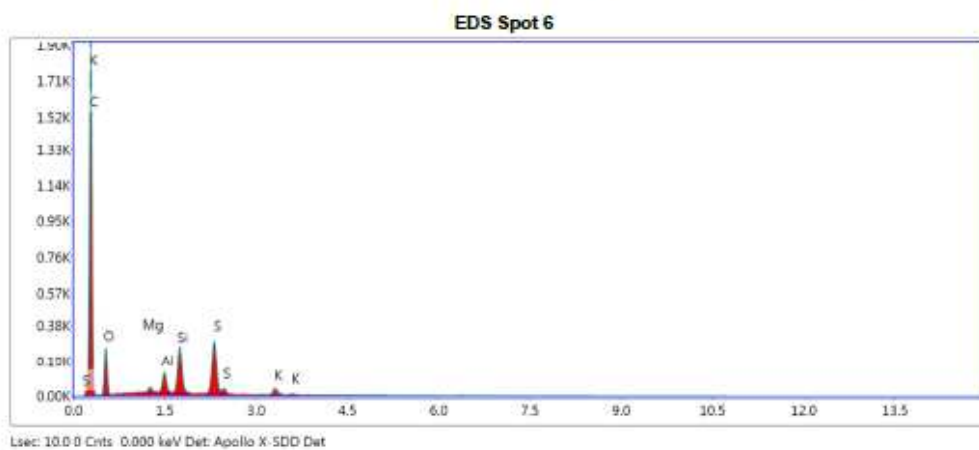
kV: 15 Mag: 3406 Takeoff: 35.5 Live Time(s): 10 Amp Time(μs): 12.8 Resolution(eV) 126.7

eZAF Smart Quant Results

Element	Weight %	Atomic %	Net Int.	Error %	Kratio	Z	R	A	F
O K	43.35	65.41	1,234.42	6.09	0.29	1.11	0.94	0.61	1
MgK	15.86	15.75	497.35	8.10	0.06	1.02	0.98	0.48	1
AlK	0.77	0.69	25.08	26.80	0.00	0.99	0.99	0.54	1
SiK	1.28	1.10	49.34	18.10	0.01	1.01	1	0.66	1
CaK	1.82	1.09	44.07	19.37	0.02	0.95	1.03	0.97	1.05
FeK	36.92	15.96	307.02	5.06	0.31	0.84	1.05	1	1

## EDS Spot 6

kV: 15      Mag: 3406      Takeoff: 35.5      Live Time(s): 10      Amp Time(μs): 12.8      Resolution:(eV) 126.7

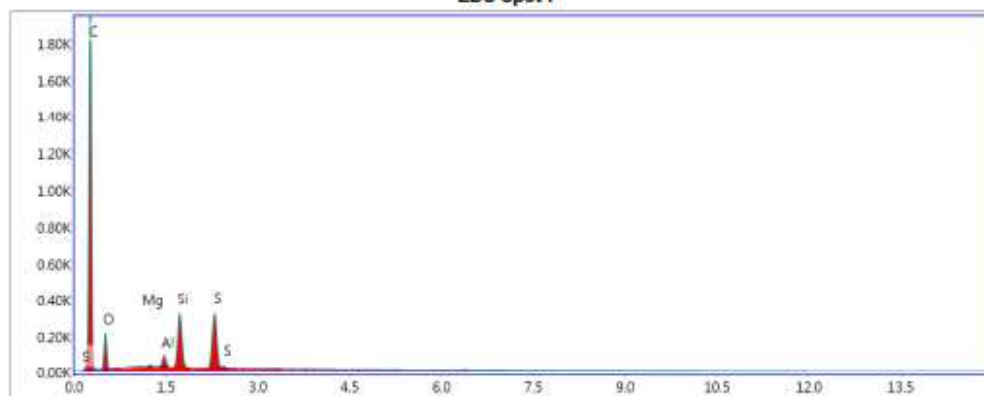
**eZAF Smart Quant Results**

Element	Weight %	Atomic %	Net Int.	Error %	Kratio	Z	R	A	F
C K	75.05	83.45	904.32	6.19	0.32	1.02	0.99	0.42	1
O K	14.09	11.76	135.50	13.45	0.02	0.97	1.01	0.17	1
MgK	0.37	0.21	21.84	18.79	0.00	0.89	1.03	0.77	1.01
AlK	1.34	0.66	83.16	6.61	0.01	0.86	1.04	0.87	1.01
SiK	3.13	1.49	199.71	5.37	0.03	0.87	1.05	0.93	1.01
S K	5.04	2.10	253.67	4.02	0.04	0.85	1.05	0.96	1
K K	0.99	0.34	33.41	19.58	0.01	0.8	1.07	1	1

## EDS Spot 7

kV: 15      Mag: 3406      Takeoff: 35.5      Live Time(s): 10      Amp Time(μs): 12.8      Resolution:(eV) 126.7

EDS Spot 7



Lsec: 10.00 Cnts 0.000 keV Det: Apollo X-SD Det

eZAF Smart Quant Results

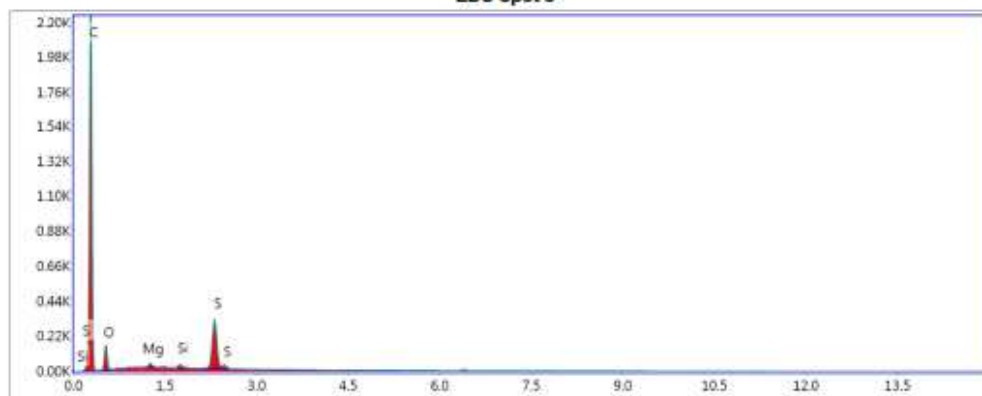
Element	Weight %	Atomic %	Net Int.	Error %	Kratio	Z	R	A	F
C K	78.69	86.19	947.68	8.01	0.34	1.02	0.99	0.42	1
O K	11.62	9.55	107.75	14.01	0.02	0.97	1.01	0.17	1
MgK	0.09	0.05	5.53	71.98	0.00	0.89	1.04	0.77	1.01
AlK	0.70	0.34	43.77	14.64	0.01	0.85	1.04	0.88	1.01
SiK	3.62	1.70	231.98	5.34	0.03	0.87	1.05	0.94	1.01
S K	5.27	2.16	263.70	5.66	0.04	0.85	1.06	0.99	1



## EDS Spot 8

kV: 15      Mag: 3406      Takeoff: 35.5      Live Time(s): 10      Amp Time(μs): 12.8      Resolution:(eV) 126.7

EDS Spot 8



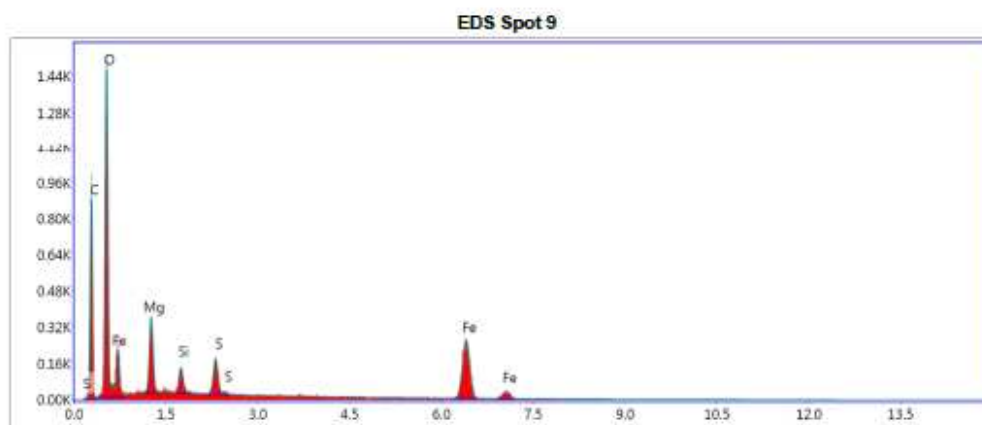
Lsec: 10.00 Cnts: 0.000 keV Det: Apollo X-SDO Det

eZAF Smart Quant Results

Element	Weight %	Atomic %	Net Int.	Error %	Kratio	Z	R	A	F
C K	83.55	89.34	1,096.09	7.16	0.42	1.01	0.99	0.5	1
O K	9.99	8.02	82.16	14.70	0.02	0.96	1.01	0.16	1
MgK	0.33	0.17	17.64	27.94	0.00	0.88	1.04	0.78	1
SiK	0.28	0.13	16.93	32.65	0.00	0.87	1.05	0.95	1.01
S K	5.85	2.34	275.99	3.99	0.05	0.84	1.06	1.01	1

## EDS Spot 9

HV: 15      Mag: 3406      Takeoff: 35.5      Live Time(s): 10      Amp Time(μs): 12.6      Resolution(eV) 126.7



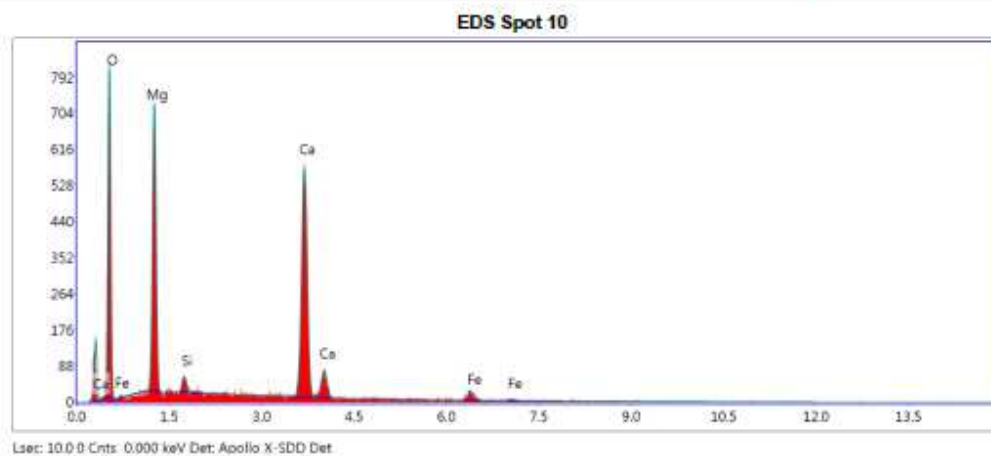
Lsec: 10.00 Cnts: 0.000 keV Det: Apollo X-5DD Det

eZAF Smart Quant Results

Element	Weight %	Atomic %	Net Int.	Error %	Kratio	Z	R	A	F
C K	33.16	49.96	439.92	9.42	0.12	1.1	0.95	0.34	1
O K	31.87	36.04	814.11	9.18	0.11	1.05	0.97	0.34	1
MgK	4.16	3.10	234.21	8.74	0.02	0.97	1	0.54	1
SiK	1.21	0.78	87.32	12.02	0.01	0.95	1.01	0.75	1
S K	2.19	1.24	140.68	10.66	0.02	0.93	1.03	0.9	1.01
FeK	27.40	8.88	367.33	4.75	0.22	0.79	1.06	1.01	1

## EDS Spot 10

kV: 15      Mag: 3406      Takeoff: 35.5      Live Time(s): 10      Amp Time(μs): 12.8      Resolution:(eV) 126.7

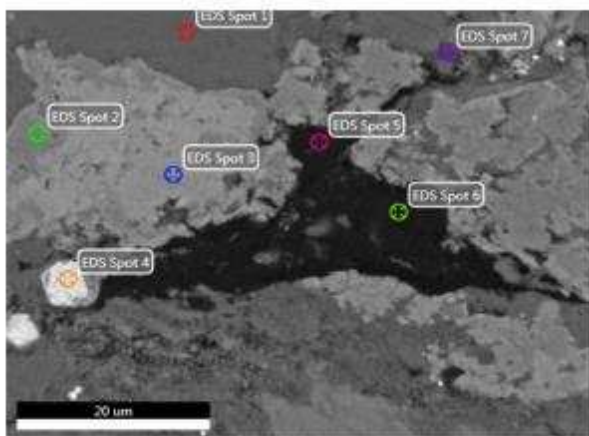
eZAF Smart Quant Results

Element	Weight %	Atomic %	Net Int.	Error %	Kratio	Z	R	A	F
O K	47.64	65.93	441.22	10.54	0.12	1.07	0.96	0.24	1
MgK	15.67	14.27	489.74	7.05	0.09	0.99	0.99	0.69	1
SiK	0.86	0.68	30.62	22.59	0.01	0.97	1.01	0.74	1.01
CaK	31.51	17.41	607.89	3.35	0.29	0.91	1.04	0.99	1
FeK	4.32	1.71	28.73	20.52	0.03	0.8	1.05	0.99	1

## Masterson

Author: segenhoff  
Creation: 3/4/2015  
Sample Name: TC-14.61-14

## Area 4

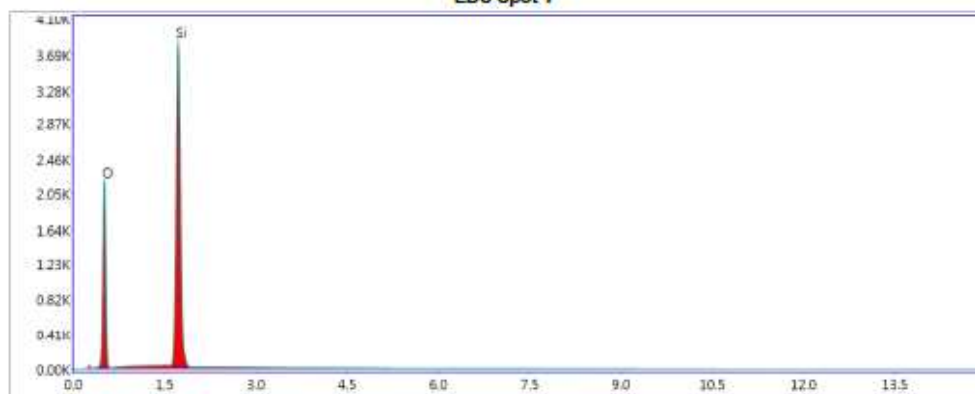


Notes:

## EDS Spot 1

kV: 15      Mag: 2668      Takeoff: 35.5      Live Time(s): 10      Amp Time(μs): 12.8      Resolution(eV) 126.7

EDS Spot 1



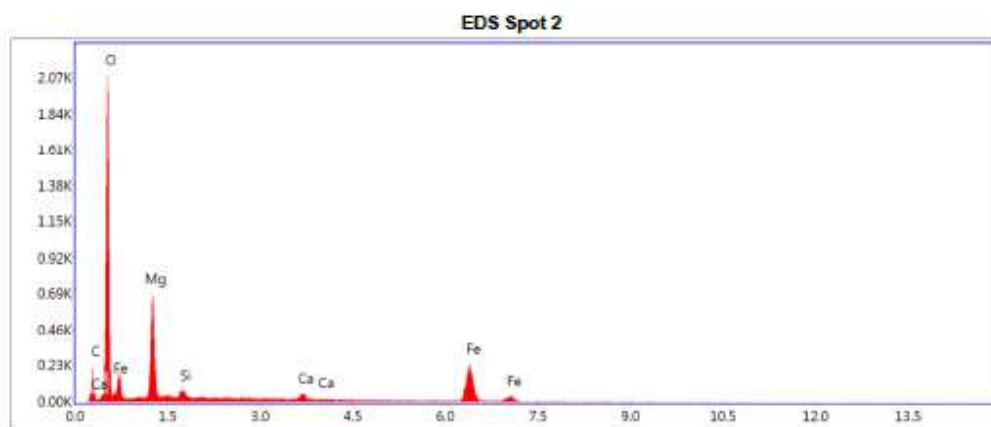
Lsec: 10.0 0 Cnts: 0.000 keV Det: Apollo X-SDD Det.

eZAF Smart Quant Results

Element	Weight %	Atomic %	Net Int.	Error %	Kratio	Z	R	A	F
O K	49.48	63.23	1,182.78	7.68	0.23	1.05	0.98	0.45	1
Si K	50.52	36.77	3,001.64	2.93	0.43	0.95	1.02	0.9	1

## EDS Spot 2

kV: 15 Mag: 2568 Takeoff: 35.5 Live Time(s): 10 Amp Time(μs): 12.8 Resolution:(eV) 126.7



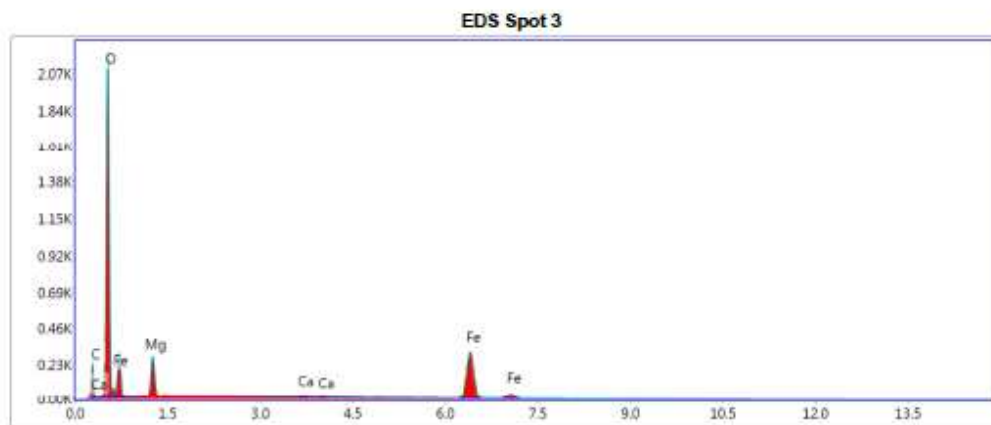
Lsec: 10.0 0 Cnts 0.000 keV Det: Apollo X-SDD Det

eZAF Smart Quant Results

Element	Weight %	Atomic %	Net Int.	Error %	Kratio	Z	R	A	F
C K	12.44	21.39	109.69	12.13	0.04	1.13	0.94	0.3	1
O K	43.52	56.17	1,206.34	7.25	0.23	1.08	0.96	0.49	1
Mg K	11.72	9.95	466.61	7.92	0.06	0.99	0.99	0.51	1
Si K	0.94	0.69	46.38	16.81	0.01	0.97	1.01	0.7	1
Ca K	1.42	0.73	41.85	18.87	0.01	0.92	1.04	0.98	1.04
Fe K	29.96	11.08	299.61	5.04	0.24	0.81	1.05	1.01	1

## EDS Spot 3

kV: 15 Mag: 2668 Takeoff: 35.5 Live Time(s): 10 Amp Time(μs): 12.8 Resolution:(eV) 126.7



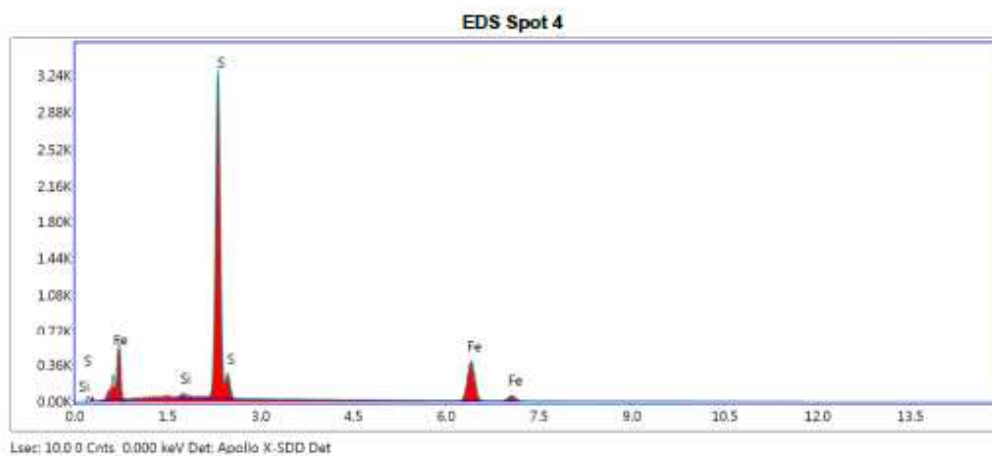
Lsec: 10.000 Cnts: 0.000 keV Det: Apollo X-SDD Det

**eZAF Smart Quant Results**

Element	Weight %	Atomic %	Net Int.	Error %	Kratio	Z	R	A	F
C K	11.39	21.34	106.95	11.96	0.04	1.16	0.92	0.32	1
O K	40.01	56.29	1,174.24	7.02	0.23	1.11	0.94	0.52	1
MgK	5.08	4.71	182.08	9.91	0.02	1.02	0.96	0.45	1
CaK	0.76	0.43	22.99	31.14	0.01	0.94	1.03	0.95	1.05
FeK	42.76	17.24	432.08	4.35	0.36	0.83	1.05	1.01	1

## EDS Spot 4

kV: 15      Mag: 2667      Takeoff: 35.5      Live Time(s): 10      Amp Time(μs): 12.8      Resolution:(eV) 126.7

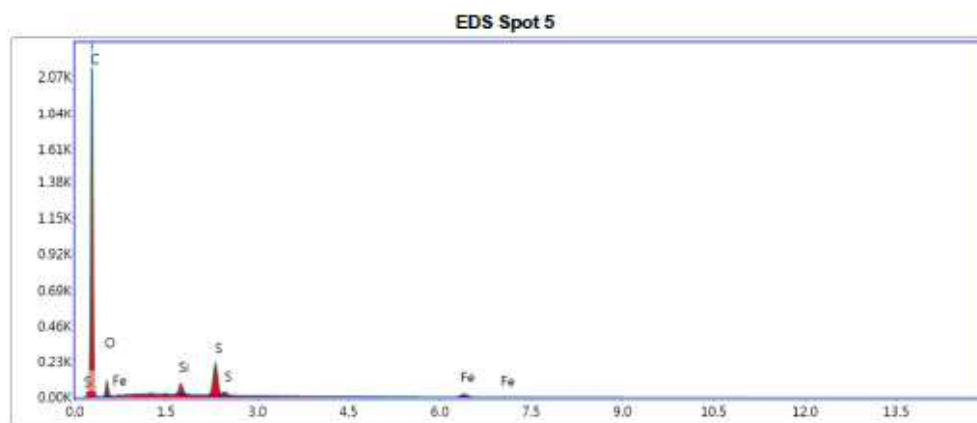
**eZAF Smart Quant Results**

Element	Weight %	Atomic %	Net Int.	Error %	Kratio	Z	R	A	F
SiK	0.37	0.52	23.24	38.05	0.00	1.09	0.96	0.74	1.04
S K	52.47	65.61	2,908.86	3.14	0.50	1.07	0.97	0.89	1
FeK	47.16	33.86	549.03	4.23	0.43	0.92	1.02	0.99	1



## EDS Spot 5

kV: 15      Mag: 2667      Takeoff: 35.5      Live Time(s): 10      Amp Time(μs): 12.6      Resolution:(eV) 126.7



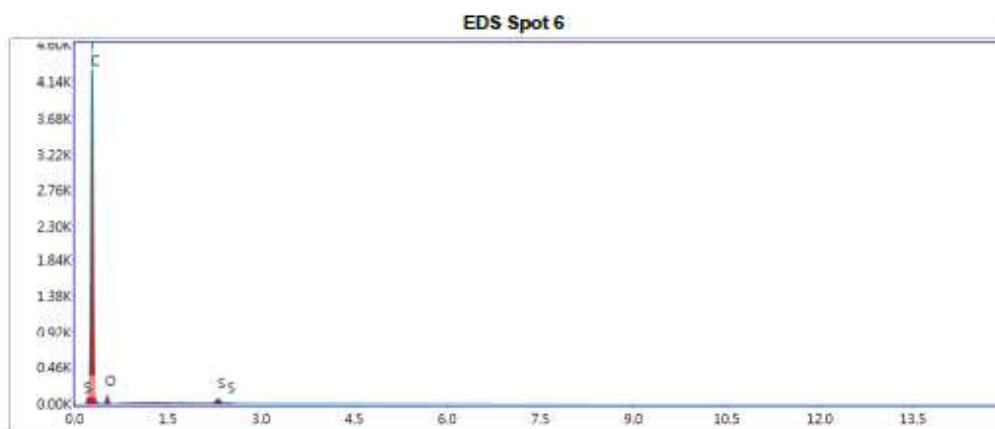
Lsec: 10.0 0 Cnts 0.000 keV Det: Apollo X-SDD Det

**eZAF Smart Quant Results**

Element	Weight %	Atomic %	Net Int.	Error %	Kratio	Z	R	A	F
C K	84.52	91.42	1,075.73	6.88	0.46	1.02	0.99	0.53	1
O K	6.88	5.59	51.77	15.96	0.01	0.97	1.01	0.16	1
Si K	1.02	0.47	55.23	11.91	0.01	0.87	1.05	0.94	1.01
S K	4.36	1.77	187.77	4.93	0.04	0.85	1.06	1	1
Fe K	3.22	0.75	26.20	19.42	0.02	0.72	1.07	1.01	1

## EDS Spot 6

kV: 15      Mag: 2567      Takeoff: 35.5      Live Time(s): 10      Amp Time(μs): 12.8      Resolution:(eV) 126.7

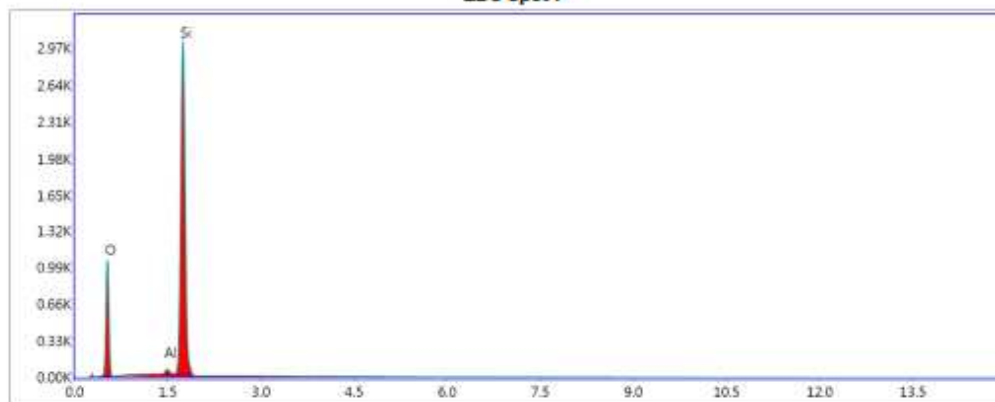
**eZAF Smart Quant Results**

Element	Weight %	Atomic %	Net Int.	Error %	Kratio	Z	R	A	F
C K	92.48	94.63	2,228.34	3.47	0.78	1	1	0.84	1
O K	6.48	4.98	55.72	15.29	0.01	0.95	1.02	0.16	1
S K	1.04	0.40	54.00	14.95	0.01	0.84	1.06	1.01	1

## EDS Spot 7

kV: 15      Mag: 2667      Takeoff: 35.5      Live Time(s): 10      Amp Time(μs): 12.8      Resolution:(eV) 126.7

EDS Spot 7



Lsec: 10.0 0 Cnts 0.000 keV Det: Apollo X-SDD Det

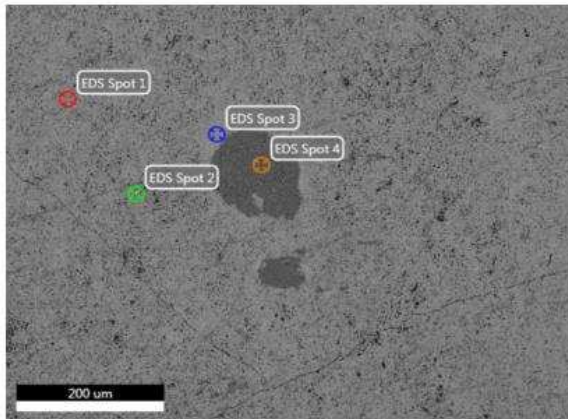
eZAF Smart Quant Results

Element	Weight %	Atomic %	Net Int.	Error %	Kratio	Z	R	A	F
O K	39.64	53.54	556.92	8.78	0.17	1.06	0.97	0.4	1
Al K	0.86	0.69	35.11	16.91	0.01	0.94	1.01	0.85	1.06
Si K	59.50	45.77	2,363.34	2.88	0.52	0.96	1.02	0.91	1

## Masterson

Author: segenhoff  
Creation: 3/4/2015  
Sample Name: D3137930-8.5

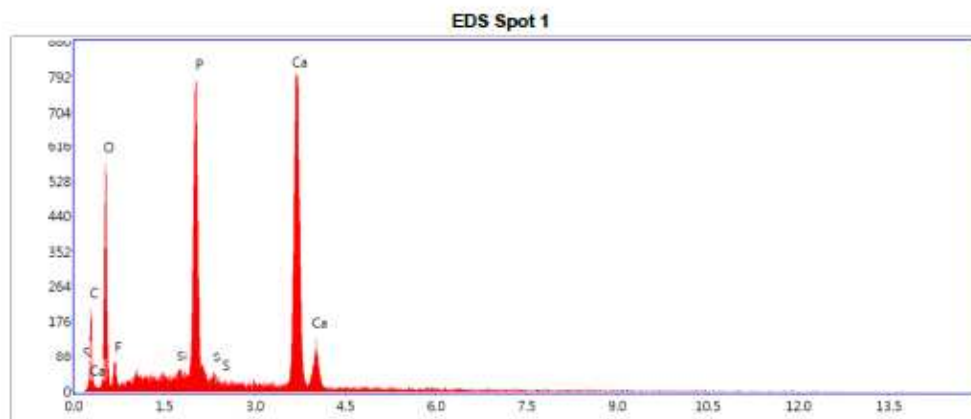
## Area 1



Notes:

## EDS Spot 1

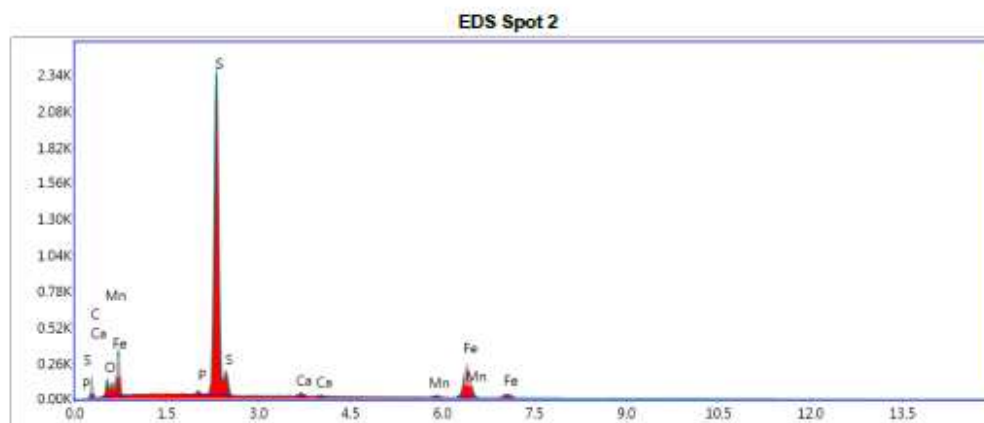
HV: 15      Mag: 211      Takeoff: 35.5      Live Time(s): 10      Amp Time(μs): 12.8      Resolution(eV) 126.7

**eZAF Smart Quant Results**

Element	Weight %	Atomic %	Net Int.	Error %	Kratio	Z	R	A	F
C K	12.21	21.68	85.37	13.85	0.04	1.12	0.94	0.26	1
O K	33.74	44.97	309.56	11.54	0.06	1.07	0.96	0.18	1
F K	3.63	4.08	42.77	17.22	0.01	0.99	0.97	0.18	1
Si K	0.52	0.40	29.09	25.01	0.00	0.97	1.01	0.84	1.03
P K	14.39	9.91	667.48	3.86	0.12	0.93	1.02	0.9	1.02
S K	0.59	0.39	25.95	29.11	0.01	0.95	1.02	0.88	1.03
Ca K	34.91	18.58	905.40	3.07	0.31	0.91	1.04	0.98	1

## EDS Spot 2

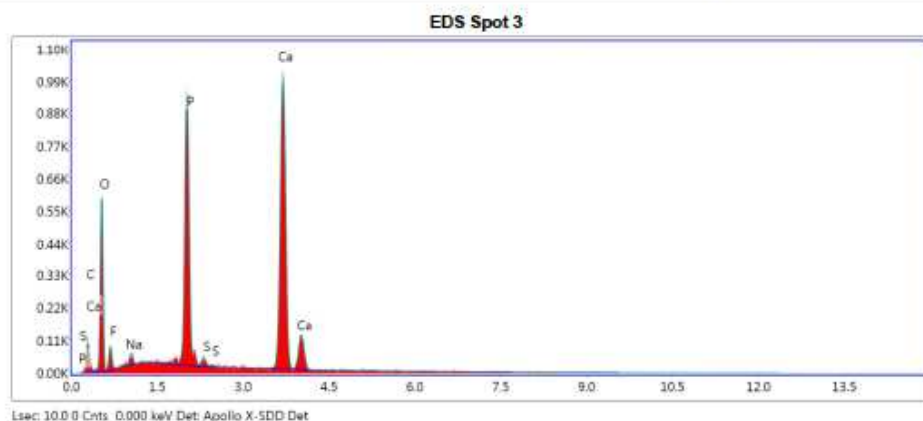
kV: 15      Mag: 211      Takeoff: 35.5      Live Time(s): 10      Amp Time(μs): 12.6      Resolution:(eV) 126.7

eZAF Smart Quant Results

Element	Weight %	Atomic %	Net Int.	Error %	Kratio	Z	R	A	F
C K	21.88	46.26	74.80	15.10	0.03	1.18	0.91	0.11	1
O K	3.85	6.11	54.81	19.39	0.01	1.12	0.93	0.23	1
P K	0.47	0.38	25.35	25.85	0.00	0.98	0.99	0.87	1.06
S K	39.93	31.62	2,119.13	2.91	0.37	1	1	0.92	1
Ca K	1.25	0.79	36.77	24.96	0.01	0.96	1.02	0.92	1.03
Mn K	1.33	0.61	17.59	36.58	0.01	0.84	1.04	0.99	1.03
Fe K	31.29	14.23	337.06	4.98	0.26	0.85	1.04	0.99	1

## EDS Spot 3

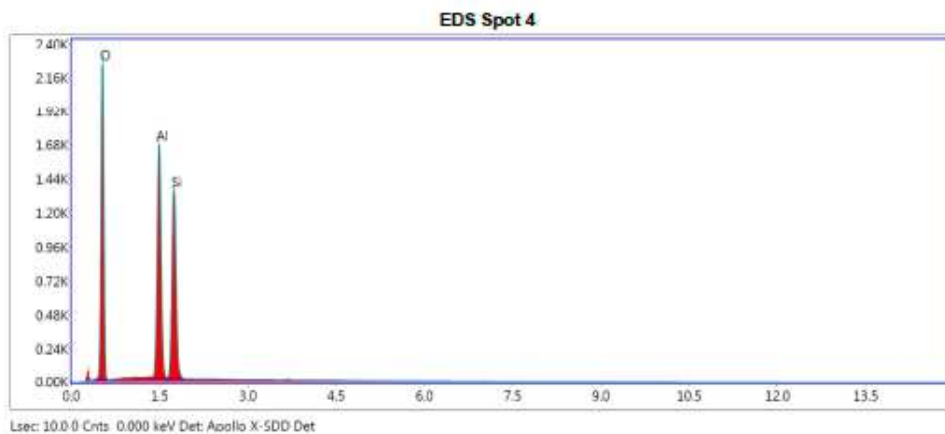
kV: 15      Mag: 211      Takeoff: 35.5      Live Time(s): 10      Amp Time(μs): 12.8      Resolution(eV) 126.7

eZAF Smart Quant Results

Element	Weight %	Atomic %	Net Int.	Error %	Kratio	Z	R	A	F
C K	5.62	10.84	38.55	18.95	0.02	1.14	0.93	0.24	1
O K	33.45	48.39	313.44	11.61	0.06	1.09	0.95	0.17	1
F K	3.67	4.47	44.72	17.21	0.01	1.01	0.96	0.18	1
Na K	0.99	0.99	26.63	22.85	0.00	0.98	0.98	0.44	1
P K	16.08	12.02	779.55	3.71	0.14	0.94	1.01	0.9	1.02
S K	0.64	0.46	29.17	27.21	0.01	0.96	1.02	0.86	1.03
Ca K	39.55	22.84	1,072.54	2.93	0.36	0.92	1.04	0.98	1

## EDS Spot 4

kV: 15      Mag: 211      Takeoff: 35.5      Live Time(s): 10      Amp Time(μs): 12.8      Resolution:(eV) 126.7

**eZAF Smart Quant Results**

Element	Weight %	Atomic %	Net Int.	Error %	Kratio	Z	R	A	F
O K	51.53	64.65	1,255.50	7.19	0.27	1.05	0.98	0.5	1
Al K	24.07	17.91	1,268.86	4.10	0.19	0.93	1.02	0.82	1.01
Si K	24.41	17.44	1,094.01	5.06	0.17	0.95	1.02	0.74	1